The University of Michigan
College of Engineering
Department of Aerospace Engineering
Gas Dynamics Laboratories

Technical Report

THE STRUCTURE OF THE REYNOLDS STRESS IN A TURBULENT BOUNDARY LAYER

Shui-Shong Lu
William W. Willmarth

under contract with

Department of the Navy
Office of Naval Research
N00014-67-A-0181-0015
Washington, D. C.

October 1972

ABSTRACT

Experimental studies of the structure of the Reynolds stress in a turbulent boundary layer on a smooth wall with zero pressure gradient are reported. The technique of conditional sampling is employed to study the signal, uv, obtained from hot wire probes. The measurements of the mean time intervals and the durations of bursts and sweeps are attempted.

In the conditional sampling method the velocity at the edge of the viscous sublayer is used as a detector for the bursts; and the signal, uv, is obtained from the x wire probe at various locations. From the measurements it is found that, when the velocity, u_w, at the edge of the viscous sublayer becomes low and decreasing, a burst occurs. On the other hand, the sweep event occurs when u_w becomes large and increasing. The convection speeds of the bursts and the sweeps are found to be equal and are about 0. 8 times the local mean velocity and 0. 425 times the free stream velocity at a distance of $y/\delta^* \approx 0.169$ from the wall. Throughout the turbulent boundary layer, the bursts are the largest contributors to $\overline{uv}$ with the sweeps the second largest. On the

average, the burst events account for 77% of $\overline{uv}$, while the sweep events have 55% to their account; the excessive percentage over 100% is due to the other small negative contributors.

Characteristic mean time intervals are obtained for both burst and sweep events from the unique features of the measurements of the fractional contributions to $\overline{uv}$ from different events. Both mean time intervals are sensibly constant for most of the turbulent boundary layer. The scaling of the mean time interval between bursts with outer flow variables is justified. The mean time interval between sweeps is roughly the same as that between bursts.

TABLE OF CONTENTS

LIST OF ILLUSTRATIONS

NOMENCLATURE

f	frequency
h	normalized uv; $h \equiv uv/u'v'$
H	hole size; $H \equiv \|h\| = \|uv/u'v'\|$
R	correlation coefficient; $R \equiv \overline{uv}/u'v'$
Re_x	Reynolds number based on the distance from the virtual origin of the turbulent boundary layer
Re_θ	Reynolds number based on the momentum thickness
S_i	indicator function for the ith quadrant in the measurements of contributions to $\overline{uv}$ from different events; see Eq. (4.4)
t	time
$\overline{T}_B$	mean time interval between bursts
$\overline{T}_{CB}$	characteristic mean time interval between bursts
$\overline{T}_{CS}$	characteristic mean time interval between sweeps
$\overline{T}_m$	characteristic time interval measured by Rao, et al. (1971)
$\overline{T}_S$	mean time interval between sweeps
u	fluctuating streamwise velocity; $u = (u_{1n} + u_{2n})/\sqrt{2}$
u_w	fluctuating streamwise velocity at the edge of the viscous sublayer
u_{1n}, u_{2n}	signal obtained from a hot wire of the x wire probe at $\pm 45^o$ to the mean flow direction, see Fig. 3

U	local mean flow speed
U_{CB}	convection speed of burst events
U_{CS}	convection speed of sweep events
U_τ	wall shear velocity
U_∞	free stream velocity
uv	$uv = u \cdot v = (u_{1n}^2 - u_{2n}^2)/2$
$\overline{uv}$	mean Reynolds stress
$\widetilde{uv}_i$	contributions to $\overline{uv}$ from ith quadrant, i = 1, 2, 3, 4, see Eq. (4.3)
v	fluctuating velocity normal to the wall; $v = (u_{1n} - u_{2n})/\sqrt{2}$
x, y, z	the coordinates; see Fig. 3
y^+	distance from the wall normalized with the wall region variables; $y^+ \equiv y U_\tau/\nu$
β_u	probability density distribution function of the u signal
β_{uv}	probability density distribution function of $uv/\overline{uv}$
β_v	probability density distribution function of the v signal
δ	boundary layer thickness
δ^*	displacement thickness
$\overline{\Delta T}_B$	time scale of bursts
$\overline{\Delta T}_{CB}$	characteristic time scale of bursts
$\overline{\Delta T}_{CS}$	characteristic time scale of sweeps
$\overline{\Delta T}_S$	time scale of sweeps

θ	momentum thickness
ν	kinematic viscosity
τ	time delay

subscripts and superscripts

1	normalized u
1	first quadrant
2	normalized v
2	second quadrant; burst
3	third quadrant
4	fourth quadrant; sweep
h	hole
i	ith quadrant; i = 1, 2, 3, 4
B	burst
S	sweep
$< >$	average of samples
$( )'$	root mean square value

I. INTRODUCTION

For decades there have been intensive investigations of the problem of the turbulent boundary layer. Yet the structure of the turbulent boundary layer has not been well understood due to the inherent complexity of the turbulent flow structure. One can divide the turbulent boundary layer roughly into two regions, i.e., the inner, or wall region and the outer, or wake region. In the outer wake region the Reynolds stress acts to retard the mean flow and extracts energy from the mean flow and transfers it to the inner wall region where most of the turbulent energy production and dissipation occur. There is an approximate balance between creation and dissipation of energy in the inner wall region with a small surplus of turbulent energy. This small surplus of turbulent energy is diffused out toward the outer region and is the major source of the turbulent energy there. This is the two-layer model of the turbulent boundary layer (Townsend (1956)). A knowledge of the structure of the inner region and its interaction with the outer region is important to the understanding of the structure of the whole turbulent boundary layer.

The initial approach to the problem of the structure of turbulent shear flow was made through the interpretation of the measurements of spatial correlations and power spectra of turbulent velocities. Representative reports are those by Townsend (1951), Schubauer and Klebanoff (1951),

Laufer (1953), Klebanoff (1954), Grant (1958) and more recently by Tritton (1967) and Clark (1968). After the measurements of space-time correlations of streamwise velocity component were introduced by Favre, Gaviglio and Dumas (1957, 1958), the structure of turbulence was inferred from the space-time correlations between various turbulent velocity components and fluctuating wall pressure such as the reports by Willmarth and Wooldridge (1962, 1963), Willmarth and Tu (1967), etc. Various structural models such as by Townsend (1957), Grant (1958) and Willmarth and Tu (1967) were proposed. However, there are difficulties in the inference of flow structure from these correlation measurements. Firstly, the inference of flow structure from the long-time-averaging measurements is not a unique process as pointed out by Townsend (1957). The turbulent velocity field cannot be uniquely specified even if complete space-time correlation measurements are available. Secondly, important information such as any intermittent feature in the flow structure will be lost owing to long-time averaging. The latter point would certainly hinder the understanding of physical mechanism involved.

More recently, flow visualization methods were employed by the group at Stanford University to study the structure of the turbulent boundary layer especially in the inner wall region. Following the experiments by Hama and his co-workers (1957, 1963) using dye and hydrogen bubbles in water to investigate the boundary layer transition problem, extensive

studies of the turbulent production in the wall region were made using similar techniques. These include the work of Schraub, et al (1964), Kline, et al (1967), Kim, et al (1968, 1971) and more recently Grass (1971). Another visual study by Corino and Brodkey (1969) used a high speed motion picture camera to photograph the trajectories of very small particles suspended in the flow. A rough structure of the flow field especially near the wall can be inferred from these measurements. In the viscous sublayer coherent spatially and temporally dependent motions are observed. These motions lead to the formation of low speed streaks in the region very near the wall, $0 < y^+ < 10$.* The streaks interact with the outer portion of the flow through a process of gradual 'lift-up', then sudden oscillation, bursting and ejection. The break-up of the streaks was found at a distance from the wall in the range $10 < y^+ < 40$. After the burst event, a larger scale high speed parcel of fluid swept into view. The retarded fluid remaining from the ejection process was then accelerated. The high speed fluid often entered almost parallel to the wall or slightly downward toward the wall. This phenomenon was called the sweep event by Corino and Brodkey (1969).

---

* $y^+ \equiv (yU_\tau)/\nu$, where y is the distance from the wall, U_τ is the wall shear velocity and ν is the kinematic viscosity.

Some quantitative measurements were also made from the visual observations. Kim, Kline and Reynolds (1968, 1971) estimated that essentially all the turbulent production (i.e., Reynolds stress) occurred during bursting periods in the zone $0 < y^+ < 90$, while Corino and Brodkey (1969) estimated that 70% of the Reynolds stress was produced during bursting in this region. Thus, the importance of the bursting process for the turbulent energy production and Reynolds stress is apparent.

However, the visual studies are still primarily qualitative in nature. The velocity at a given point can not be measured using the photographs of bubble trajectories downstream of the bubble generating wire unless the bubbles happen to pass through the given point. In the method used by Corino and Brodkey (1969) in which motion picture photographs were made of numerous small suspended particles in the flow, one must ensure that the depth of field is small if accurate measurements of the velocity at a point are to be made.

Hot wire measurements at one or more points in the flow can provide better quantitative information. Willmarth and Lu (1971) used hot wire anemometers in an x array to measure instantaneous values of the Reynolds stress at a point near the wall. With the aid of conditional sampling techniques (an extension of the methods pioneered by Kovasznay, et al (1970)) they found that, when the streamwise fluctuating velocity at the edge of the viscous sublayer was negative and decreasing, the burst

occurred. The burst was found to be very energetic and of short duration. Using an array of hot wires to measure streamwise velocity fluctuations and a different technique of conditional sampling, Blackwelder and Kaplan (1971) showed that, during the burst, there was a substantial streamwise momentum defect followed by an extremely rapid acceleration. These results are in agreement with the visual studies.

The idea that the bursting process is important for the production was supported by these quantitative measurements. In addition, the importance of sweep events was also supported, since Willmarth and Lu (1971) estimated the contribution to Reynolds stress from the sweep events to be about 43.5% while bursting events account for 80.5% with the excessive percentage over 100% due to the negative contributions from other weaker interactions. In an oil channel flow, Wallace et al (1972) used a technique similar to that used by Willmarth and Lu (1971) and found that, for $y^+ > 15$, burst events had more contributions to Reynold stress than sweep events, but the situation was reversed when $y^+ < 15$. This last point is not in agreement with the other reports.

It was postulated by Townsend (1957) and Grant (1958) that an eddy structure consistent with velocity correlation measurements could take the form of jets of low momentum fluid issuing from the

boundary region. This has thus been partially supported by the above mentioned results. Based on the analysis of their various pressure-velocity and velocity-velocity space-time correlation measurements, Willmarth and Tu (1967) proposed a qualitative model for the generation of turbulence near the wall. This model outlined the sequence of events that resulted in the production of intensive pressure and velocity fluctuations by stretching of the vorticity after it was produced by viscous stresses within and near the edge of the viscous sublayer. This model has further been supported by Willmarth and Lu (1971).

By appropriate eigen-function decomposition of streamwise fluctuating velocities in the region near the wall in a turbulent pipe flow, Bakewell and Lumley (1967) proposed a model for the flow field near the wall region very similar to that of Willmarth and Tu (1967). They suggested that, in the wall region, pairs of counter-rotating eddies of elongated streamwise extent occurring at random were responsible for the streaky structure near the wall region.

There were also speculations on the possibility of the interaction between outer and inner flow regions. In their study of the motion and shape of the turbulent bulges in the outer intermittent region, Kovasznay, et al (1970) suggested that the violent bursts near the viscous sublayer might have some bearing on the turbulent bulges in the outer flow.

Rao, et al (1971) estimated the mean time interval between bursts from specially processed turbulent signals obtained from the hot wire measurements of streamwise velocity fluctuations in a turbulent boundary layer. They found that the mean time interval between bursts scaled with outer rather than inner variables and that the probability distribution of the time interval between bursts is log-normal. They found that the mean time interval, $\overline{T}_{CB}$, between bursts can be expressed as

$$\frac{U_\infty \overline{T}_{CB}}{\delta^*} = 32 \quad , \tag{1.1}$$

or,

$$\frac{U_\tau^2/\overline{T}_{CB}}{\nu} = 0.65\ Re_\theta^{0.75} \quad , \tag{1.2}$$

where U_∞ is the free stream velocity, δ^* is the displacement thickness and Re_θ is the Reynolds number based on the momentum thickness. It was also pointed out by Laufer and Badri Narayanan (1971) that the mean frequency of the inner bursts was of the same order as that of the turbulent bulges in the outer intermittent region.

The objective of the present experimental study is to provide more information on the structure of the turbulent boundary layer on a flat plate with no pressure gradient. The present study is an

extension of the work by Willmarth and Lu (1971) and provides further information about the interaction between inner and outer wake-like flow. Some statistical properties are investigated. Attempts were made to measure the mean time interval between bursts and sweeps and their scale as a function of distance from the wall. A tape recorded run from the high Reynolds number investigation of Willmarth and Tu (1967) was used to evaluate the effect of high Reynolds number since their measurement of auto-correlation coefficient yielded a high Reynolds number data point for Rao, et al (1971).

The present study will be divided into three parts. The first part will deal with conditional sampling method. The second part will study some statistical properties of the turbulent velocities. Finally, mean time interval between bursts and sweeps and the scales of them will be discussed.

II. EXPERIMENTAL APPARATUS AND PROCEDURE

A. WIND TUNNEL AND FLOW CONDITIONS

The experiments were carried out on the floor of the 5 by 7 ft low speed wind tunnel of the Department of Aerospace Engineering at The University of Michigan. The test section of the wind tunnel is 25 ft long and is indoors. The settling chamber, fan and steel ducting that recirculate the air are out of doors. The contraction ratio is 15:1.

For the low speed measurements ($U_\infty \approx 20$ ft/sec), the bottom floor of the wind tunnel was fitted with smooth 1/2 in. plywood sheets to make the wall aerodynamically smooth. The measurements were made at the rearmost station of the test section in a thick turbulent boundary layer. The transition to turbulence was developed naturally. No tripping device was introduced. With natural transition, the lowest possible flow speed to achieve a fully developed turbulent boundary layer at the rearmost station of the test section was 20 ft/sec. Most of the measurements were made at this low speed. Only a few were made at a higher free stream speed, $U_\infty \approx 200$ ft/sec.

The mean velocity profiles measured with an impact pressure tube and with a hot wire are displayed in Fig. 1. The flow parameters for the two fully developed turbulent boundary layers are listed in Table I, which also includes the properties of Coles' ideal turbulent

boundary layer (Coles (1954)) for comparison. For the high flow speed measurements, the mean wall shear stress of the turbulent boundary layer used in the present investigation was measured by Willmarth and Wooldridge (1962, 1963) using a Stanton tube. For the low speed measurements, the Clauser plot (Clauser (1956)) was used to measure the mean wall shear stress.

B. HOT WIRE ANEMOMETER PROBES AND EQUIPMENT

Two types of hot wire probes were used in the measurements. For the low flow speed measurements, the wires were soldered to the tips of needles protruding through the wall. These wires, which were used to produce the detecting signals for use in the conditional sampling measurements, were at a distance of 0.037 in. from the wall and had lengths of 0.10 in. and 0.045 in. The wires were made by etching the silver away from the platinum wire, soldering the wire to one needle tip and letting it hang, with a small weight on the end, near the lower needle tip. Then the hanging wire was soldered to the lower needle tip. The surface tension of the molten solder was very effective in pulling the wire onto the needle tip. The wire had a diameter of 1.5×10^{-4} in.

The Reynolds stress was measured using the usual x wire configuration of 2×10^{-4} in. diameter copper plated tungsten wires. Each wire was soldered on needles 0.07 in. apart at angles of $\pm 45^{o}$

to the flow. The distance between the wire centers was 0.04 in. and the wires were 0.035 in. long. The wire resistance was approximately three ohms when cold and the difference in resistance between a pair of wires was less than three percent of the nominal wire resistance.

Each wire of the x wire probe was separately heated at a constant current and a separate channel of amplification and compensation was used for each wire. The wires, amplifier gain and amount of compensation in each channel were carefully matched so that they were identical within a few percent. Each wire was separately calibrated in a steady laminar flow at various velocities. The calibrations differed by less than three percent and obeyed King's law with good accuracy. The wires were operated at an overheating ratio of one-half. The time constant of each wire was approximately 9.5×10^{-4} sec near the wall in the low speed boundary layer and 5×10^{-4} sec in the high speed boundary layer. The above values represent the maximum amount of compensation necessary near the wall. The gain and phase shift of each channel with compensation network operating over the entire frequency band, $1 < f < 20,000$ Hz, were compared using a Lissajous figure displayed on matched x and y channels of a Hewlett Packard Model 130 BR oscilloscope. The gain and phase shift did not differ by more than three percent over the entire frequency band.

The streamwise velocity signal at the edge of the sublayer was produced with a Miller constant temperature hot wire set or occasionally with a DISA Model 55 D05 constant temperature hot wire set. The Miller hot wire set is based on a design by Kovasznay, et al (1963).

C. DATA PROCESSING FACILITIES

The fluctuating signals from the hot wires were recorded on magnetic tape using a three-channel Ampex Model FR-1100 tape recorder. A six-channel Ampex Model 300A tape recorder with the same frequency-modulated electronic system was also used. The frequency response of the tape recorder was DC-20,000 Hz. The magnetic tape was half inch wide. The signals from the hot wires were recorded at a tape speed of 60 in./sec.

It was decided that the large IBM 360/67 digital computer at the Computing Center of The University of Michigan was to be used to reduce the data. First the analog data stored on reels of magnetic tapes had to be converted into digital form. Two different systems were used to do the analog-to-digital (A/D) conversions.

1. Low speed measurements: The tapes containing the analog data were converted to digital form using a Control Data Corporation Model 160A digital computer, a Redcor Model 608 Multiplexer, a Redcor Model 632 A/D converter and a

Control Data Corporation Model 164 digital magnetic tape recorder. The system can operate with one to four-channel input at a rate of 1000 conversions per second for each channel with 12 bit data in 2's complement. This conversion rate was deemed adequate for a 100 Hz signal (i.e., one would have ten data points per cycle). The analog magnetic tape was played back using the FM analog tape recorder at a slower tape speed of 7.5 in./sec, which was a factor of eight slower than that at which the analog data were recorded. Thus, the digitized data were accurate to frequencies of the order of 1000 Hz. This frequency response was broad enough for the signals from the hot wires for the low speed, $U_{\infty} \approx 20$ ft/sec, measurements. The digitized data were stored on 200-BPI 7-track digital magnetic tapes.

2. High speed measurements: Higher frequency response was needed in this case. The data acquisition system in the Cooley Laboratory of The University of Michigan was used. This system operates with two-channel input at a rate of 21,000 conversions per second for each channel. With the analog tape played back at a speed reduced by a factor of eight, the digitized data were accurate to frequencies of 16,800 Hz.

This system was composed of a Raytheon Model DM-120 Multiplexer, a Raytheon Model AD-10A A/D converter, an IBM 729 II Magnetic Tape Unit and a Raytheon Format Generator.

A block diagram for this phase of A/D conversion is shown in Fig. 2. The signals shown in Fig. 2 were obtained from the hot wires as sketched in Fig. 3. AC coupling was used to block out the DC component. The analog filter was a low pass Butterworth filter of third order with half power point at 10 Hz. The filter was constructed on an Applied Dynamics AD-24PB Analog Computer. Since the analog data was played back at a speed of one-eighth the recording speed, the filter half power point was actually at 80 Hz in real time. There were no conditional sampling measurements for the high speed case. Only the signals, u_{1n} and u_{2n} (see Fig. 3) from the x wire probes were converted into digital form. Thus, a filter is not used in this case. The characteristics of the filter can be found in Appendix A.

After A/D conversion, the digitized magnetic tapes were then taken to the Computing Center for processing. The data reduction was done by several simple FORTRAN programs and a few assembly language subroutines.

III. CONDITIONALLY SAMPLED MEASUREMENTS OF REYNOLDS STRESS

A. INTRODUCTION

The method of conditional sampling was first used by Kovasznay, et al (1970)(also Kibens (1968)) in the study of the motion and shape of the turbulent bulges in the outer intermittent region of a turbulent boundary layer. Their concepts of conditional sampling were extended by Willmarth and Lu (1971) in a study of the structure of the Reynolds stress near the wall. The fluctuating streamwise velocity, u_w, at the edge of the sublayer provided a detector signal. They found that, when u_w became low and decreasing, a burst occurred. It was also found that "the filtered signal, u_w, provides better criteria for the identification of samples of uv that contribute to the Reynolds stress when u_w decreases." Thus, it was decided to use the filtered fluctuating streamwise velocity, u_w, at the edge of the sublayer as the detector signal in the present study.

This part studies the spatial distribution of the sampled Reynolds stress using the same method employed by Willmarth and Lu (1971). However, the sampled Reynolds stress is further sorted according to the different events involved. Thus, the spatial distribution and decay of the different events can be investigated from these sampled and sorted Reynolds stresses.

B. METHOD OF MEASUREMENTS

Two methods of conditional sampling were employed in the present measurement. The arrangement of the hot wires for these measurements is sketched in Fig. 3. The filtered fluctuating streamwise velocity, u_w, at the edge of the sublayer was used for detection for both methods. If the u_w signal satisfied certain conditions, then one sample of Reynolds stress was found. A program was required to compare the velocity, u_w, with a desired constant level and the slope of u_w was also determined when the constant level was reached. The sampled uv data were treated in the following two ways:

1. The sampled uv time segments (zero time referred to the time of detection) were stored and averaged to give the average value of the samples. This is the same method used by Willmarth and Lu (1971). The signals, u, v and uv, were obtained using

$$u = (u_{1n} + u_{2n})/\sqrt{2} \quad ,$$

$$v = (u_{1n} - u_{2n})/\sqrt{2} \qquad (3.1)$$

and

$$uv = u \cdot v = (u_{1n}^2 - u_{2n}^2)/2 \quad .$$

Let $\langle uv \rangle$ denote the average value of the samples, then,

$$\langle uv \rangle = \frac{1}{N} \sum_{i=1}^{N} (uv)_i \quad , \tag{3.2}$$

where N is the number of stored samples.

2. The sampled uv time segment was sorted into four parts depending on which quadrant in the u-v plane the uv signal at any instant belongs to. To make the method clearer, define $h_i(\tau)$ as

$$h_i(\tau) \equiv \begin{cases} 1 & \text{for any time } \tau \text{ that the point, } (u, v), \text{ is in the ith quadrant in the u-v plane,} \\ 0 & \text{otherwise} \end{cases} \tag{3.3}$$

for i = 1, 2, 3, 4. Next, define the four segments, $uv_i(\tau)$, as

$$uv_i(\tau) \equiv h_i(\tau) \cdot uv(\tau) \quad . \tag{3.4}$$

Then, the average values of the sampled samples are

$$\langle uv_i \rangle = \frac{1}{N} \sum_{j=1}^{N} [uv_i(\tau)]_j \quad , \tag{3.5}$$

where N is the number of samples. Note that the first method is related to the second method through

$$\langle uv \rangle = \sum_{i=1}^{4} \langle uv_i \rangle \quad . \tag{3.6}$$

$\langle uv_2 \rangle$ comes from the second quadrant in the u-v plane and is associated with the bursting events while $\langle uv_4 \rangle$ comes from fourth quadrant and is associated with the sweeping or inrush events. $\langle uv_1 \rangle$ and $\langle uv_3 \rangle$ are the other interactions.

C. RESULTS OF MEASUREMENTS

Extensive measurements at low speed (20 ft/sec) were made using these methods. Figures 4 through 21 show the results of non-dimensional $\langle uv_i \rangle / \overline{uv}$ as functions of the non-dimensional time, $U_\infty \tau / \delta^*$, with different sampling conditions. The u_w wire was located at y = 0.037 in. from the wall, or, $y^+ = 16.2$. This location was chosen based on the observation by Corino and Brodkey (1969) that the approximate center of the low speed region near the wall was at $y^+ \approx 15$. The sampling conditions for Figs. 4 through 7 were that u_w was equal to the trigger level of $\pm 1 \cdot u_w'$ with $\pm$ slope at the trigger level. The location of the x wire was directly above the point where u_w was measured. The center of the x wire was at y = 0.07 in. or $y^+ = 30.5$. The sampling conditions for Figs. 8 through 21 were either that the slope of u_w was negative at the trigger level of $-1 \cdot u_w'$ or that

the slope of u_w was positive at the trigger level of $+1 \cdot u_w'$. The x wire was at various locations downstream of the u_w wire on the plane normal to the wall and parallel to the mean flow direction, or, $z = 0$.

Figures 24 through 32 show the results of non-dimensional $\langle uv \rangle / \overline{uv}$ as functions of the non-dimensional time delay, $U_\infty \tau / \delta^*$, with x wire at various locations relative to the u_w wire which was at $y^+ = 16.2$. The sampling conditions for these figures (except Fig. 32) were that the trigger level was $-1 \cdot u_w'$ and the slope of u_w was negative at the trigger level. Figure 32 was obtained using the sampling conditions that the trigger level was $+1 \cdot u_w'$ and the slope of u_w was positive at the trigger level.

It is seen from Figs. 4 and 5 that there are peaks in $\langle uv_2 \rangle / \overline{uv}$ plots and valleys in $\langle uv_4 \rangle / \overline{uv}$ plots. At the time when the peak in $\langle uv_2 \rangle$ occurs, there are only small contributions to $\overline{uv}$ from other $\langle uv_i \rangle$. Thus, there is large contribution to $\overline{uv}$ from bursting events when u_w is low. However, the locations of peaks in these two plots are different. For the case $u_w/u_w' = -1$ with the slope of u_w positive (the low speed fluid is being accelerated), the peak occurs before the sampling conditions are detected. For the other case ($u_w/u_w' = -1$ with negative u_w slope, i.e., the fluid speed is low and being decelerated), the peak occurs after the detection. This is in agreement

with the visual studies by Kim, et al (1968, 1971) and Corino and Brodkey (1969) that the flow speed near the wall was low during bursting and the velocity profile was inflectional. This result also clarifies the finding of Willmarth and Lu (1971) who measured $<uv>/\overline{uv}$ only. Thus, these plots show that the burst occurs when the velocity at the edge of the sublayer becomes low and decreasing.

Figures 6 and 7 were obtained with the trigger level set at $+1 \cdot u_w'$ and the slope of u_w being positive and negative respectively. Peaks are seen in the $<uv_4>/\overline{uv}$ plots while there are valleys in $<uv_2>/\overline{uv}$ plots. At the time when the peak in $<uv_4>$ occurs, there are only small contributions to $\overline{uv}$ from the other $<uv_i>$. Also the peak in $<uv_4>/\overline{uv}$ plot occurs earlier when u_w is of negative slope. The peak occurs at the same time as the u_w signal reaches $+1 \cdot u_w'$ with positive slope. Since $<uv_4>$ is associated with sweep events, this finding provides additional information about the acceleration phase as observed in the visual study of Corino and Brodkey (1969). Thus, the sweep occurs when the velocity at the edge of the sublayer becomes high and increasing.

The contributions to $\overline{uv}$ from the sweep events are smaller than from the burst events as can be seen from the magnitude of the peaks in Figs. 5 and 6. The peak observed in the $<uv_2>/\overline{uv}$ plot for the burst is 2.6 times the average Reynolds stress while the peak

observed in the $<uv_4>$ plot associated with sweep events is 1.35 times the mean Reynolds stress. The ratio is 1.92. As the time lag becomes large, or at a time remote from the detection time, each $<uv_i>$ approaches a constant value. As τ becomes large, $<uv_2>/\overline{uv}$ $\rightarrow$ 0.85, $<uv_4>/\overline{uv} \rightarrow$ 0.5 and $<uv_1>/\overline{uv}$ and $<uv_3>/\overline{uv}$ have small negative numbers. The inequality of the two values, $<uv_2>/\overline{uv}$ and $<uv_4>/\overline{uv}$, is striking. The ratio of contributions to $\overline{uv}$ from $<uv_2>$ and from $<uv_4>$ is 1.7 to 1. The contributions to $\overline{uv}$ from the bursts are considerably larger than from the sweeps. This important fact will be further studied later when the statistical properties of the uv signal are surveyed.

Results similar to above can also be observed in Figs. 8 through 21, which were obtained at various stations downstream of the u_w wire. At each station two sets of $<uv_i>$ were obtained using these two different sampling conditions: (1) trigger level at $-1 \cdot u_w'$ and the slope of u_w negative at the trigger level and (2) trigger level at $+1 \cdot u_w'$ and the slope of u_w positive at the trigger level. For case (1) peaks exist in $<uv_2>/\overline{uv}$ plots and valleys in $<uv_4>/\overline{uv}$ plots. At the time when the peak in $<uv_2>$ occurs, there are only smaller contributions to $\overline{uv}$ from the other $<uv_i>$. For case (2) peaks exist in $<uv_4>/\overline{uv}$ plots and valleys in $<uv_2>/\overline{uv}$ plots. At the time when the peak in $<uv_4>$ occurs, there are only smaller contributions to $\overline{uv}$ from the other

$\langle uv_i \rangle$. Regardless of the location of the x wire probe relative to the u_w wire, it is generally observed that the contributions to $\overline{uv}$ from the sweep events (case (2)) are smaller than from the burst events (case (1)).

At a time remote from the detection time for both cases, the product, $\overline{uv}$, will not correlate with the sampling criteria. The quantity, u, measured at the x wire station at this large time lag will be unrelated to the detection criterion. However, to ensure a negative value of the mean Reynolds stress, the product, uv, must occur at a point in the second or fourth quadrants of the u-v plane more often than in the other quadrants. Thus, the absolute values of $\langle uv_2 \rangle$ and $\langle uv_4 \rangle$ will be larger than that of $\langle uv_1 \rangle$ and $\langle uv_3 \rangle$. This was observed in the above measurements for both case (1) and case (2), see Figs. 4 to 21.

Consider now at a time close to the detection time and with the x wire probe not too remote from the detection wire. In case (1) the fluid is being retarded at the detection and measuring stations. The turbulent streamwise velocity, u, measured at the x wire station will most likely be less than zero. The product, uv, will then come from a point in the half plane, $u < 0$, of the u-v plane most of the time. Thus, larger absolute values of $\langle uv_2 \rangle$ and $\langle uv_3 \rangle$, and smaller absolute values of $\langle uv_1 \rangle$ and $\langle uv_4 \rangle$ will be observed than at times remote from the detection time. This argument explains the presence of peaks

and valleys in the plots of the sampled and sorted Reynolds stress for case (1). To ensure a negative value of mean Reynolds stress requires that at times close to the detection time the absolute peak value of $\langle uv_2 \rangle$ be larger than that of $\langle uv_3 \rangle$ as was observed from the measurements, see Figs. 8-21. Similar arguments can be applied to case (2). In this case the fluid is being accelerated. Thus, the product, uv, will most likely come from a point in the half plane, $u > 0$, of the u-v plane. This leads to the presence of peaks and valleys in the plots of the sampled and sorted Reynolds stress. Also, the absolute peak value of $\langle uv_4 \rangle$ will be larger than that of $\langle uv_1 \rangle$. All these facts were observed from the above measurements.

The relation between $\langle uv \rangle$ and $\langle uv_i \rangle$ is given in Eq. (3.6). Figs. 5 and 24(c) were obtained using the sampling conditions (case (1); $-1 \cdot u_w'$ and negative slope of u_w) with the x wire probe at the same location. There is a large peak in the $\langle uv \rangle / \overline{uv}$ plot (Fig. 24(c)), case (1). This figure was obtained by adding the four $\langle uv_i \rangle / \overline{uv}$ in Fig. 5, thus $\langle uv_2 \rangle / \overline{uv}$ is the main contributor. Therefore, large contributions to $\overline{uv}$ occur when u_w is low and decreasing. However, when the other case (case (2)) is considered, the major contributor to $\overline{uv}$ is $\langle uv_4 \rangle / \overline{uv}$ (see Fig. 6), but the contribution is not as large as that of $\langle uv_2 \rangle / \overline{uv}$ obtained with the sampling condition of case (1) above (see Fig. 5). The result for case (2) is that in Fig. 32 there

is no discernable peak in $\langle uv \rangle / \overline{uv}$. Nevertheless, almost the entire contribution to $\langle uv \rangle / \overline{uv}$ for case (2) is caused by the sweep event (note that the other three quadrants contribute nothing to $\langle uv \rangle$ at the time given by case (2)). These results demonstrate the validity of the detection criteria, namely; that bursts or sweeps occur near the wall when the velocity near the wall is low and decreasing or high and increasing respectively.

D. SPATIAL DISTRIBUTION AND DECAY OF SAMPLED REYNOLDS STRESSES $\langle uv \rangle$ AND $\langle uv_i \rangle$

Consider first the burst related events, i.e., the sampling conditions were set at trigger level of $-1 \cdot u_w'$ and negative slope of u_w at the trigger level. The sampled sorted Reynolds stresses, $\langle uv_i \rangle / \overline{uv}$, are shown in Figs. 5, 8, 10, 12, 14, 16, 18 and 20; and more extensive measurements of sampled Reynolds stress $\langle uv \rangle / \overline{uv}$ are shown in Figs. 24 through 32. The magnitude of the peak in $\langle uv_2 \rangle / \overline{uv}$ plot is seen to decrease as one travels outward from the wall (see Figs. 8 and 10, 12 and 14, and 16 and 18). The magnitude of the peak in $\langle uv_2 \rangle / \overline{uv}$ also decreases as one travels downstream at a fixed distance from the wall. This result is shown in Fig. 22, which was obtained at a fixed distance of $y/\delta^* \approx 0.169$ from the wall downstream of the u_w wire ($z = 0$). Also seen in this figure is the shift of time lag for the peak in $\langle uv_2 \rangle / \overline{uv}$ plot. The ordinate of each plot in this figure is

located in proportion to the distance, x, of the x wire probe from the u_w wire. Thus, the dashed line in the figure represents the speed of convection of the burst events. The burst convection speed, U_{CB}, at this distance from the wall was found to be about 8.5 ft/sec, which is somewhat less than the local mean flow velocity ($U_{CB}/U \approx 0.8$) and $U_{CB}/U_\infty \approx 0.425$.

Similar results are also observed in Figs. 24 through 32. The magnitude of the peak in $\langle uv \rangle / \overline{uv}$ plot decreases as one travels outward from the wall and spanwise at a fixed downstream station from the u_w wire. The decrease in magnitude of the peak is also observed as one travels downstream at a fixed distance from the wall. From these more extensive measurements of $\langle uv \rangle / \overline{uv}$, it is apparent that the burst events are confined to a narrow region in the spanwise direction near the wall and downstream from the u_w wire. However, the region of disturbance in the direction normal to the wall increases from a size of $y/\delta^* = 0.506$ at $x/\delta^* = 0$ to a size of $y/\delta^* = 0.912$ at $x/\delta^* = 1.686$ and more as one travels further downstream. There is still some contribution to $\overline{uv}$ even at a station of $x/\delta^* = 2.53$ downstream of the u_w wire.

At a fixed station downstream of the u_w wire ($z = 0$, x fixed, y variable), one can find that, at a certain distance from the wall, the peak in the $\langle uv \rangle / \overline{uv}$ curve will occur at no time delay. This distance

from the wall increases as one moves downstream. The line in the x-y plane on which the peaks occur at no time delay travels outward from the surface at an angle of 16 - 20^{o}.

Consider now the sweep related events, i.e., the sampling conditions were set at trigger level of $+1 \cdot u_w'$ and positive slope of u_w at the trigger level. The sampled sorted Reynolds stresses, $\langle uv_i \rangle / \overline{uv}$, are shown in Figs. 6, 9, 11, 13, 15, 17, 19 and 21. No measurements of sampled Reynolds stress $\langle uv \rangle / \overline{uv}$ were made since there would be no peak in the $\langle uv \rangle / \overline{uv}$ plot as was noted in the last section. The magnitude of the peak in $\langle uv_4 \rangle / \overline{uv}$ behaves similarly as in the case of burst events. It decreases as one travels outward from the wall or downstream at a fixed distance from the wall. A figure similar to Fig. 22 is shown in Fig. 23, which was obtained at the same fixed distance of $y/\delta^* \approx 0.169$ from the wall as Fig. 22. The speed of convection of the sweep events is represented by the dashed line in the figure. The sweep convection speed, U_{CS}, was found to be nearly the same as the burst convection speed. Thus,

$$\frac{U_{CS}}{U_\infty} \approx \frac{U_{CB}}{U_\infty} \approx 0.425$$

and

$$\frac{U_{CB}}{U} \approx \frac{U_{CS}}{U} \approx 0.8 \quad .$$

Rough estimates of the speed of convection of the burst events were also made at various larger distances from the wall. The burst convection speed, U_{CB}, was found to increase with the distance from the wall.

IV. STATISTICAL PROPERTIES OF uv SIGNAL IN A TURBULENT BOUNDARY LAYER

A. INTRODUCTION

The probability density distribution function of the uv signal measured by Willmarth and Lu (1971) near the wall ($y^+ \approx 30$) in a turbulent boundary layer showed an odd shaped distribution with long tails at both ends and a large peak at uv = 0. Similar results were also obtained recently by Gupta and Kaplan (1972) very near the wall ($y^+ \approx 2 \sim 35$) in a turbulent boundary layer. As will be seen later, the odd shaped probability density distribution of the uv signal is not surprising if the joint-normality of u and v signals is assumed. The joint-probability-density distribution function, $P(u_1, u_2)$, is normal if

$$P(u_1, u_2) = \frac{1}{2(1 - R^2)^{1/2}} \cdot \exp\left\{ \frac{-1}{2(1 - R^2)} (u_1^2 - 2R\, u_1 u_2 + u_2^2) \right\} \quad , \quad (4.1)$$

where

$$u_1 = \frac{u}{u'} \quad , \quad u_2 = \frac{v}{v'}$$

and

$$R = \overline{u_1 u_2} = \frac{\overline{uv}}{u'v'} = \text{correlation coefficient} \quad .$$

The revealing measurements of correlation maps, which showed the fractional contributions to $\overline{uv}$ from different events such as burst and sweep, were made by Willmarth and Lu (1971) at a distance of $y^+ \approx 30$ from the wall. More extensive measurements were made in the present study across the whole turbulent boundary layer to study the distribution of the contributions to $\overline{uv}$ from different events. Comparisons were made with the predicted results obtained from the joint-normality assumption of u and v signals.

Some statistical properties of the uv signal were measured in a flat plate turbulent boundary layer with zero pressure gradient. Probability density distributions of the uv signal were also measured across the turbulent boundary layer. Comparisons were made between the measured results and the predicted results obtained from the joint-normality assumption of u and v signals. When computing the predicted results, the measured local correlation coefficient was used for R in $P(u_1, u_2)$. A study of the two dimensional joint normal distribution can be found in Appendix B, which also includes some comparison with other known results.

B. CORRELATION COEFFICIENT MEASUREMENTS

The correlation coefficient, $\overline{uv}/u'v'$, is shown in Fig. 33 as a function of y/δ, where δ is the boundary layer thickness. The correlation coefficient is nearly constant throughout the boundary layer and assumes a mean value of - 0.44. Some previous results are given

here for comparison. Townsend (1951) reported a value of - 0.48 for most of the turbulent boundary layer. Klebanoff (1954) gave a value of - 0.5 while Laufer (1953) showed a value of - 0.45 for $y^+ > 15$ in a pipe flow. Tritton (1967) reported a value of - 0.46. A value of - 0.5 was given by Kim, et al (1968) for $y^+ < 100$. In the greater part of the channel flow the correlation coefficient was - 0.4 to - 0.5 as reported by Reichardt (1938), Eckelmann (1970) and Wallace, et al (1972). Even at a location very close to the wall, or as one approaches the wall, a value of - 0.45 is approached as was shown by Coantic (1965), who used the Navier-Stokes equation with a power series expansion of each turbulent variable in the neighborhood of the wall to give an expression for the correlation coefficient in terms of some measured quantities. Thus, a value of - 0.45 for the correlation coefficient can be assumed for most of the turbulent boundary layer even very close to the wall. This checks with the present measurements.

C. PROBABILITY DENSITY DISTRIBUTIONS

The probability density distributions of u and v are shown in Fig. 34, which were measured at a distance of 0.07 in. from the wall or $y^+ = 30.5$. Gaussian distribution is also shown for reference. The turbulent velocity, u, is seen to follow the normal Gaussian distribution closely. However, the deviation from the normal Gaussian

distribution is observed in the probability density distribution ov v. A rather high value of 0.5 is reached at v = 0 as compared to a value of 0.4 for the normal Gaussian distribution. Also, the curve is slightly skewed to the positive side of v/v'.

The probability density distributions of uv fluctuations were measured at various distance from the wall. The results were found to be very similar to that reported by Willmarth and Lu (1971) at $y^+ \approx 30$. This distribution has the features of long tails at both ends and a sharp peak at uv = 0. A typical distribution is shown in Fig. 35, which was measured at a distance of 0.54 in. from wall, or, $y/\delta^* = 0.912$.

The odd shaped probability density distribution of the uv signal is not surprising if one assumes that the u and v signals are two statistically dependent random variables with correlation coefficient, R. The normal joint-probability-density distribution function is shown in Eq. (4.1). After some transformations and integrations (see Appendix B, Sec. B for details), the probability density distribution of the normalized $uv/\overline{uv}$ signal, denoted by β_{uv}, can be found from Eq. (4.1). The result is

$$\beta_{uv}(uv/\overline{uv}) = \frac{1}{\pi} \frac{|R|}{(1-R^2)^{1/2}} \cdot \exp\left(\frac{R^2 \cdot (uv/\overline{uv})}{1-R^2}\right) \cdot K_o\left(\left|\frac{R \cdot (uv/\overline{uv})}{1-R^2}\right|\right), \tag{4.2}$$

where K_0 is the zeroth order K Bessel function. This distribution is also included in Fig. 35. The agreement is satisfactory. Note that, as uv → 0, the Bessel function approaches infinity. Thus, $\beta_{uv} \to \infty$, as uv → 0. The peak at uv = 0 in the measured probability density distribution is thus expected. From the shape of this distribution, the intermittent feature of uv signal is expected since most of the time the uv signal will stay around uv = 0.

D. CONTRIBUTIONS TO $\overline{uv}$ FROM DIFFERENT EVENTS

1. Introduction and Methods

To better understand the nature of contributions to $\overline{uv}$ from the different events, contributions to $\overline{uv}$ from different regions in the u-v plane were measured. The measurements were made with the x wire at various distances from the wall. The u-v plane was divided into five regions as shown in Fig. 36. In the figure, the cross-thatched region is called the "hole", which is bounded by the curves $|uv|$ = constant. The four quadrants excluding the "hole" are the other four regions. The size of the "hole" is decided by the curves, $|uv|$ = constant. Introduce the parameter, H, and let $|uv| = H \cdot u'v'$, where u' and v' are the local root mean square values of u and v signals. The parameter, H, is called the hole size. With this scheme, large contributors to $\overline{uv}$ from each quadrant can be extracted leaving the smaller fluctuating uv signal in the "hole". The contribution to $\overline{uv}$

from the "hole" would mean the contribution during the quiescent period, while the second quadrant represents the burst events and the fourth quadrant the sweep events.

The contributions to $\overline{uv}$ from the four quadrants were computed from the following equations:

$$\frac{\tilde{uv}_i(H)}{\overline{uv}} = \frac{1}{\overline{uv}} \lim_{T\to\infty} \frac{1}{T} \cdot \int_0^T uv(t) \cdot S_i(t, H)\, dt \quad , \tag{4.3}$$

$$i = 1,\ 2,\ 3,\ 4 \quad ,$$

where the subscript i refers to the ith quadrant and

$$S_i(t, H) \equiv \begin{cases} 1 \quad , & \text{if } |uv(t)| > H \cdot u'v' \text{ and the point } (u, v) \text{ in the } u\text{-}v \text{ plane is in the ith quadrant} \\ 0 \quad , & \text{otherwise} \quad . \end{cases} \tag{4.4}$$

The contribution to $\overline{uv}$ from the "hole" region was obtained from

$$\frac{\tilde{uv}_h(H)}{\overline{uv}} = \frac{1}{\overline{uv}} \lim_{T\to\infty} \frac{1}{T} \cdot \int_0^T uv(t) \cdot S_h(t, H)\, dt \quad , \tag{4.5}$$

where

$$S_h(t, H) = \begin{cases} 1 \quad , & \text{if } |uv(t)| \leq H \cdot u'v' \quad , \\ 0 \quad , & \text{otherwise} \quad . \end{cases}$$

These five contributions, $\widetilde{uv}_i$ and $\widetilde{uv}_h$, are all functions of the hole size, H, and

$$\sum_{i=1}^{4} \frac{\widetilde{uv}_i(H)}{\overline{uv}} + \frac{\widetilde{uv}_h(H)}{\overline{uv}} = 1 \quad . \tag{4.6}$$

2. Results of Measurements

The results of the measurements are shown in Figs. 37a-37g and Fig. 38. There was only one measurement for the case of high speed flow which was made at a distance of $y^+ = 265$ from the wall. This result is shown in Fig. 38. As for the low speed measurements, the results were obtained with x wire at various distance from the wall. The results were very similar for both high and low Reynolds number measurement and regardless of the x wire probe location in the turbulent boundary layer. In these figures, curves representing the fraction of total time that uv signal spent in the "hole" region were also included. As can be seen, for a large portion of the time, $|uv|$ is very small. This is expected from the probability density distribution of the uv signal. This can also be seen from a trace of the uv signal that, for a large fraction of time, the uv signal is approximately zero. This fact is also seen from the contribution curve related to the "hole" that the contribution remains small in spite of large time of occupancy. As a matter of fact, these two curves, i.e., the fraction of the total

time in "hole" and the contribution to $\overline{uv}$ from the "hole" region, can be derived from the assumption of joint-normality of u and v signals (see Appendix B, Sec. C). The predicted curves are also included in Figs. 37a through 37g and in Fig. 38 for comparison. The agreements between measurements and predictions are very good except at the point very close to the wall and in the outer intermittent region.

The assumption of joint-normality of u and v signals implies that the contribution to $\overline{uv}$ from the second quadrant, $\widetilde{uv}_2$, should equal that from the fourth quadrant, $\widetilde{uv}_4$. Similarly, $\widetilde{uv}_1 = \widetilde{uv}_3$. The predicted curves for them are also shown on the figures. The deviation from the joint-normality is apparent regardless of the flow speed and the location in the turbulent boundary layer. As can be seen, the largest contribution comes from the second quadrant which is burst related. The second largest contribution is $\widetilde{uv}_4$ and is sweep related. The contributions from $\widetilde{uv}_1$ and $\widetilde{uv}_3$ are negative and relatively small. Especially, when the hole size, H, becomes large, there are only two contributors. One is $\widetilde{uv}_2$ and the other one comes from the "hole" region. Thus the importance of the burst events in the turbulent boundary layer is obvious. At the hole size of H = 4.5, which amounts to $|uv| > 10 \cdot |\overline{uv}|$, there is still a 15 to 30% contribution to $\overline{uv}$ from the second quadrant, i.e., $\widetilde{uv}_2/\overline{uv} \approx 0.15$ to 0.30. At this level there are almost no contributions from the other quadrants.

E. SOME RESULTS FOR THE BURST AND SWEEP EVENTS

Some results will be discussed here regarding the contributions to $\overline{uv}$ from bursts and sweeps in general. Figure 39 shows plots of $\tilde{uv}_2/u'v'$, $\tilde{uv}_4/u'v'$, their average values and the predicted average values with H = 0. It is understood that the hole size is set at zero (H = 0) in the study of this section, since bursts and sweeps in general are concerned here. Both $\tilde{uv}_2/\overline{uv}$ and $\tilde{uv}_4/\overline{uv}$ are nearly constant in the boundary layer except very close to the wall and near the edge of boundary layer. It is found that $\tilde{uv}_2/u'v' \approx -0.34$ and $\tilde{uv}_4/u'v' \approx -0.24$, or, $\tilde{uv}_2/\overline{uv} \approx 0.77$ and $\tilde{uv}_4/\overline{uv} \approx 0.55$. Thus, bursting events account for 77% of the local Reynolds stress and the sweep events have 55% to their account. This leaves - 32% of local Reynolds stress to the other two negative contributors. As can be seen from Fig. 39, the mean values of $\tilde{uv}_2/u'v'$ and $\tilde{uv}_4/u'v'$ predicted from the assumption of the joint-normality of u and v are in satisfactory agreement with the measured values. It should be pointed out here that, even though the u and v signals are not jointly normal as noted in this study and the v signal is not Gaussian distributed as noted before (Sec.IV-C), the assumption of the joint-normality of u and v leads to a reasonably good prediction such as the fraction of time spent in hole, the fractional contribution to $\overline{uv}$ from hole, the probability density distribution of the uv signal and the mean value, $(\tilde{uv}_2 + \tilde{uv}_4)/(2\,u'v')$.

The ratio of the contribution to $\overline{uv}$ from the burst events and that from the sweep events is plotted in Fig. 40 as a function of y/δ. There is a sharp rise near the wall while for most of the boundary layer the ratio is nearly constant with a value of 1.35. The single high speed measurement gave a value of 1.25, which was measured at $y/\delta = 0.014$ or $y^+ = 265$. The results are replotted in Fig. 41 as a function of y^+. In this figure the results obtained by Wallace, et al (1972) at a much lower Reynolds number in a channel flow are included. The disagreement is apparent especially near the wall. The reason for this disagreement might be due to the Reynolds number effect. But, from the present measurements, the results seem to scale with the wall region variables with the two flow conditions considered ($Re_\theta = 4,230$ and $38,000$). Although there is only one measurement for the high Reynolds number flow, it is conjectured that the Reynolds number similarity may hold. Further studies on the case of high Reynolds number flow are needed.

The closest distance to the wall obtainable for the present measurement was $y^+ = 30.5$ for the case of $Re_\theta = 4,230$ because of the size of the x wire probe. The ratio, $\tilde{uv}_2/\tilde{uv}_4$, is 1.8 at this distance from the wall. In the section describing the conditional sampling measurements (Sec. III-B), it is recalled that with x wire probe at this distance from the wall the ratio of the contributions to $\overline{uv}$ from $\langle uv_2 \rangle$ and from $\langle uv_4 \rangle$ at large time lag was found to be 1.7:1 (see Figs. 4 through 7).

Thus, this provides another check since at very large time lag from the detection (the time when sampling conditions are detected) the ratio, $(\langle uv_2\rangle/\langle uv_4\rangle)_{\tau\to\infty}$, should be the same as $(\tilde{uv}_2/\tilde{uv}_4)_{H=0}$ if the x wire probes are at the same distance from the wall.

V. MEAN PERIODS AND SCALES OF BURSTS AND SWEEPS

A. INTRODUCTION

In the visual studies by Runstadler, et al. (1963), Schraub and Kline (1965) and Kim, et al. (1968, 1971), the mean time intervals, $\overline{T}_{CB'}$ between bursts were measured by visual counting of the violent motion of ejection near the wall in a turbulent boundary layer. Kim, et al. found that the mean time interval, $\overline{T}_{CB'}$ was nearly the same as the time lag required to obtain the second mild maximum in the curve of the auto-correlation coefficient of the fluctuating streamwise velocity, u. By properly processing a hot wire signal in a turbulent boundary layer in the air, Rao, et al. (1969, 1971) were able to measure the mean time interval between bursts. They showed, from the data over wide range of Reynolds number, that the mean burst period, $\overline{T}_{CB'}$ scaled with outer rather than inner flow variables (see Eq. (1.1)). Among the data, there was only one measurement for the high Reynolds number flow (Re_θ = 38,000) by Tu and Willmarth (1966). Rao, et al. used their measurement to obtain the mean burst period.

In the process of counting the number of bursts a definitive identification of bursts is required. This represents difficulties both in visual studies and in hot wire measurements. In the visual studies bursts of varying magnitude were observed embedded in a background of other turbulent fluctuations. When an event is not extremely violent

and coherent, it is up to the observer to decide whether it is a burst or not. More difficulties are present in the measurement of the mean burst period from a trace of a single hot wire signal because only the velocity at one point is known. In the hot wire measurements by Rao, et al. (1969, 1971), the signal, u, was differentiated and filtered to make "bursts" stand out more clearly. Firstly, as pointed out by Kim, et al. (1971), it remains to be checked whether this process will show the same phenomenon as the "oscillatory motion" as observed in the second stage of the bursting process observed by Kim, et al. (1968, 1971). Secondly, even if this technique does make the burst stand out, counting the number of bursts using human eyes is somewhat arbitrary since the "bursts" are not too well organized or clearly identifiable in the traces of their processed u signal (see Fig. 1 of the paper by Rao, et al. (1971)). However, Rao, et al. arrived at a characteristic time, called $\overline{T}_m$, for the burst period. The procedures they followed are:

(a) Hot wire signals filtered with narrow pass band were projected onto graph paper.

(b) After blocking out central strips of various width (amplitude discriminator setting), bursts were presumed to occur only if the time interval after the previous burst was greater than twice the period of the center frequency of the pass band of step (a).

(c) Mean burst rates were plotted against the amplitude discriminator settings.

(d) An optimum range of the discriminator settings over which the precise value of the setting was immaterial was found. The burst rate found in this range was the characteristic time, $\overline{T}_m$.

As pointed out by Rao, et al. (1971) the optimum range of discriminator levels was not as wide as one might wish. In procedure (b), "the periods of activity, i.e., stretches of signal beyond this strip, were counted as separate bursts only if the time interval between them was greater than twice the basic period corresponding to the mid frequency in the selected pass band". This leads one to speculate what the situation will be if, instead of "twice the basic period", some other factor times the basic period is used. The burst rate will then be a function of this factor. Then, the optimum range obtained in procedure (d) may shift to another discriminator setting depending on the value of the factor. Thus, the characteristic time, $\overline{T}_m$, will not be the same.

In the present study some characteristic times related to bursts and sweeps and their durations are attempted. Similar difficulties, mainly definitive identification of bursts and sweeps, will be encountered.

Extensive measurements were made for the low speed flow across the turbulent boundary layer. A single high speed measurement was also made to study the Reynolds number effect on the burst and sweep rates.

B. MEASUREMENTS

As is evident from the measurements of sampled sorted Reynolds stress, during the occurrence of bursts, there is large contribution to $\overline{uv}$. A large peak in uv signal was observed (see the measurements of Willmarth and Lu (1971)) and came from the second quadrant of the u-v plane. Difficulties are encountered when a definitive identification of bursts is desired. Assume that, if the uv signal reaches a certain specified level or larger in the second quadrant, a burst occurs. By counting the number of times the above conditions are detected in a given time interval, the mean time interval between bursts, called $\overline{T}_B$, can be found. Of course, the mean time interval between bursts so measured will depend on the setting of the specified level that the uv signal must reach. Thus, the burst rate certainly is a function of the hole size, H. However, after a close examination of the plots of the contributions to $\overline{uv}$ from different events (Figs. 37a through 37g and Fig. 38), a unique feature is seen that, as the hole size becomes large, the contributions to $\overline{uv}$ from quadrant one, three and four vanish more rapidly than contributions from the second quadrant. It is observed

that, when H reaches a value of 4 to 4.5, only $\tilde{uv}_2/\overline{uv}$ is not zero. This contribution must have come from the large spikes in the uv signal related to the bursts. For a hole size of H = 4 ~ 4.5, |uv| is about ten times the absolute value of the local mean Reynolds stress. These bursts certainly are very violent. From this unique feature, one can obtain a characteristic time interval between large bursts by setting the specified level at H = 4 to 4.5.

A similar scheme was used to measure the mean time interval between sweeps, denoted by $\overline{T}_S$. A sweep is assumed to occur if the uv signal in the fourth quadrant reaches a specified value or larger. Thus, as in the case of bursts, the mean time interval, $\overline{T}_S$, between sweeps is also a function of the hole size, H. A characteristic time interval between sweeps can also be found using another unique feature in the plots of the contributions to $\overline{uv}$ from different events. At a hole size of $H \simeq 2.25 \sim 2.75$, $\tilde{uv}_1/\overline{uv}$ and $\tilde{uv}_3/\overline{uv}$ vanish. Thus, the characteristic time interval between large sweeps is obtained by setting the level at $H \simeq 2.25 \sim 2.75$. From the study of the statistical properties of the uv signal, the contribution to $\overline{uv}$ from the second quadrant is found to be larger than that from the fourth quadrant. Thus, the sweeps are not as violent as the bursts. This was also observed in the measurements of sampled sorted Reynolds stress. Thus, a lower specified level for sweeps may yield a characteristic time interval more representative of sweep events.

The time scale of the burst was obtained by measuring the mean time during which the uv signal exceeded the specified level. In other words, the time scale, $\overline{\Delta T}_B$, can be expressed as

$$\overline{\Delta T}_B(H) = \lim_{T\to\infty} \frac{1}{T} \int_0^T S_2(t, H)\, dt \quad , \tag{5.1}$$

where $S_2(t, H)$ is the function shown in Eq. (4.4). Similar expression can be written for the scale of sweep, $\overline{\Delta T}_S$, as

$$\overline{\Delta T}_S(H) = \lim_{T\to\infty} \frac{1}{T} \int_0^T S_4(t, H)\, dt \quad , \tag{5.2}$$

where $S_4(t, H)$ is the function in Eq. (4.4).

The counting of the number of bursts and sweeps and the computations of $\overline{\Delta T}_B$ and $\overline{\Delta T}_S$ were accomplished at the same time that the contributions to $\overline{uv}$ from different events were computed.

C. RESULTS

The non-dimensional mean time interval, $U_\infty \overline{T}_B/\delta^*$, between bursts is shown in Fig. 42 as a function of the hole size, H, with the distance from the wall, y/δ, as a parameter. This was obtained from the low speed ($U_\infty \approx 20$ ft/sec) measurements. As is seen, the mean time interval between bursts is nearly independent of the location in the turbulent boundary layer. And so is the characteristic time interval between bursts as shown in Fig. 43, which was obtained from Fig. 42

by setting a level of $H \approx 4 \sim 4.5$. A value of $U_\infty \overline{T}_{CB}/\delta^* \approx 32$ is found for most of the boundary layer. Measurements from the single high flow speed run are also included in Fig. 43. It is believed that this characteristic time interval, called $\overline{T}_{CB}$, is related to that of Rao, et al. (1971). For the two flow conditions with $Re_\theta = 4,230$ and $38,000$, $U_\infty \overline{T}_{CB}/\delta^* \approx 32$. This confirms the scaling of the mean period between bursts with outer flow variables as reported by Rao, et al. (1971).

The mean time interval between sweeps in non-dimensional form, $U_\infty \overline{T}_S/\delta^*$, is shown in Fig. 44 as a function of the hole size, H, with y/δ as a parameter. The data are more scattered. However, the dependency of $U_\infty \overline{T}_S/\delta^*$ on the distance from the wall is not too large. The characteristic time interval, called $\overline{T}_{CS}$, obtained from Fig. 44 by setting a level of $H \approx 2.25 \sim 2.75$ is shown in Fig. 45 as a function of the distance from the wall, y/δ. A value of about 30 for $U_\infty \overline{T}_{CS}/\delta^*$ is found in most of the boundary layer. Thus, $U_\infty \overline{T}_{CB}/\delta^*$ and $U_\infty \overline{T}_{CS}/\delta^*$ are essentially equal. Same result was obtained for the high speed flow measurement. Thus, $\overline{T}_{CS}$ might also scale with the outer flow variables as $\overline{T}_{CB}$. Further studies on the sweep events are needed.

The fact that $\overline{T}_{CB}$ is nearly the same as $\overline{T}_{CS}$ can also be justified from the measurements of $\overline{T}_m$ by Rao, et al. (1971) (see also Sec. V-A). The mean time interval, $\overline{T}_m$, is found to be about one half of $\overline{T}_{CB}$, i.e.,

$\overline{T}_{CB}/\overline{T}_m \approx 2$ for $500 < Re_\theta < 1 \times 10^4$. It is possible that $\overline{T}_m$, determined by Rao, et al. (1971), may indicate the mean time interval between a burst and a sweep (mean time interval between violent events regardless of whether they are bursts or sweeps). Furthermore, Kim, et al. (1968, 1971) found that the mean time interval between visually observed bursts was nearly the same as the time lag required to obtain the second mild maximum in the curve of the auto-correlation coefficient of the fluctuating streamwise velocity, u. If a sweep event occurs after a burst event the average value of the time interval between bursts and between sweeps should be the same.

As noted before, there are difficulties in the process of counting the number of bursts and sweeps. It is suggested that, in order to obtain the characteristic time intervals that are representative of the different events, one should try to find these time intervals from the measurements of the auto-correlation coefficient of the signals sorted for the different events. For example, one can first sort the u signal into two parts: one positive sign and the other negative sign. Then the curves of the auto-correlation coefficient can be found from these two sorted signals. One then defines the characteristic time intervals to be the time lags required to obtain the second mild maximum in these two curves. One of these time intervals is burst related (the one that is obtained from the sorted signal with negative sign). The other is then sweep related.

The time scale of the burst in non-dimensional form, $U_\infty \overline{\Delta T}_B/\delta^*$, is shown in Fig. 46 as a function of hole size for the low speed measurements. The time scale is seen to increase as one moves away from the wall. The characteristic time scale, $\overline{\Delta T}_{CB}$, for bursts is shown in Fig. 47, which was obtained from Fig. 46 by setting the level of $H \approx 4 \sim 4.5$. The single measurement for high Reynolds number flow gave a value of 0.21, which is somewhat small compared to that for low speed measurements. The time scale of the sweep is shown in Fig. 48. The general trend that the scale increases as the distance from the wall increases is also observed. Figure 49 shows the characteristic time scale, $\overline{\Delta T}_{CS}$, for sweeps. This figure was obtained by setting a level of $H \approx 2.25 \sim 2.75$. A lower value of 0.16 for $U_\infty \overline{\Delta T}_{CS}/\delta^*$ is obtained for the high speed measurement. The variation of the time scale, $\overline{\Delta T}_{CB}$, is very small within the range of hole size considered. It is found to be less than one percent. The variation of the time scale, $\overline{\Delta T}_{CS}$ is larger. Within the range of hole size considered ($H \approx 2.25 \sim 2.75$), the variation is about 10% at most.

VI. DISCUSSIONS OF MEASUREMENTS

The ejection of low momentum fluid from the wall is a dominant feature of the structure of the turbulent boundary layer. The importance of burst events is obvious from the study of the ratio, $\tilde{uv}_2/\tilde{uv}_4$, at H = 0. Near the wall, the ratio is the highest with a value of 1.8, while in outer region a smaller value of 1.35 is obtained (see Fig. 40). Thus the ejection is more violent near the wall as was better illustrated by the measurements of Willmarth and Lu (1971) in which very large individual contributions to $\overline{uv}$ were identified near the wall. It is likely that the ejection can reach a station remote from the wall in a turbulent boundary layer. This is in agreement with the results of Grass (1971).

Although definitive identification of bursts and sweeps is difficult, some characteristic mean time intervals between bursts and sweeps have been found. The scaling of the mean time interval between bursts, $\overline{T}_{CB}$, with the outer flow variables (see Eq. (1.1)) is confirmed. As for the sweep events, the mean sweep rates were obtained for two flow conditions with Reynolds numbers, Re_θ, of 4,230 and 38,000. The mean time interval between sweeps is roughly the same as that between bursts. It is too early to draw any conclusion about the scaling of the sweep rate, although both cases yielded roughly the same value of about

30 for $U_\infty \overline{T}_{CS}/\delta^*$ using the methods of Section V. However, if the measurements of $\overline{T}_m$ by Rao, et al. (1971) are an indication of the mean time interval between a burst and a sweep, it is conjectured that the mean sweep period may also scale with the outer flow parameters and $U_\infty \overline{T}_{CS}/\delta^* \approx U_\infty \overline{T}_{CB}/\delta^* \approx 32$.

The contributions to $\overline{uv}$ from the burst events is about 77%, which is in essential agreement with the measurements by others (e.g., Kim, et al. (1968), Corino and Brodkey (1969) and Grass (1971), etc.) However, Wallace, et al. (1971), reported a larger contribution to $\overline{uv}$ from the sweep events for $y^+ < 15$ in a channel flow. The reason for this discrepancy is not clear. It might be due to the nature of flow involved.

Whether the sweep events follow the burst events is not clear. However, from the facts that the sweep events contribute to $\overline{uv}$ (about 55%) less than the burst events and that the mean time interval between bursts is nearly the same as that between sweeps, sweep events may follow the burst as was observed by Corino and Brodkey (1969).

It has been speculated that the bursts may have some bearing on the turbulent "bulges" in the outer intermittent flow region. See, e.g., Kovasznay, et al. (1970) and Laufer and Badri Narayanan (1971). Present measurements of the mean time interval between bursts and the time scale seem to confirm the idea. The mean burst period,

$\overline{T}_{CB}$, is constant for most of the boundary layer while the time scale, $\overline{\Delta T}_{CB}$, increases with increasing distance from the wall.

From the scaling of the burst rate with outer flow variables and the scaling of $\tilde{uv}_2/\tilde{uv}_4)_{H=0}$ (Fig. 41) with inner flow variables, it seems that the occurrence of bursts is determined by the outer flow conditions while the ensuing events after the burst sets in are related to the wall region variables.

The dominant feature of ejection in a turbulent boundary layer can be seen in the plots of contributions to $\overline{uv}$ from different events (Figs. 37a-37g and 38). Besides this, other statistical characteristics of the uv signal are fairly predictable from the assumption of joint-normality for u and v signals except very close to the wall ($90 < y^+$) and in the outer intermittent region. These facts lead one to speculate that the turbulence in the inner part of the turbulent boundary layer may be considered as a 'universal motion' plus an 'irrelevant motion' as suggested by Townsend (1957, 1961). The 'universal motion' may be considered as random occurrence (both temporally and spatially) of bursts, which is controlled by the outer flow, plus the ensuing more diffuse return flow, which may be related to the sweep events. The 'irrelevant motion' may be considered as the accumulation of the remnants of what has happened upstream. The contribution to $\overline{uv}$ from the latter would be small.

From the measurements of sampled Reynolds stress, $\langle uv \rangle$, using the sampling criteria that the velocity, u_w, at the edge of the viscous sublayer is low and decreasing, it is found that the line in the x-y plane on which the peak values of $\langle uv \rangle$ occur at no time delay travels outward from the wall at an angle of $16\text{-}20^{o}$. This may be thought of as, when a burst occurs, a certain pattern such as the hair-pin-vorticity model proposed by Willmarth and Tu (1967) is being convected and swept by the measuring stations. As a matter of fact, this pattern may also be used to describe the time sequence of the instantaneous velocity profiles near the wall as observed by Kim, et al. (1968) (see Fig. 4.13 in their report). Since the sampled Reynolds stress, $\langle uv \rangle$, was obtained with a sampling procedure that is favorable to the occurrence of bursts, it is likely that the model of Willmarth and Tu (1967) may describe the flow structure near the wall and may well be a part of 'universal motion' as mentioned above.

VII. SUMMARY AND CONCLUSIONS

A. SUMMARY

The structure of Reynolds stress in a turbulent boundary layer on a smooth wall with zero pressure gradient has been investigated. The method of conditional sampling has been employed. Some statistical characteristics of the uv signal were measured. An attempt was made to measure the mean time interval and time scale of bursts and sweeps.

1. Conditional Sampling Method

Using the hot-wire signal at the edge of the sublayer as a detector, the averages of sampled Reynolds stress, $\langle uv \rangle$ and $\langle uv_i \rangle$, were measured with the x wire probes at various locations. The striking feature is the appearance of peaks and valleys in the sampled sorted Reynolds stress. As the velocity at the edge of the viscous sublayer becomes low and decreasing, a burst occurs. On the other hand, when the flow velocity at the edge of the sublayer becomes large and increasing, the sweep event occurs. The burst events make greater contributions to $\overline{uv}$ than the sweep events.

The size and the decay of the sampled Reynolds stress, $\langle uv \rangle$, and the sampled sorted Reynolds stress, $\langle uv_2 \rangle$, are also measured using sampling criteria favorable to the occurrence of bursts (the

fluctuating streamwise velocity, u_w, at the edge of the viscous sublayer is low and decreasing). The region of disturbance is relatively narrow in spanwise direction and grows as it is convected downstream. The convection speed of the bursts is somewhat lower than the local mean flow velocity ($U_{CB}/U \approx 0.8$) at a distance of $y/\delta^* \approx 0.169$ from the wall. The burst convection speed is found to increase with the distance from the wall.

The size and the decay of the sampled sorted Reynolds stress, $<uv_4>$, for sweep events are measured using sampling criteria favorable to the occurrence of sweeps (u_w is high and increasing). The region of disturbance grows as it is convected downstream. The convection speed of the sweeps at a distance of $y/\delta^* \approx 0.169$ from the is nearly the same as that of the bursts; and $U_{CB}/U_\infty \approx U_{CS}/U_\infty \approx 0.425$ and $U_{CB}/U \approx U_{CS}/U \approx 0.8$.

2. Statistical Characteristics of the uv Signal

Many statistical properties of the uv signal were measured. When the product, uv, is considered the assumption of joint-normality for u and v predicts reasonably well the measured results. However, if the details of u and v signals are considered, deviations from the joint-normality are found. The contribution to $\overline{uv}$ from bursts is larger than that from sweeps. Near the wall, the bursts are much more violent. The ratio, $(\tilde{uv}_2/\tilde{uv}_4)_{H=0}$, was found to scale with the wall

region variables (see Fig. 41). Thus, the importance of the bursting events in turbulence generation is also confirmed in this part of the study.

The plots of contributions to $\overline{uv}$ from different events (Figs. 37a-37b and 38) show a definite feature that the bursts are the largest contributor throughout the boundary layer. The intermittent feature of the uv signal is also apparent, since most of the time the signal is spent at small hole size. If the internal intermittency is defined to be the fraction of time spent during the violent ejection period, the value was found to be 1 ~ 2%. This value is obtained from the curves of fraction of total time spent in hole when the hole size is 4 ~ 4.5.

3. Burst and Sweep Measurements

From the plots of contributions to $\overline{uv}$ from different events, definite characteristic times are obtained for both burst and sweep events. These characteristic times are believed to be the mean time intervals between bursts and sweeps. Both mean time intervals are found to be sensibly constant for most of the turbulent boundary layer. The scaling of the time interval between bursts with outer flow variables is confirmed. The characteristic time scale of the bursts increases with the distance from the wall. The mean time interval between sweeps is roughly the same as that between bursts. And the scale also increases with the distance from the wall.

B. CONCLUSIONS

The largest contributors of local Reynolds stress are the burst events, which account for 77% of $\overline{uv}$, while the sweep events account for 55%. The excessive percentage over 100% is due to the other negative contributors.

The scaling of the burst rate with outer flow variables is checked. The measurements of sweep rates imply the same scaling, since both rates are nearly equal.

The size of the burst is narrow, but it is growing as the disturbance is convected downstream. The convection speed of the burst events is somewhat lower than the local speed of the mean flow at the distance of $y/\delta^* \approx 0.169$ from the wall. As for the sweeps, the size is believed to be narrow. The convection speed is the same as that of the burst events and $U_{CB}/U_\infty \approx U_{CS}/U_\infty \approx 0.425$, and $U_{CB}/U \approx U_{CS}/U \approx 0.8$.

The model proposed by Willmarth and Tu (1967) for the flow structure near the wall is pertinent to the description of ejection process, which is due to the stretching of the vorticities produced by viscous stresses within and near the edge of the viscous sublayer and is responsible for the generation of turbulence.

APPENDIX A

THIRD ORDER LOW PASS BUTTERWORTH FILTER

It was part of the sampling procedure that the hot wire signal, u_w, obtained from the edge of the viscous sublayer, was filtered through a low pass filter. The third order Butterworth filter was used. The characteristics of this filter can be obtained from the governing differential equation of the filter,

$$\frac{1}{\omega_o^3}\dddot{e}_o + \frac{2}{\omega_o^2}\ddot{e}_o + \frac{2}{\omega_o}\dot{e}_o + e_o = e_i \quad , \tag{A.1}$$

where e_i is the input signal to the filter, e_o is the output signal and $\omega_o = 1/2\pi f_o$, where f_o is called half power point frequency. Assume that e_i and e_o are of the forms

$$e_i = A_i e^{i\omega t}$$

and

$$e_o = A_o e^{i\omega t}$$

Then, from Eq. (A1), one obtains

$$\frac{A_o}{A_i} = \frac{1}{\sqrt{1+\xi^6}} \cdot e^{i\phi} \quad \text{and} \quad \left|\frac{A_o}{A_i}\right| = \frac{1}{\sqrt{1+\xi^6}} \quad , \tag{A.2}$$

where $\xi = \omega/\omega_o = f/f_o$ and $\phi = \tan^{-1}\left[(\xi^3 - 2\xi)/(1 - 2\xi^2)\right]$. ϕ is called the phase shift.

The time lag for the signal after passing through the filter is given by

$$\Delta T = \frac{\phi}{2\pi f} = \frac{1}{2\pi f_o} \cdot \frac{1}{\xi} \tan^{-1}\left(\frac{\xi^3 - 2\xi}{1 - 2\xi^2}\right) \quad . \qquad \text{(A.3)}$$

As $\xi \to 0$, $\Delta T \to 1/\pi f_o = 0.318/f_o$.

The gain of the filter is shown in Fig. A1 as a function of the non-dimensional frequency, $\xi = f/f_o$. The non-dimensional time lag, $\Delta T \cdot f_o$, is shown in Fig. A2. It is seen that the time lag is nearly constant for the range of frequencies of interest, $0 < \xi < 1$. Thus, a signal passing through this filter is delayed by an amount of time of about $0.34/f_o$ sec., where f_o is the half power point in unit of Hz.

APPENDIX B

A STUDY OF THE TWO DIMENSIONAL JOINT NORMAL DISTRIBUTION

A. HIGHER ORDER MOMENTS, $\overline{(u_1 u_2)^n}$

Consider two statistically dependent random variables, u and v, with the correlation coefficient, $R \equiv \overline{uv}/u'v'$, where u' and v' are the root mean square values of u and v respectively. Let $P(u_1, u_2)$ be the joint-probability-density distribution function of u_1 and u_2. Let $u_1 = u/u'$ and $u_2 = v/v'$. Then, $P(u_1, u_2)$ is normal if

$$P(u_1, u_2) = \frac{1}{2} \frac{1}{(1 - R^2)^{1/2}} \cdot \exp\left\{ - \frac{1}{2(1 - R^2)} (u_1^2 - 2R\, u_1 u_2 + u_2^2) \right\} , \tag{B.1}$$

which has the following features:

(1) The marginal distributions of u_1 and u_2 are normal Gaussian distributions.

(2) All uneven moments are zero:

$$\overline{u_1^m u_2^n} = \int_{-\infty}^{+\infty} P(u_1, u_2)\, u_1^m u_2^n \, du_1 \, du_2 = 0 \tag{B.2}$$

for m and n integers and m + n = uneven. (See Hinze (1959).)

For any integer n, $\overline{(u_1 u_2)^n}$ will not vanish. The results are as follows:

$$\overline{u_1 u_2} = R \quad , \quad \overline{(u_1 u_2)^2} = 2R^2 + 1 \quad ,$$

$$\overline{(u_1 u_2)^3} = 6R^3 + 9R \quad , \quad \overline{(u_1 u_2)^4} = 24R^4 + 72R^2 + 9 \quad ,$$

. . .

$$\overline{(u_1 u_2)^n} = (1/2)^n \, 1 \cdot 3 \cdot 5 \ldots (2n - 1) \left[(1 + R)^n + (1 - R)^n \right] \qquad \text{(B. 3)}$$

$$+ (1/2)^n \sum_{i=1}^{n-1} (-1)^i \, {}_nC_i \; 1 \cdot 3 \cdot 5 \ldots (2i - 1) \cdot 1 \cdot 3 \cdot 5 \ldots$$

$$\cdot [2(n - i) - 1] \; (1 - R)^i \, (1 + R)^{n-i} \quad ,$$

where

$${}_nC_i = \frac{(n - i + 1) \cdot (n - i + 2) \ldots n}{1 \cdot 2 \cdot \ldots (n - i)} \quad .$$

Some comparisons can be made with the experimental measurements. Recently, $\overline{(uv)^3}/[\overline{(uv)^2}]^{3/2}$ and $\overline{(uv)^4}/[\overline{(uv)^2}]^2$ were measured by Gupta and Kaplan (1972) in a turbulent boundary layer with two different flow speeds. Both quantities remain constant in the boundary layer except very close to the wall and in the wake region. They found that $\overline{(uv)^3}/[\overline{(uv)^2}]^{3/2}$ had values between - 1 and - 2 while $\overline{(uv)^4}/[\overline{(uv)^2}]^2$ had a value of approximately 10. From Eq. (B. 3), one obtains

$$\frac{\overline{(uv)^3}}{[\overline{(uv)^2}]^{3/2}} = \frac{6R^3 + 9R}{[(2R^2 + 1)]^{3/2}} \simeq -3.2$$

and

$$\frac{\overline{(uv)^4}}{[\overline{(uv)^2}]^2} = \frac{24R^4 + 72R^2 + 3}{(2R^2 + 1)^2} \simeq 12.4 \quad \text{for} \quad R = -0.44 \ .$$

These results are comparable with the experimental measurements.

B. PROBABILITY DENSITY DISTRIBUTION, P_{uv}

In order to find the probability density distribution function for the uv signal, some transformations and integrations are needed. Consider the following transformation

$$\alpha = 2u_1u_2 \quad , \quad \beta = u_1^2 - u_2^2 \ . \tag{B.4}$$

This transformation would transform the half plane, $u_1 > 0$, into the whole α - β plane. This is also true for the other half plane, $u_1 < 0$. However, from the symmetry of the function, $P(u_1, u_2)$, about the origin, the real probability density distribution function is, except a factor of two, the same function which would be obtained by considering only the half plane, $u_1 > 0$.

Let $P_{\alpha\beta}(\alpha, \beta)$ be the probability density distribution function of α and β variables. Then,

$$P(u_1, u_2)\ du_1\ du_2 = P_{\alpha\beta}(\alpha, \beta)\ d\alpha\ d\beta \ .$$

From Eq. (B. 4), one obtains

$$du_1\, du_2 = \frac{1}{4\,(\alpha^2 + \beta^2)^{1/2}}\, d\alpha\, d\beta \quad . \tag{B. 5}$$

From Eqs. (B. 1) and (B. 5), one has

$$P(u_1, u_2)\, du_1\, du_2 = \frac{1}{8}\,\frac{1}{(1 - R^2)^{1/2}}\,\frac{1}{(\alpha^2 + \beta^2)^{1/2}}$$

$$\cdot \exp\left\{-\frac{1}{2(1 - R^2)}\cdot\left[(\alpha^2 + \beta^2)^{1/2} - R\alpha\right]\right\} d\alpha\, d\beta \quad .$$

Thus,

$$P_{\alpha\beta}(\alpha, \beta) = \frac{1}{4}\,\frac{1}{(1 - R^2)^{1/2}}\,\frac{1}{(\alpha^2 + \beta^2)^{1/2}}$$

$$\cdot \exp\left\{-\frac{1}{2(1 - R^2)}\cdot\left[(\alpha^2 + \beta^2)^{1/2} - R\alpha\right]\right\} \quad . \tag{B. 6}$$

Note that a factor of two has been included in this expression. The marginal probability density distribution function of α is

$$P_\alpha(\alpha) = \int_{-\infty}^{+\infty} P_{\alpha\beta}(\alpha, \beta)\, d\beta$$

$$= \frac{1}{2}\,\frac{1}{(1 - R^2)^{1/2}}\cdot\exp\left(\frac{R\alpha}{2(1 - R^2)}\right)\cdot\int_0^{\infty}\frac{1}{(\alpha^2 + \beta^2)^{1/2}}$$

$$\cdot \exp\left(-\frac{(\alpha^2 + \beta^2)^{1/2}}{2(1 - R^2)}\right) d\beta \quad . \tag{B. 7}$$

Let $I(\alpha)$ denote the integral in this equation. By change of variables one obtains

$$I(\alpha) = \exp\left(\frac{-|\alpha|}{2(1-R^2)}\right)\cdot\int_0^\infty \frac{\exp(-t)}{t^{1/2}}\,\frac{1}{\left(t+\left|\frac{\alpha}{1-R^2}\right|\right)^{1/2}}\,dt$$

$$= K_o\left(\left|\frac{\alpha}{2(1-R^2)}\right|\right) \quad , \tag{B.8}$$

where K_o is the zeroth order K Bessel function. See Grobner and Hofreiter (1966) for this integration.

Since

$$P_\alpha(\alpha)\,d\alpha = 2P_\alpha(2u_1u_2)\,d(u_1u_2) = 2RP_\alpha(2u_1u_2)\,d(uv/\overline{uv}) \quad ,$$

the probability density distribution function, $P_{uv}(uv/\overline{uv})$, of the variable $uv/\overline{uv}$, can be written as

$$P_{uv}\left(\frac{uv}{\overline{uv}}\right) = \frac{1}{\pi}\,\frac{|R|}{(1-R^2)^{1/2}}\exp\left(\frac{R^2}{(1-R^2)}\cdot\frac{uv}{\overline{uv}}\right)$$

$$\cdot K_o\left(\left|\frac{R}{1-R^2}\cdot\frac{uv}{\overline{uv}}\right|\right) \quad . \tag{B.9}$$

This function is plotted in Fig. 35 with $R = -0.4$. Note that, as $uv \to 0$, $P_{uv} \to \infty$, since $K_o \to \infty$.

For the variable, $h = uv/u'v'$, the probability density distribution function, $P_H(h)$, is, from Eq. (B.9),

$$P_H(h) = \frac{1}{\pi} \frac{1}{(1 - R^2)^{1/2}} \exp\left(\frac{Rh}{1 - R^2}\right) K_o\left(\left|\frac{h}{1 - R^2}\right|\right) \qquad \text{(B. 10)}$$

C. CONTRIBUTIONS TO $\overline{uv}$ FROM DIFFERENT EVENTS AND FRACTION OF TOTAL TIME IN "HOLE"

The fraction of total time in "hole", $P_T(H)$, can be considered as the probability that the uv signal stays in the range, $|uv/u'v'| \leq H$. Thus,

$$P_T(H) = \int_{-H}^{H} P_H(h)\, dh \quad . \qquad \text{(B. 11)}$$

The contribution to $\overline{uv}$ from "hole" is given by

$$\frac{\tilde{uv}_h}{\overline{uv}}(H) = \int_{-H}^{H} \frac{uv}{\overline{uv}} P_H(h)\, dh = \frac{1}{R} \int_{-H}^{H} h \cdot P_H(h)\, dh \quad . \qquad \text{(B. 12)}$$

Other contributions are computed as follows:

(1) Burst and sweep:

$$\frac{\tilde{uv}_2}{\overline{uv}}(H) = \frac{\tilde{uv}_4}{\overline{uv}}(H) = \frac{1}{2R} \int_{H}^{\infty} h \cdot P_H(h)\, dh \qquad \text{(B. 13)}$$

(2) Other two quadrants:

$$\frac{\tilde{uv}_1}{\overline{uv}}(H) = \frac{\tilde{uv}_3}{\overline{uv}}(H) = \frac{1}{2R} \int_{-\infty}^{H} h \cdot P_H(h)\, dh \qquad \text{(B. 14)}$$

Similarly, the fraction of total time spent in each quadrant can be computed. For the case, H = 0, the fraction of total time for bursts or sweeps is

$$\int_{-\infty}^{0}\int_{0}^{\infty} F(u_1, u_2)\, du_1 du_2 = \frac{1}{\pi}\cos^{-1} R \quad . \tag{B.15}$$

Also, for H = 0

$$\frac{\widetilde{uv}_2}{\overline{uv}}(0) = \frac{\widetilde{uv}_4}{\overline{uv}}(0) = \int_{-\infty}^{0}\int_{0}^{\infty} u_1 u_2 \cdot F(u_1, u_2)\, du_1 du_2$$

$$= -\frac{(1 - R^2)^{1/2}}{2} + \frac{R \cos^{-1} R}{2} \tag{B.16}$$

and

$$\frac{\widetilde{uv}_1}{\overline{uv}}(0) = \frac{\widetilde{uv}_3}{\overline{uv}}(0) = \frac{R}{2} - \frac{\widetilde{uv}_2}{\overline{uv}}(0) \quad . \tag{B.17}$$

Using the locally measured correlation coefficient for R, the computed contributions to $\overline{uv}$ from different events are found from Eqs. (B.12)-(14) and are included in Figs. 37a through 37g and 38. Included also in these figures is the computed percentage of total time spent in "hole", $P_T(H)$, as computed from Eq. (B.11). The predicted values in Fig. 39 are computed from Eq. (B.16).

REFERENCES

Bakewell, H. P. and Lumley, J. L. (1967), "Viscous Sublayer and Adjacent Wall Region in Turbulent Pipe Flow," Phys. Fluids, vol. 10, no. 9, part 1, pp. 1880-1889.

Blackwelder, R. F. and Kaplan, R. E. (1971), "Intermittent Stucture in Turbulent Boundary Layer," AGARD Conference Proceedings No. 93 on Turbulent Shear Flow, p. 5, September 1971.

Clark, J. A. (1968), "A Study of Incompressible Turbulent Boundary Layer in Channel Flow," J. Basic Engng., Trans. ASME, vol. 90, series D, no. 4, pp. 455-468.

Clauser, F. H. (1956), "The Turbulent Boundary Layer," Advance in Applied Mechanics, vol. 4, Academic Press Inc., Publisher, New York, pp. 1-51.

Coantic, M. (1965), "Remarques sur la Structure de la Turbulence a Proximite d'une Paroi," Compte Rendus Acad. Sci., Paris, t. 260, Groupe 2, pp. 2981-2984.

Coles, D. E. (1954), "The Problem of the Turbulent Boundary Layer," Z. A. M. P., vol. 5, pp. 181-202.

Corino, E. R. and Brodkey, R. S. (1969), "A Visual Investigation of the Wall Region in Turbulent Flow," J. Fluid Mech., vol. 37, part 1, pp. 1-30.

Eckelmann, H. (1970), "Mitteilungen MPI fur Stromungsforschung und der AVA," Gottingen, No. 48.

Favre, A. J., Gaviglio, J. J. and Dumas, R. J. (1957), "Space-Time Correlations and Spectra in a Turbulent Boundary Layer," J. Fluid Mech., vol. 2, part 4, pp. 313-342.

Favre, A. J., Gaviglio, J. J. and Dumas, R. J. (1958), "Further Space-Time Correlations of Velocity in a Turbulent Boundary Layer," J. Fluid Mech., vol. 3, part 4, pp. 344-356.

Grant, H. L. (1958), "The Large Eddies of Turbulent Motion," J. Fluid Mech., vol. 4, part 2, pp. 149-190.

Grass, A.J. (1971), "Structural Features of Turbulent Flow over Smooth and Rough Boundaries," J. Fluid Mech., vol. 50, part 2, pp. 233-255.

Grobner, W. and Hofreiter, N. (1966), Integraltafel, Zweiter Teil, Springer Verlag, p. 57.

Gupta, A.K. and Kaplan, R.E. (1972), "Statistical Characteristics of Reynolds Stress in a Turbulent Boundary Layer," Phys. Fluids, vol. 15, no. 6, pp. 981-985.

Hama, F.R., Long, J.D. and Hegarty, J.C. (1957), "On Transition from Laminar to Turbulent Flow," J. Appl. Phys., vol. 28, no. 4, pp. 388-394.

Hama, F.R. and Nutant, J. (1963), "Detailed Flow-Field Observations in the Transition Process in a Boundary Layer," Proc. 1963 Heat Transfer and Fluid Mech. Inst., pp. 77-93, Stanford Univ. Press, Stanford.

Hinze, J.O. (1959), Turbulence, McGraw-Hill Book Co., New York, pp. 347-348.

Kibens, V. (1968), "The Intermittent Region of a Turbulent Boundary Layer," Ph.D. Dissertation, The Johns Hopkins University, February 1968.

Kim, H.T., Kline, S.J. and Reynolds, W.C. (1968), "An Experimental Study of Turbulence Production near a Smooth Wall in a Turbulent Boundary Layer with Zero Pressure Gradient," Report MD-20, Thermosciences Division, Dept. of Mech. Engng., Stanford University, January 1968.

Kim, H.T., Kline, S.J. and Reynolds, W.C. (1971), "The Production of Turbulence near a Smooth Wall in a Turbulent Boundary Layer," J. Fluid Mech., vol. 50, part 1, pp. 133-160.

Klebanoff, P.S. (1954), "Characteristics of Turbulence in a Boundary Layer with Zero Pressure Gradient," NACA TN 3178.

Kline, S.J., Reynolds, W.C., Schraub, F.A. and Runstadler, P.W. (1967), "The Structure of Turbulent Boundary Layers," J. Fluid Mech., vol. 30, part 4, pp. 741-743.

Kovasznay, L. S. G., Miller, L. T. and Vasudeva, B. R. (1963), "A Simple Hot Wire Anemometer," Project SQUID Tech. Rept. JHU-22-P, July 1963.

Kovasznay, L. S. G., Kibens, V. and Blackwelder, R. F. (1970), "Large Scale Motion in the Intermittent Region of a Turbulent Boundary Layer," J. Fluid Mech., vol. 41, part 2, pp. 283-325.

Laufer, J. (1953), "The Structure of Turbulence in a Fully Developed Pipe Flow," NACA TN 2954.

Laufer, J. and Badri Narayanan, M. A. (1971), "Mean Period of the Turbulent Production Mechanism in a Boundary Layer," Phys. Fluids, vol. 14, no. 1, pp. 182-183.

Rao, K. N., Narasimha, R. and Badri Narayanan, M. A. (1969), "Hot Wire Measurements of Burst Parameter in a Turbulent Boundary Layer," Report 69 FM 8, Department of Aeronautical Engineering, Indian Institute of Science, Bangalore.

Rao, K. N., Narasimha, R. and Badri Narayanan, M. A. (1971), "The 'Bursting' Phenomenon in a Turbulent Boundary Layer," J. Fluid Mech., vol. 48, part 2, pp. 339-352.

Reichardt, H. (1938), "Messungen Turbulenter Schwangkungen," Die Naturwissenschaften, 26. Jahrgang, Heft 24/25, pp. 404-408.

Runstadler, P. W., Kline, S. J. and Reynolds, W. C. (1963), "An Investigation of the Flow Structure of the Turbulent Boundary Layer," Report MD-8, Thermosciences Division, Mech. Engng. Dept., Stanford University, Stanford.

Schraub, F. A. and Kline, S. J. (1965), "Study of the Structure of the Turbulent Boundary Layer with and without Longitudinal Pressure Gradients," Report MD-12, Thermosciences Division, Mech. Engng. Dept., Stanford University.

Schraub, F. A. Kline, S. J., Henry J., Runstadler, P. W. and Littell, A. (1964), "Use of Hydrogen Bubbles for Quantitative Determination of Time-Dependent Velocity Field in Low-Speed Water Flows," J. Basic Engng., Trans. ASME, vol. 87, series D, no. 2, pp. 429-444.

Schubauer, G. B. and Klebanoff, P. S. (1951), "Investigations of the Separation of Turbulent Boundary Layers," NACA Report 1030.

Townsend, A.A. (1951), "The Structure of the Turbulent Boundary Layer," Proc. Camb. Phil. Soc., vol. 47, pp. 375-395.

Townsend, A.A. (1956), The Structure of Turbulent Shear Flow, Cambridge University Press, pp. 232-237.

Townsend, A.A. (1957), "The Tubulent Boundary Layer," IUTAM Symp., Freiburg, Berlin: Springer, pp. 1-15.

Townsend, A.A. (1961), "Equilibrium Layers and Wall Turbulence," J. Fluid Mech., vol. 11, part 1, pp. 97-120.

Tritton, D.J. (1967), "Some New Correlation Measurements in a Turbulent Boundary Layer," J. Fluid Mech., vol. 28, part 3, pp. 439-462.

Tu, B.J. and Willmarth, W.W. (1966), "An Experimental Study of the Structure of Turbulence Near the Wall Through Correlation Measurements in a Thick Turbulent Boundary Layer," The University of Michigan Tech. Rept. ORA 02920-3-T.

Wallace, J.M., Eckelmann, H. and Brodkey, R.S. (1972), "The Wall Region in Turbulent Shear Flow," J. Fluid Mech., vol. 54, part 1, pp. 39-48.

Willmarth, W.W. and Lu, S.S. (1971), "Structure of the Reynolds Stress near the Wall," AGARD Conference Proceedings No. 93 on Turbulent Shear Flow, p. 3, September 1971. (Also, submitted to J. Fluid Mech. for publication.)

Willmarth, W.W. and Tu, B.J. (1967), "Structure of Turbulence in the Boundary Layer near the Wall," Phys. Fluids, vol. 10, no. 9, part 2, Supplement, pp. S134-S137.

Willmarth, W.W. and Wooldridge, C.E. (1962), "Measurements of the Fluctuating Pressure at the Wall beneath a Thick Turbulent Boundary Layer," J. Fluid Mech., vol. 14, part 2, pp. 187-210.

Willmarth, W.W. and Wooldridge, C.E. (1963), "Measurements of the Correlation between the Fluctuating Velocities and the Fluctuating Pressure in a Thick Turbulent Boundary Layer," AGARD-NATO Tech. Rept. 456, April 1963.

U_∞ ft/sec	Re_θ	δ ft	δ^* ft	θ ft	δ^*/θ	U_τ/U_∞	Re_x	Remarks
19.7	4,230	0.405	0.0494	0.0363	1.365	0.0386	---	Transition Location Unknown
---	3,800	---	---	---	1.383	0.0387	2.1×10^6	Coles' Ideal Boundary Layer
204	38,000	0.42	0.041	0.0315	1.30	0.0326	3.1×10^7	Willmarth and Tu (1967)
---	39,000	---	---	---	1.30	0.0318	3.2×10^7	Coles' Ideal Boundary Layer

Table I. Properties of the Actual and Ideal Turbulent Boundary Layer.

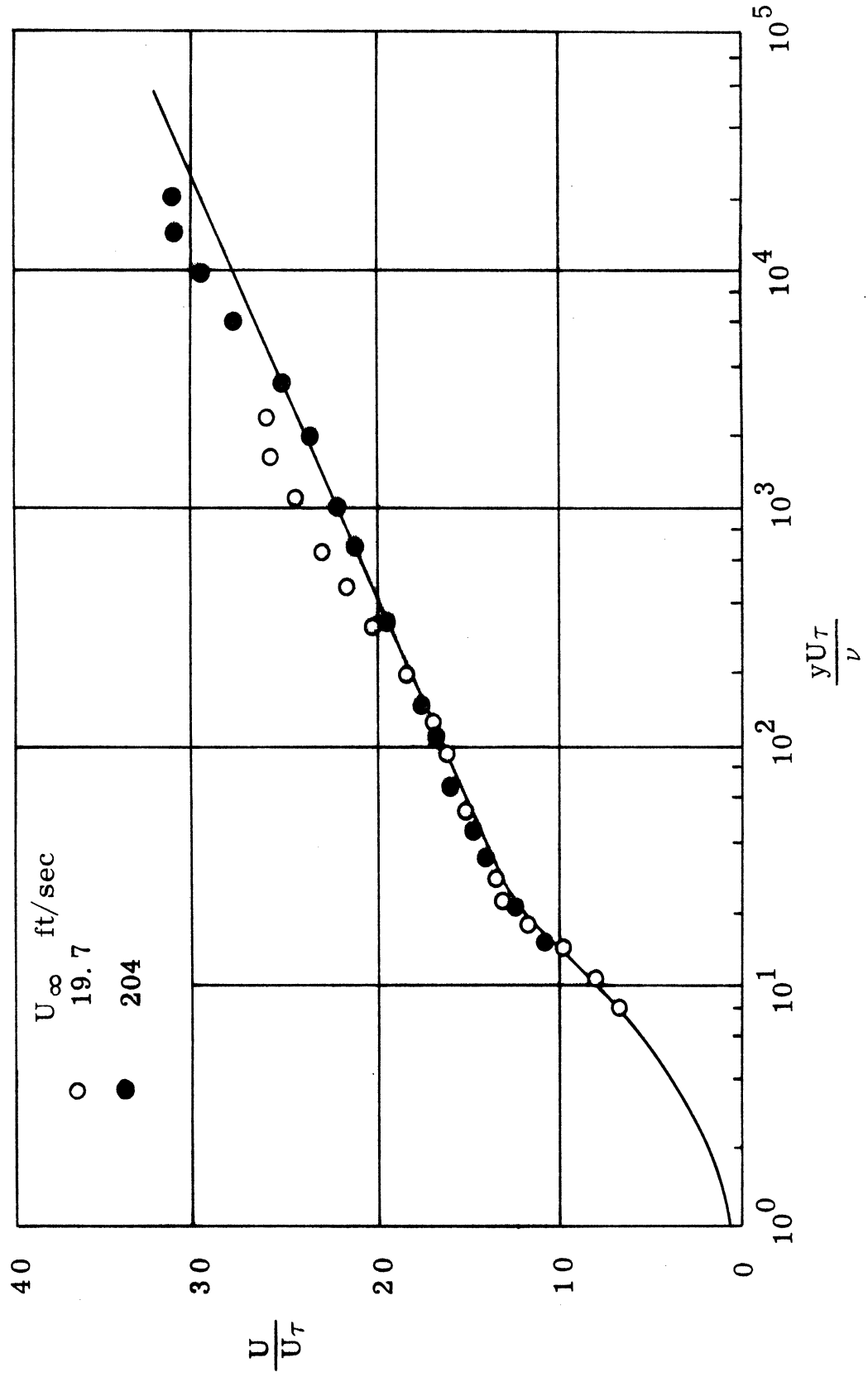

Fig. 1. Mean Velocity Profiles.

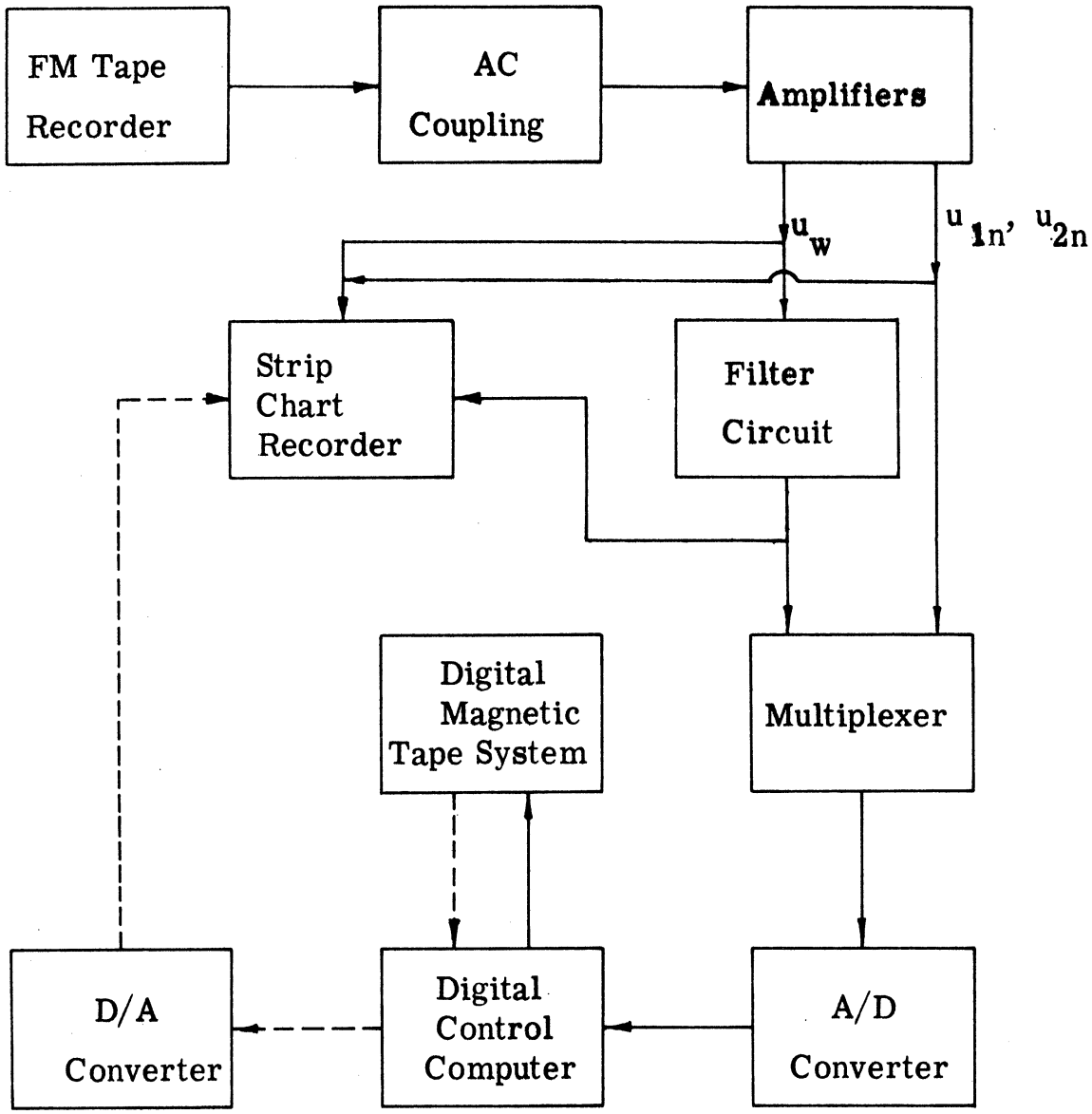

Fig. 2. Flow Diagram for A/D Conversion.

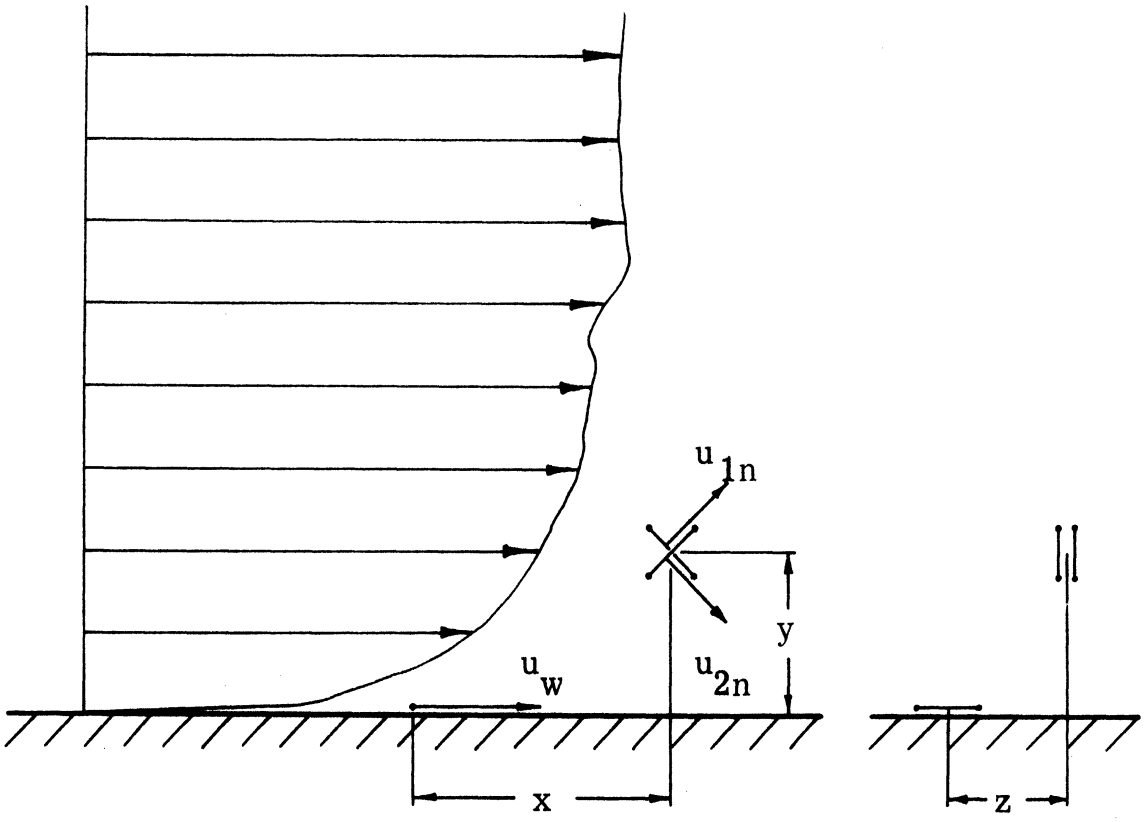

Fig. 3. Sketch of Arrangement of Hot Wires for Measurements of u_w, u_{1n} and u_{2n}.

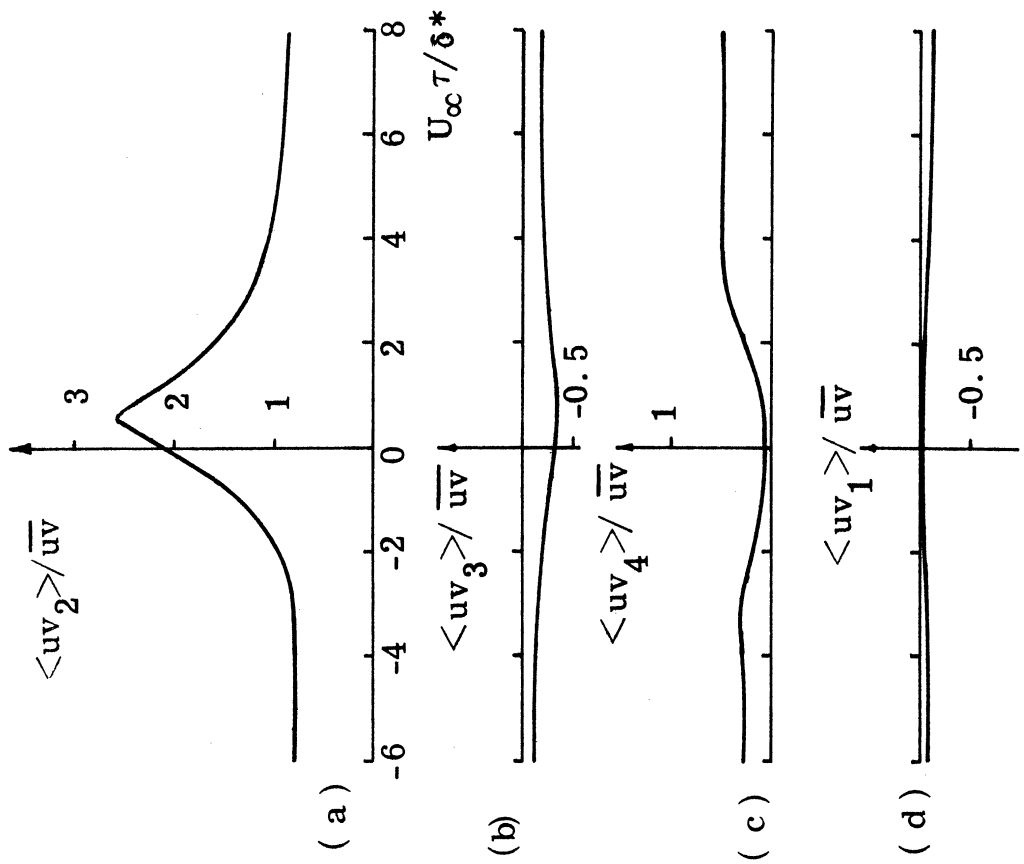

Fig. 5. Sampled Sorted Reynolds Stress.
u_w/u'_w=-1, - slope,
x/δ^*=0, y/δ^*=0.118, z/δ^*=0.

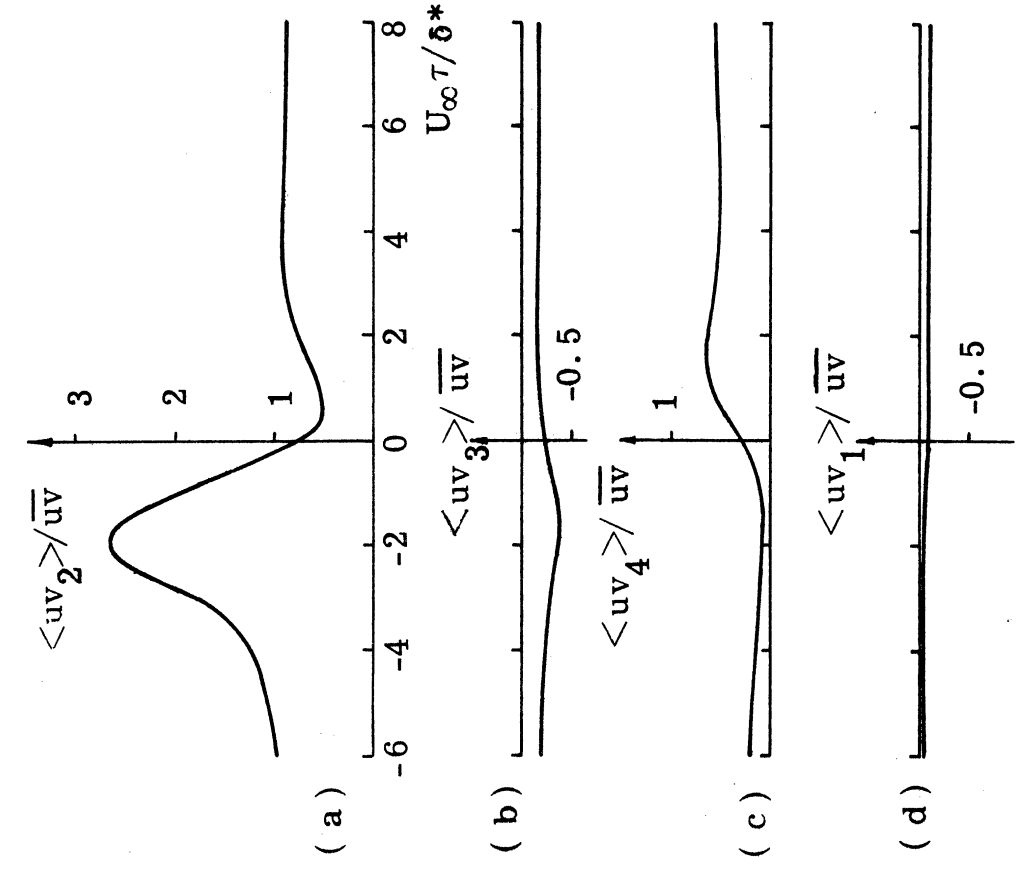

Fig. 4. Sampled Sorted Reynolds Stress.
u_w/u'_w=-1, + slope, x/δ^*=0,
y/δ^*=0.118, z/δ^*=0.

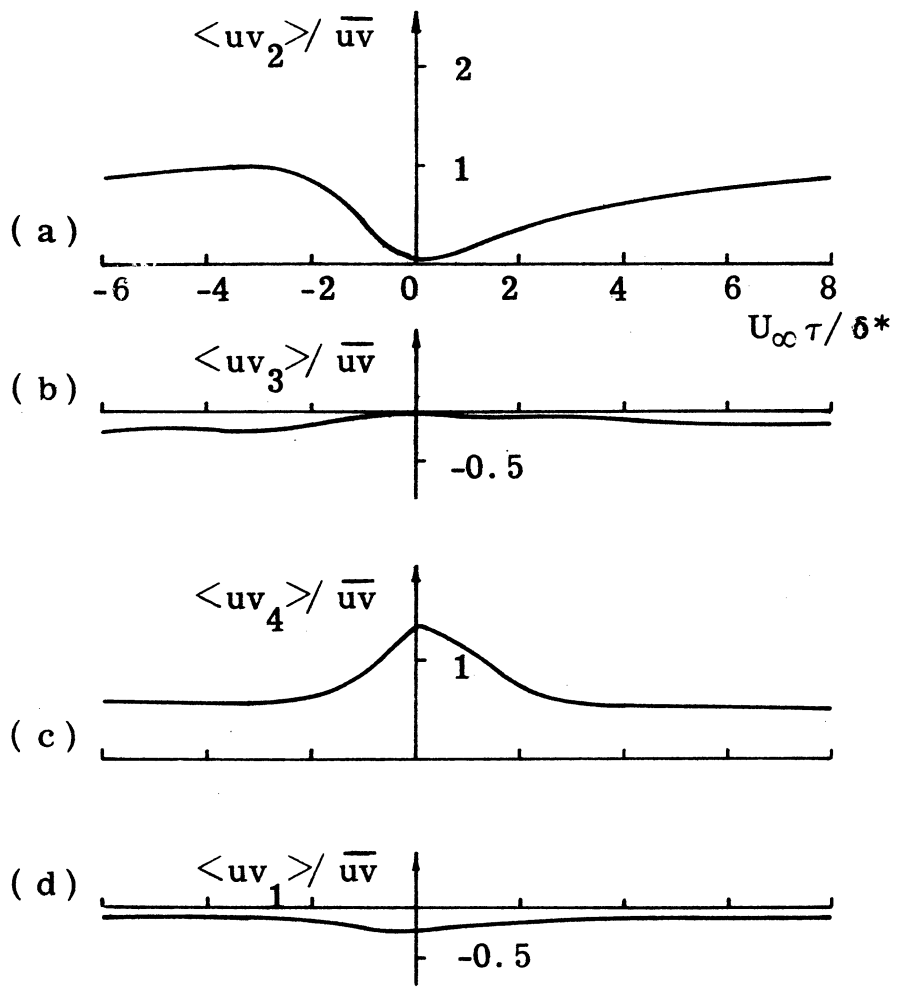

Fig. 6. Sampled sorted Reynolds Stress.
$u_w/u'_w = +1$, + slope,
$x/\delta^* = 0$, $y/\delta^* = 0.118$, $z/\delta^* = 0$.

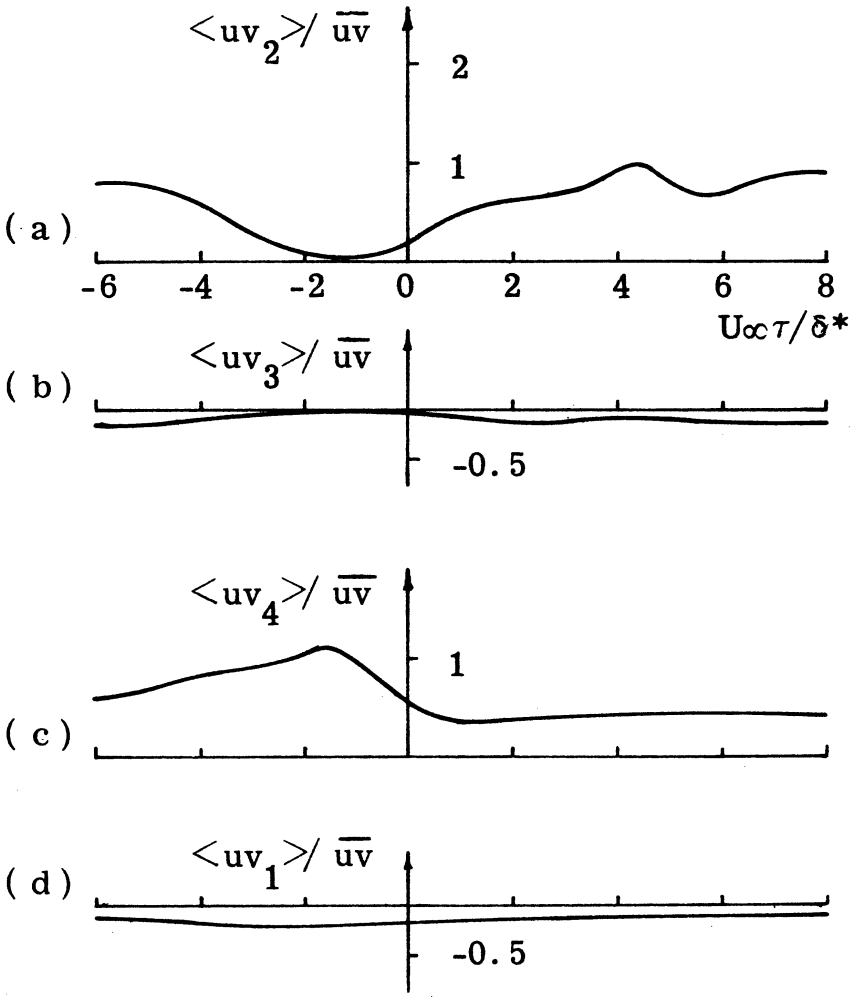

Fig. 7. Sampled Sorted Reynolds Stress.
$u_w/u'_w = +1$, - slope,
$x/\delta^* = 0$, $y/\delta^* = 0.118$, $z/\delta^* = 0$.

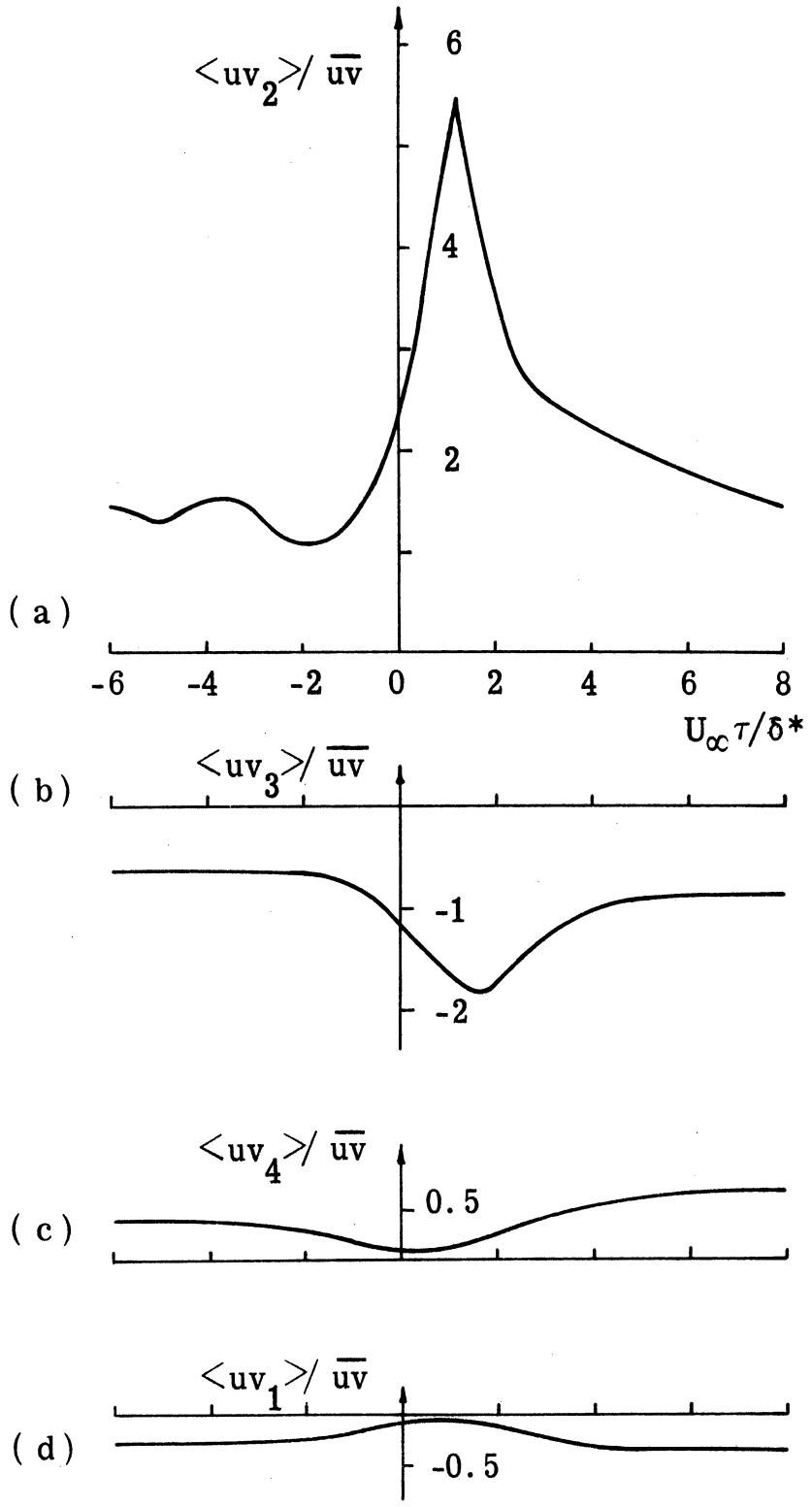

Fig. 8. Sampled sorted Reynolds Stress.
$u_w / u'_w = -1$, - slope,
$x/\delta^* = 0.337$, $y/\delta^* = 0.118$, $z/\delta^* = 0$.

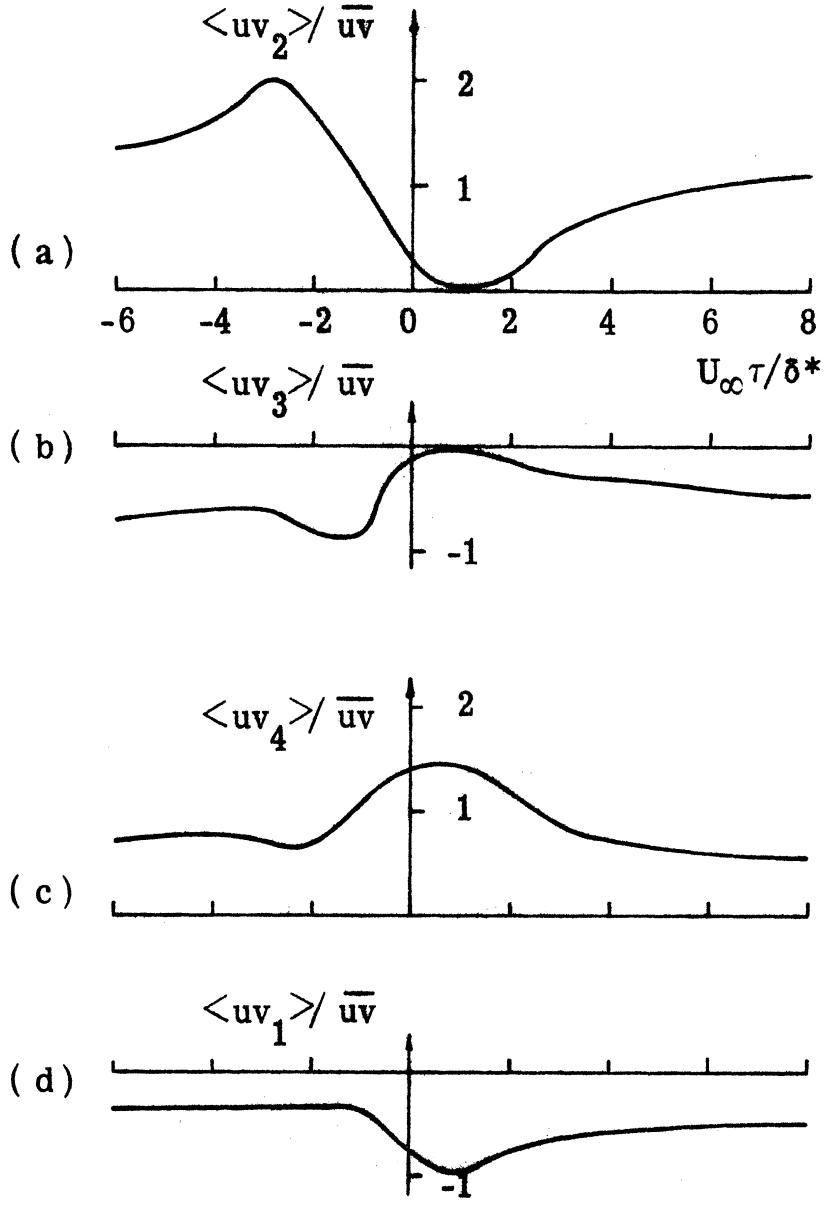

Fig. 9. Sampled Sorted Reynolds Stress.
$u_w/u'_w = +1$, + slope,
$x/\delta^* = 0.337$, $y/\delta^* = 0.118$, $z/\delta^* = 0$.

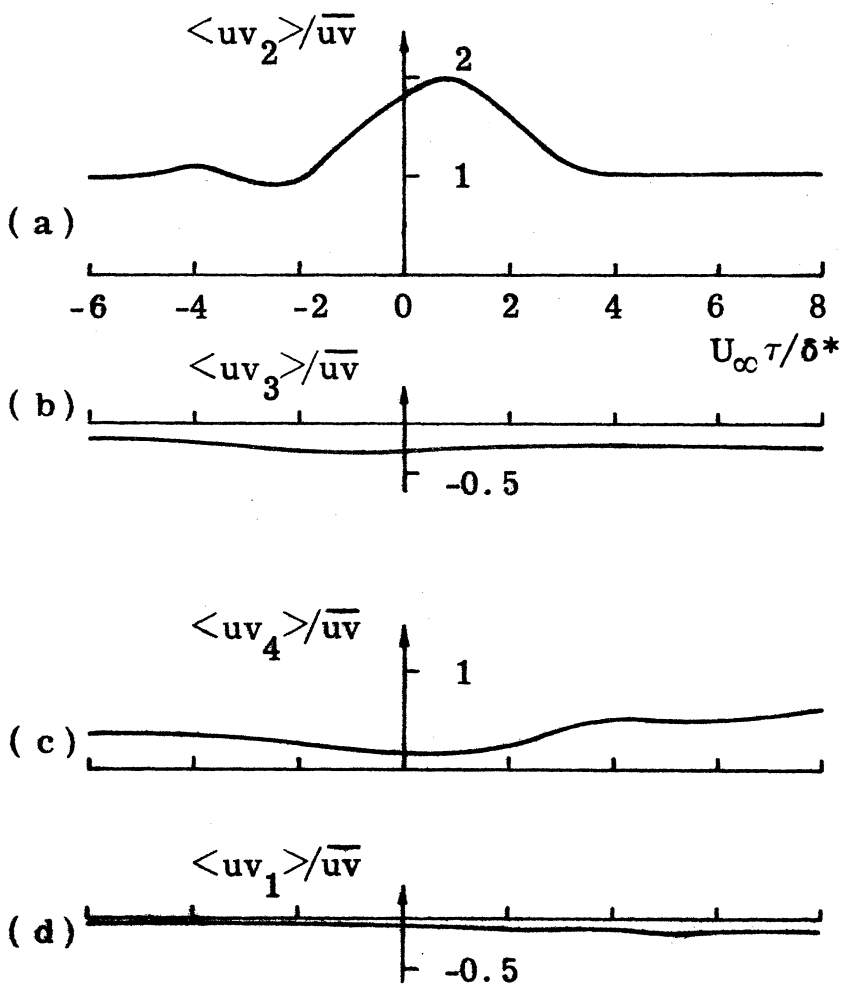

Fig. 10. Sampled Sorted Reynolds Stress.
$u_w/u'_w = -1$, - slope,
$x/\delta^* = 0.337$, $y/\delta^* = 0.253$, $z/\delta^* = 0$.

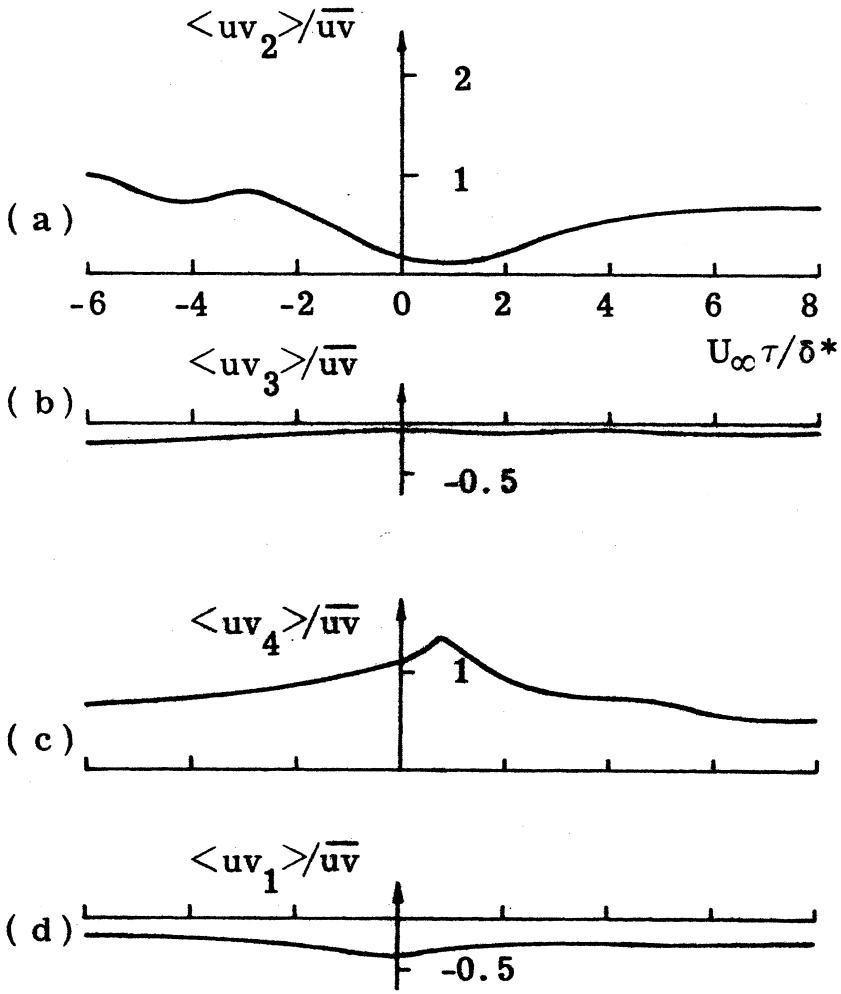

Fig. 11. Sampled Sorted Reynolds Stress.
$u_w/u'_w = +1$, + slope,
$x/\delta^* = 0.337$, $y/\delta^* = 0.253$, $z/\delta^* = 0$.

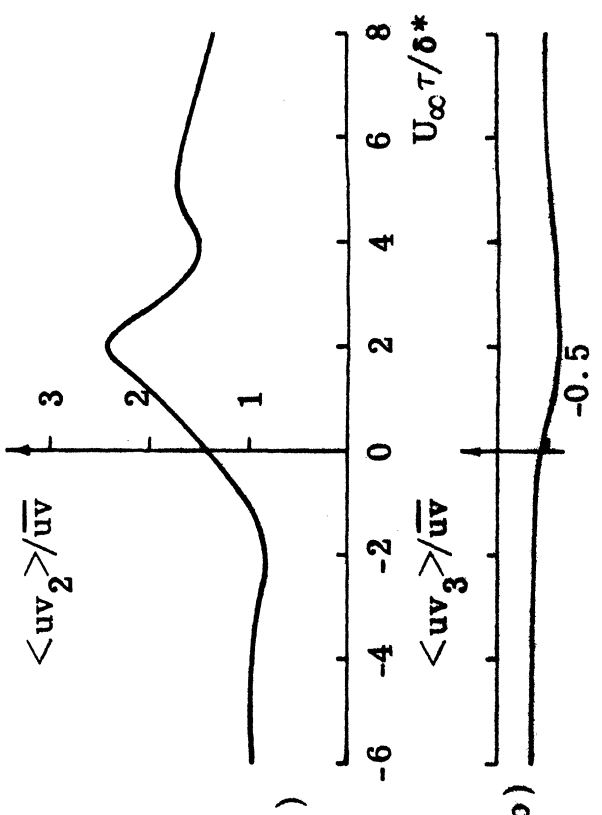

Fig. 12. Sampled Sorted Reynolds Stress.
$u_w/u'_w = -1$, - slope,
$x/\delta^* = 0.843$, $y/\delta^* = 0.211$, $z/\delta^* = 0.$

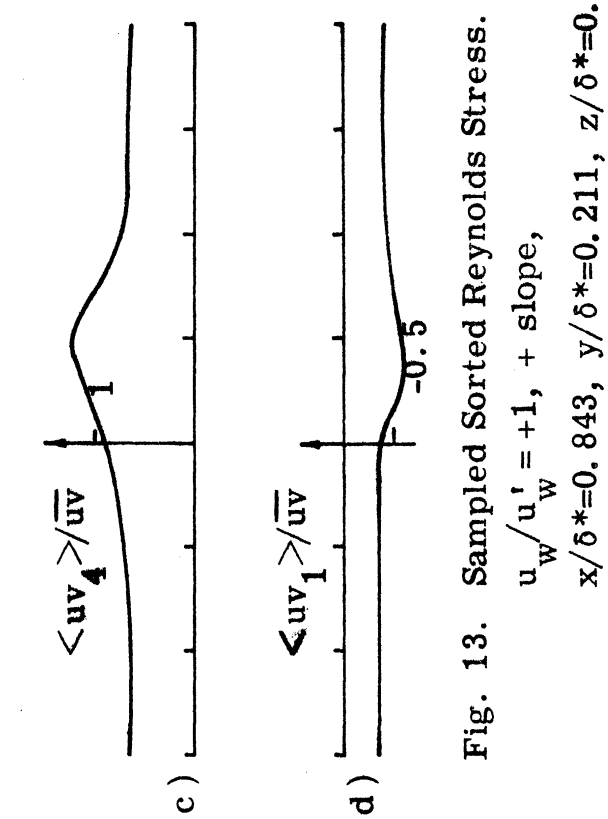

Fig. 13. Sampled Sorted Reynolds Stress.
$u_w/u'_w = +1$, + slope,
$x/\delta^* = 0.843$, $y/\delta^* = 0.211$, $z/\delta^* = 0.$

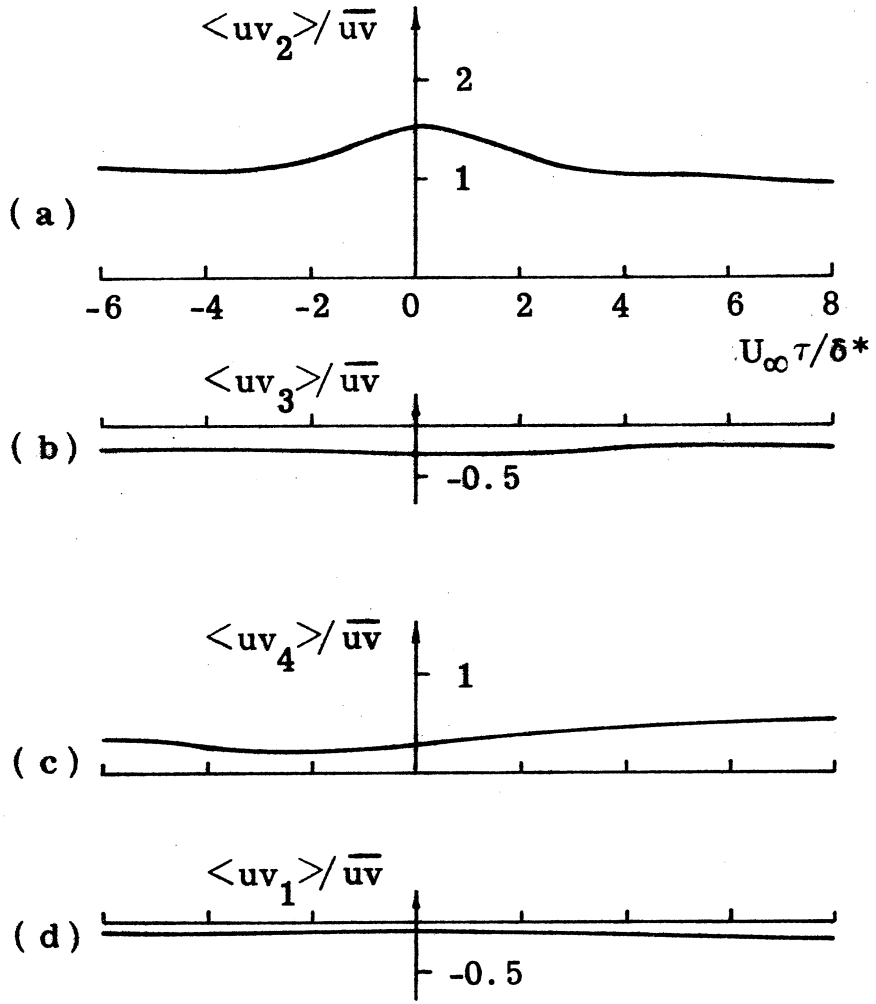

Fig. 14. Sampled Sorted Reynolds Stress.
$u_w/u'_w = -1$, - slope,
$x/\delta^*=0.843$, $y/\delta^*=0.506$, $z/\delta^*=0$.

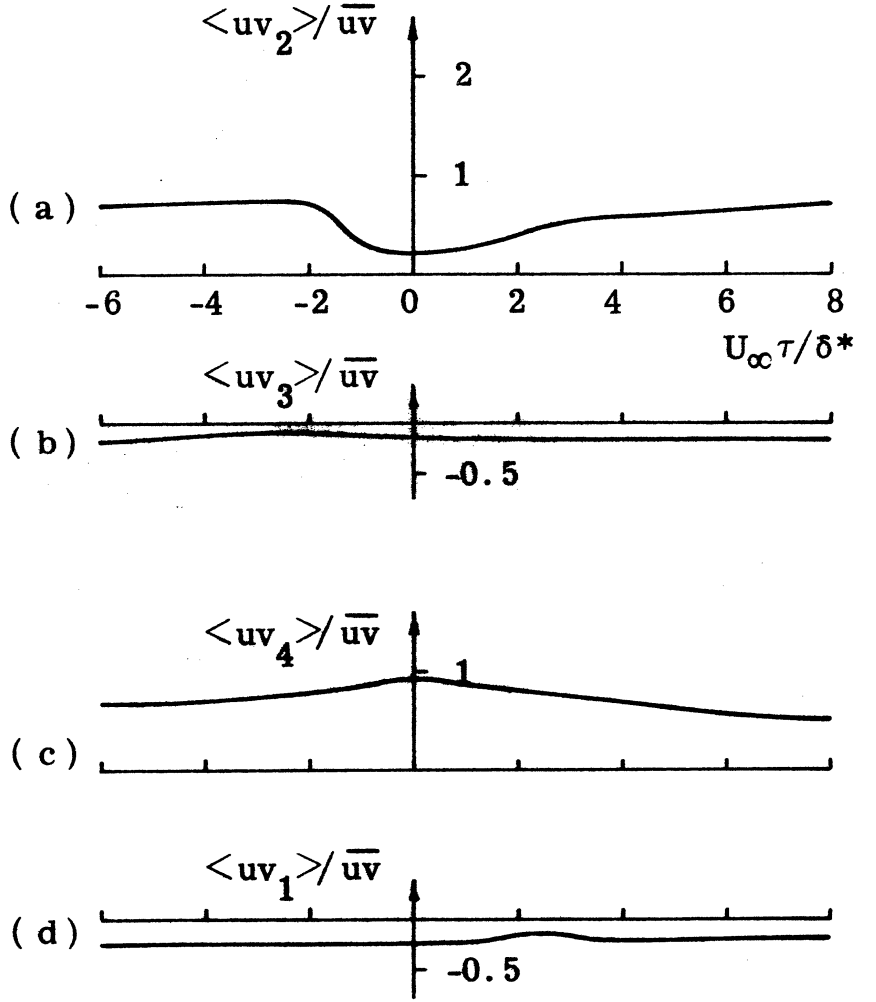

Fig. 15. Sampled Sorted Reynolds Stress.
$u_w/u'_w = +1$, + slope,
$x/\delta^*=0.843$, $y/\delta^*=0.506$, $z/\delta^*=0$.

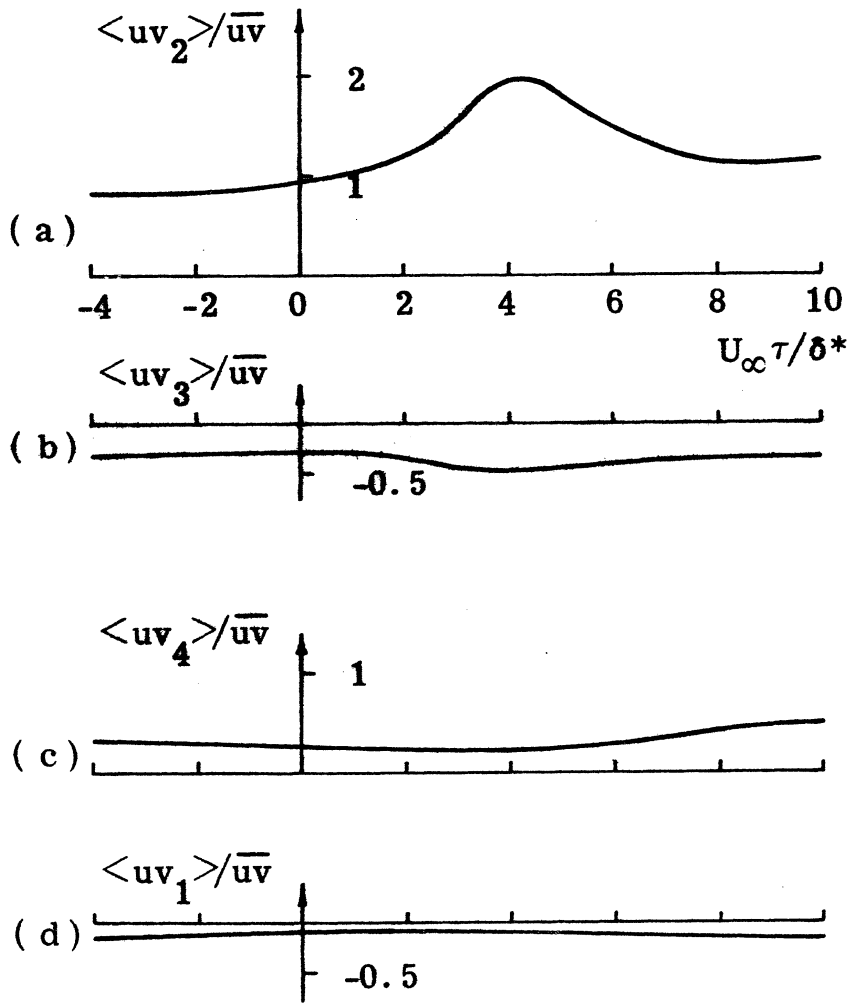

Fig. 16. Sampled Sorted Reynolds Stress.
$u_w/u'_w = -1$, - slope,
$x/\delta^*=1.686$, $y/\delta^*=0.169$, $z/\delta^*=0$.

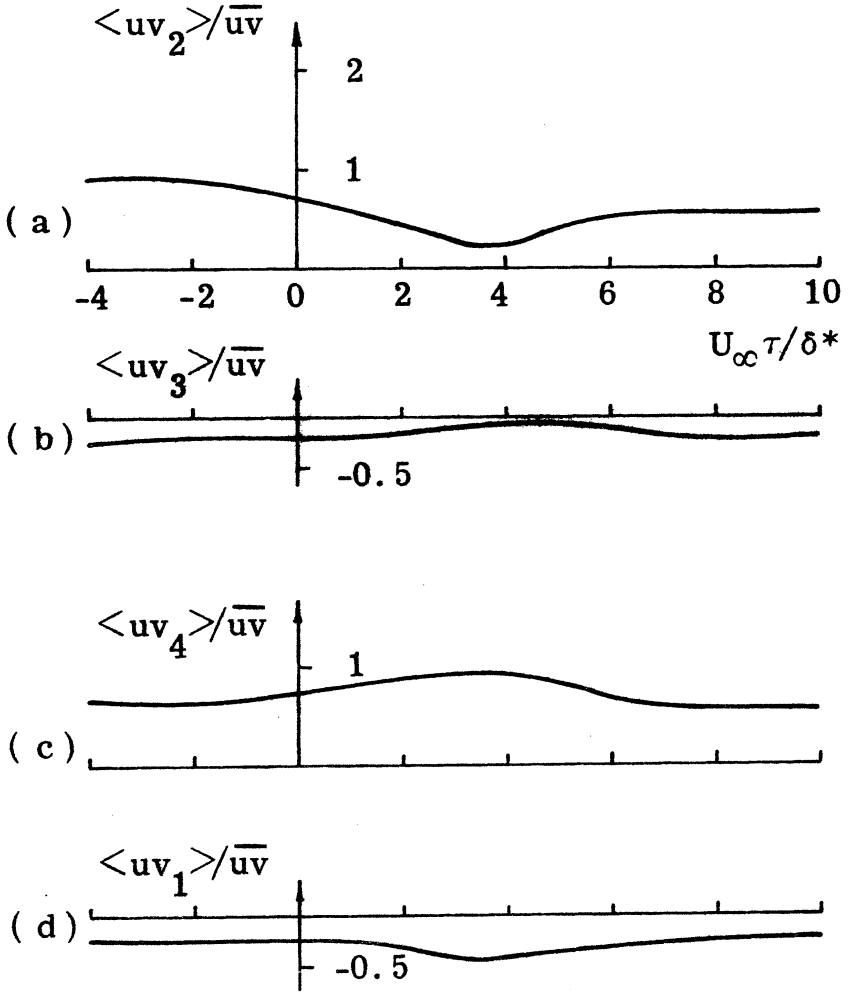

Fig. 17. Sampled Sorted Reynolds Stress.
$u_w/u'_w = +1$, + slope,
$x/\delta^*=1.686$, $y/\delta^*=0.169$, $z/\delta^*=0$.

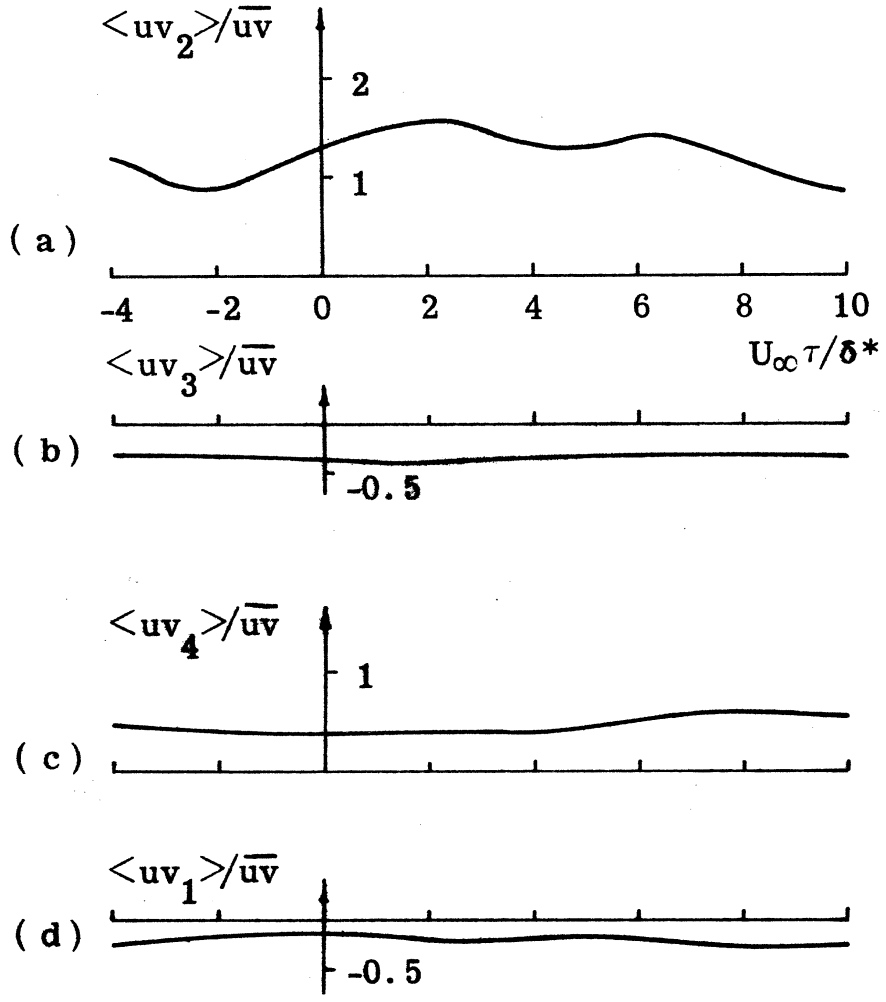

Fig. 18. Sampled Sorted Reynolds Stress.
u_w/u'_w = -1, - slope,
x/δ^*=1.686, y/δ^*=0.388, z/δ^*=0.

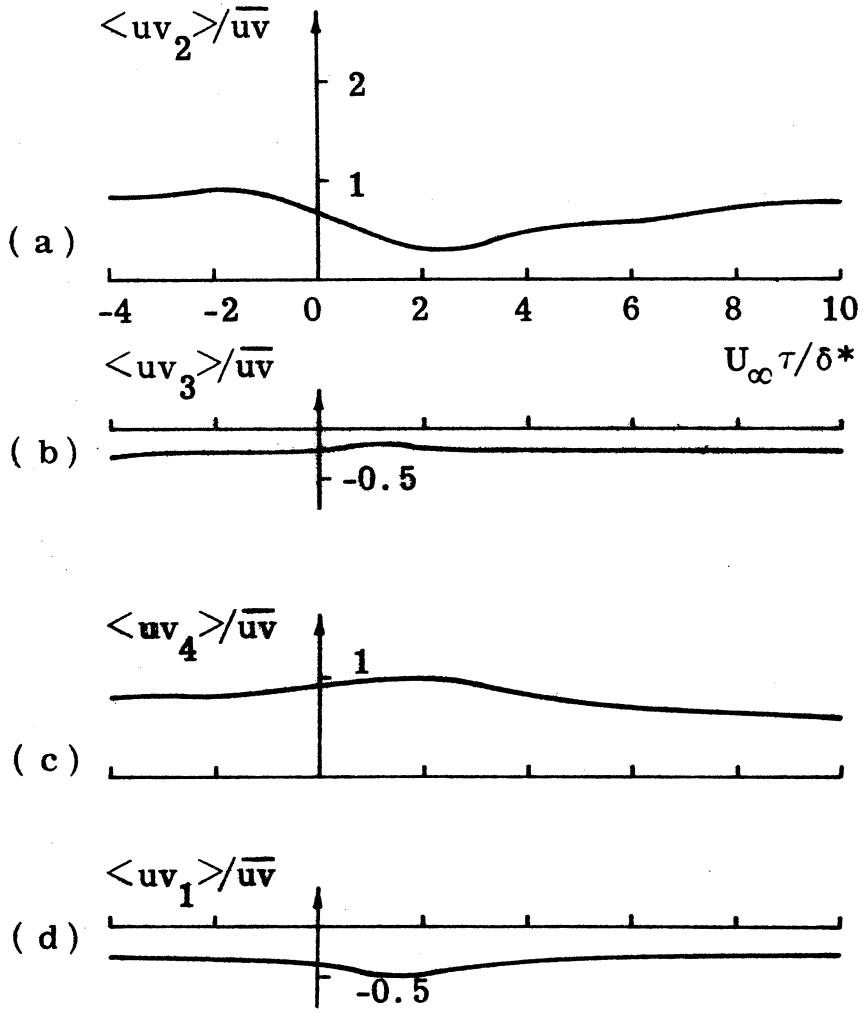

Fig. 19. Sampled Sorted Reynolds Stress.
u_w/u'_w = +1, + slope,
x/δ^*=1.686, y/δ^*=0.388, z/δ^*=0.

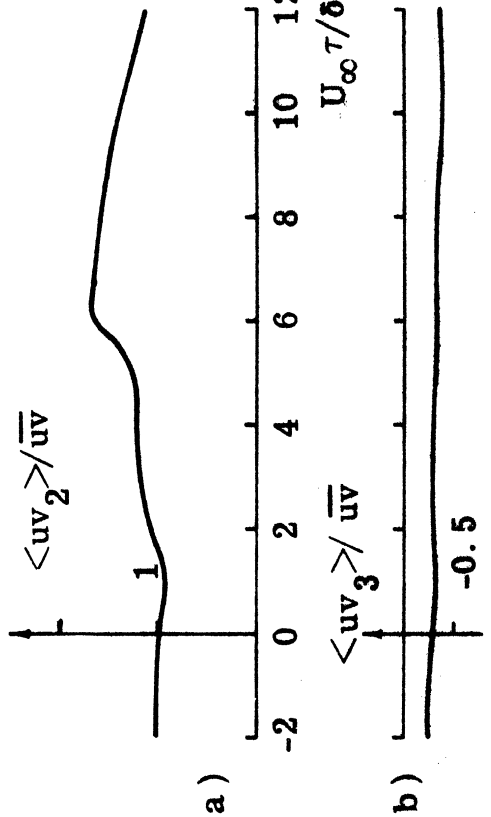

Fig. 20. Sampled Sorted Reynolds Stress.
$u_w/u'_w = -1$, - slope,
$x/\delta^* = 2.53$, $y/\delta^* = 0.169$, $z/\delta^* = 0$.

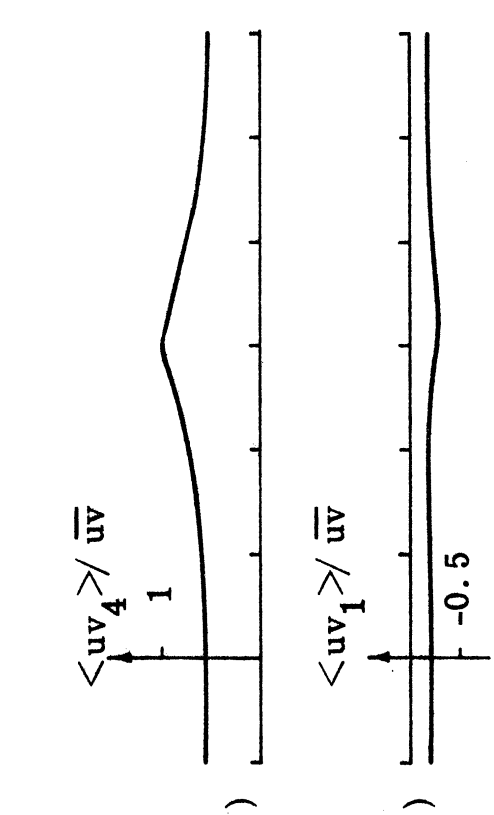

Fig. 21. Sampled Sorted Reynolds Stress.
$u_w/u'_w = +1$, + slope,
$x/\delta^* = 2.53$, $y/\delta^* = 0.169$, $z/\delta^* = 0$.

Fig. 22. Convection and Decay of Sampled Sorted Reynolds Stress, $\langle uv_2 \rangle / \overline{uv}$, with Sampling Conditions of $u_w/u'_w = -1$ and Negative Slope of u_w; $y/\delta^* \approx 0.169$, $z/\delta^* = 0$.

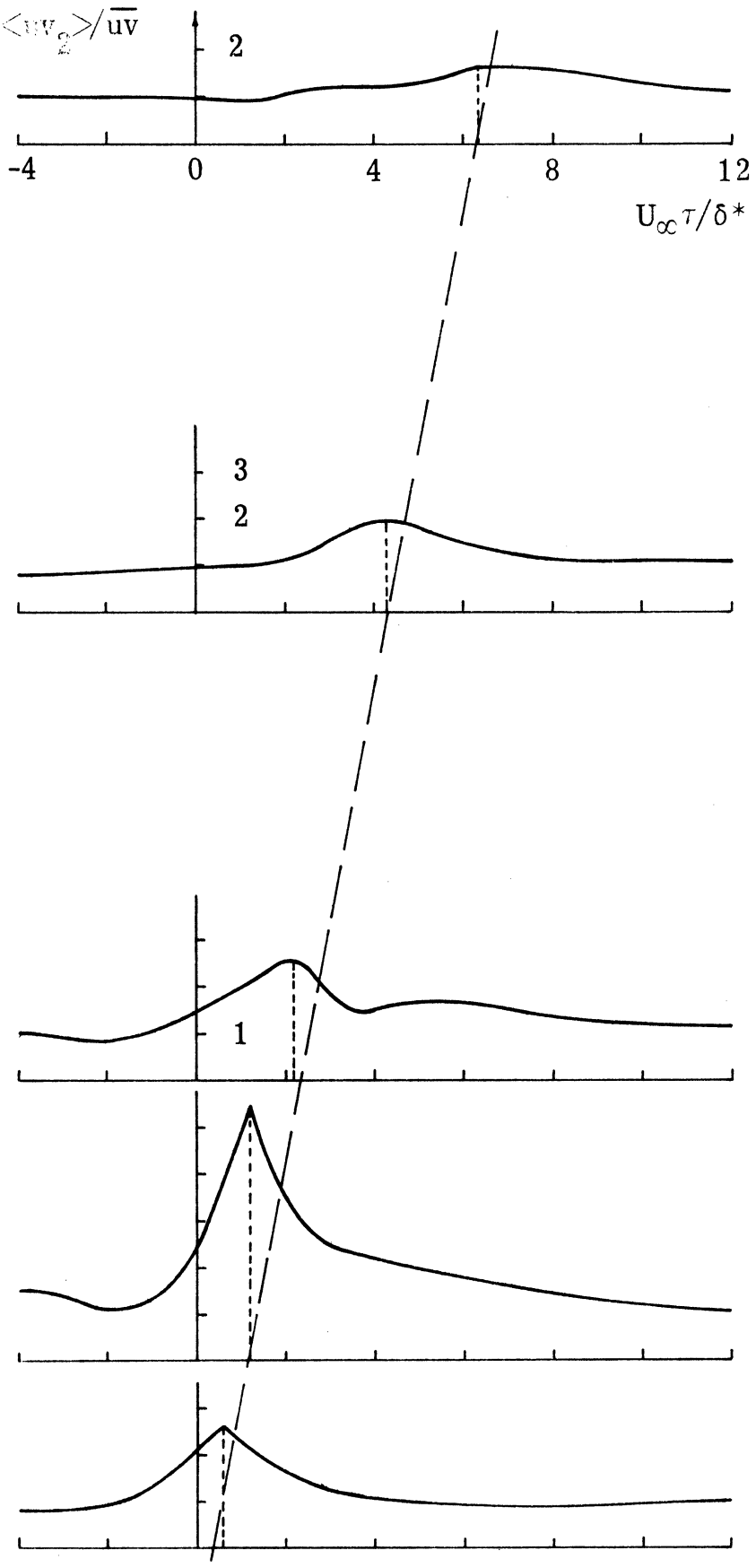

Fig. 22.

Fig. 23. Convection and Decay of Sampled Sorted Reynolds Stress, $\langle uv_4 \rangle / \overline{uv}$, with Sampling Conditions of $u_w/u'_w = +1$ and Positive Slope of u_w; $y/\delta^* \approx 0.169$, $z/\delta^* = 0$.

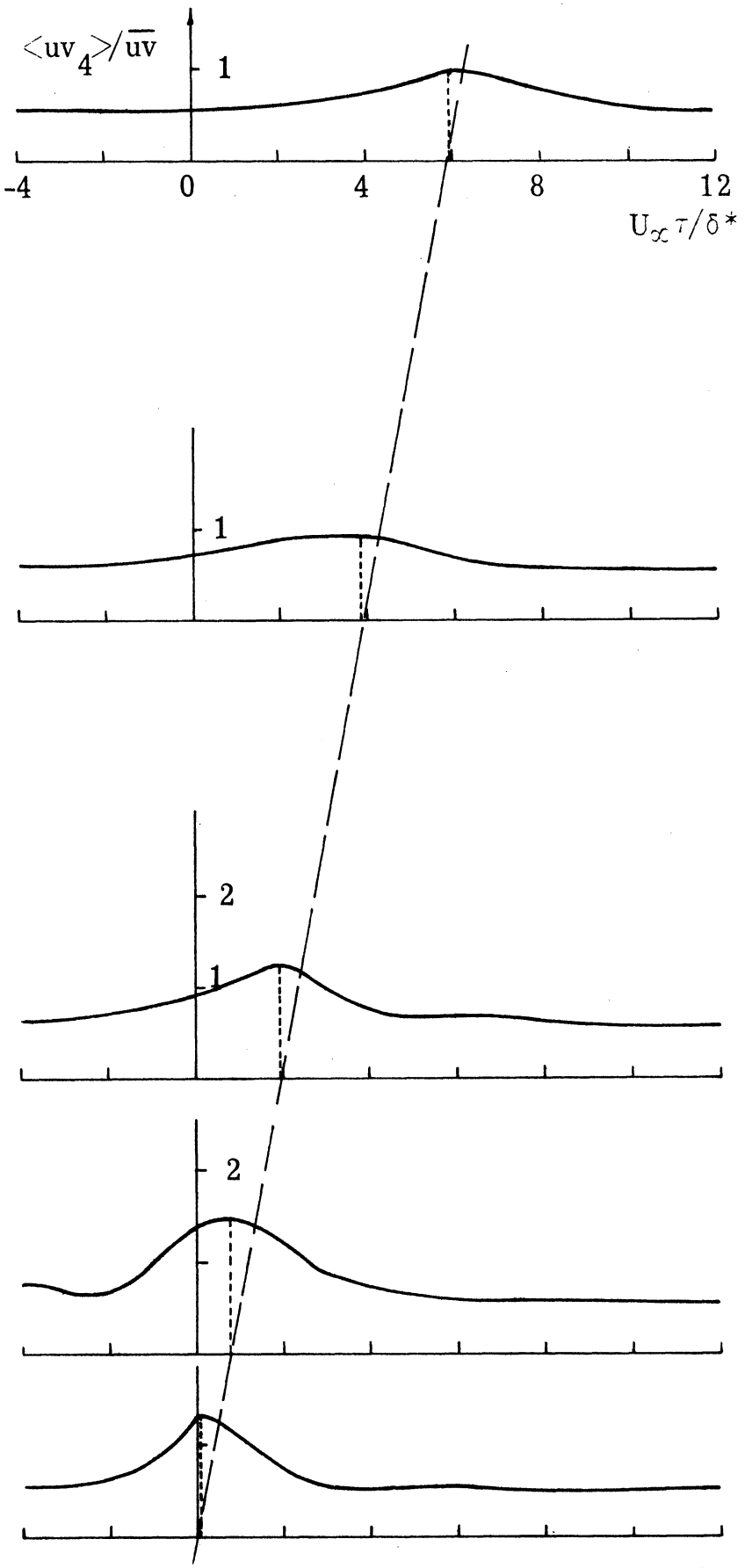

Fig. 23.

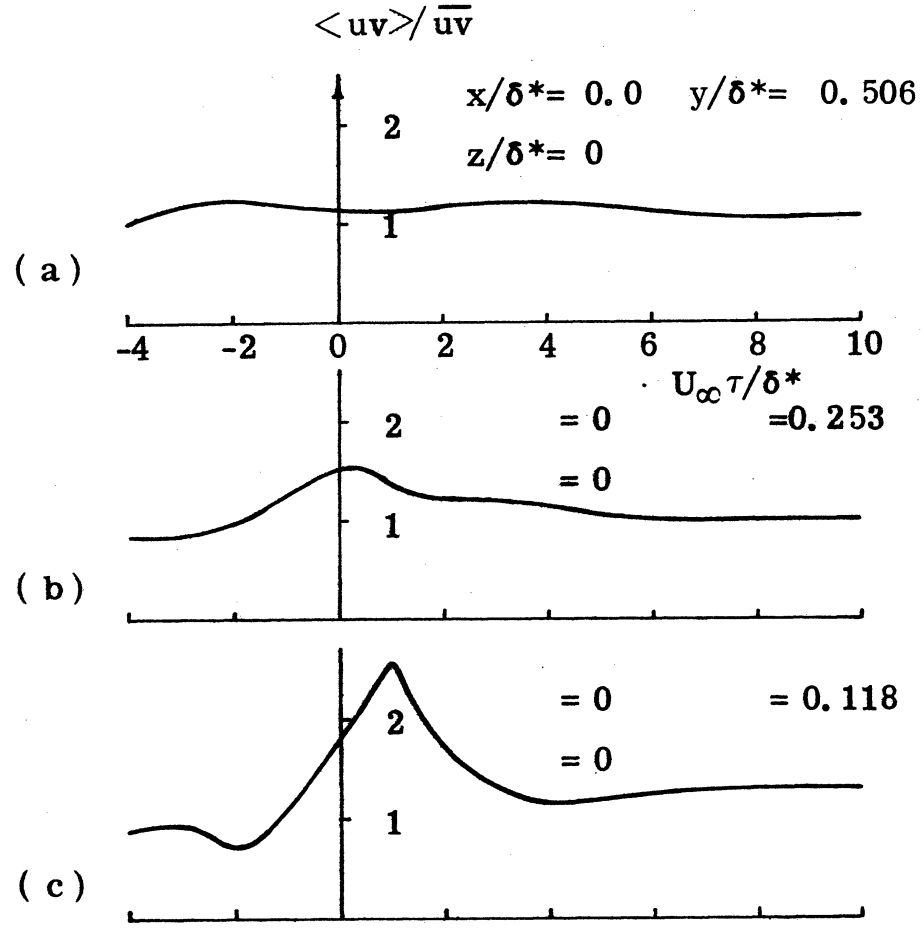

Fig. 24. Sampled Reynolds Stress.
$u_w/u'_w = -1$, -slope.

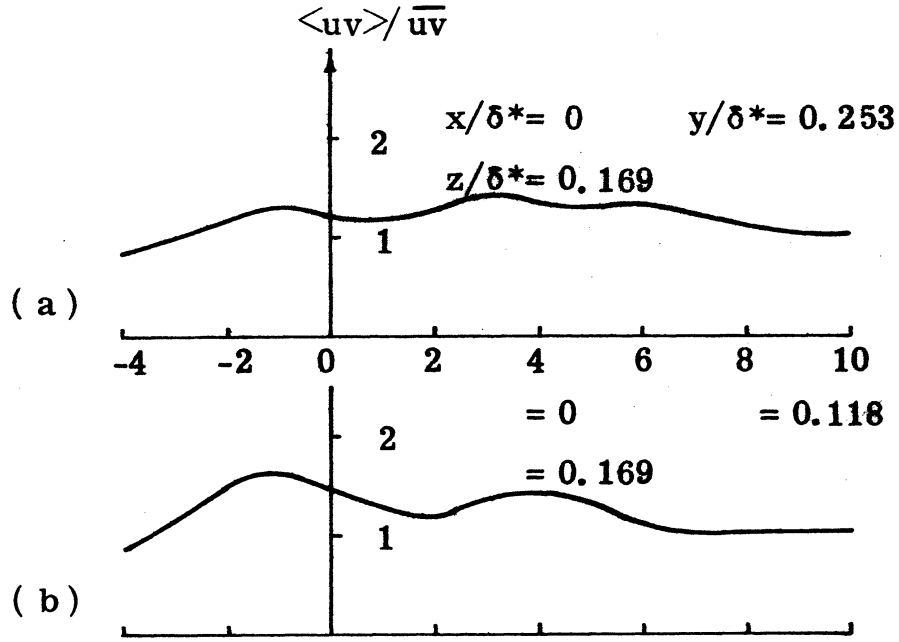

Fig. 25. Sampled Reynolds Stress.
$u_w/u'_w = -1$, - slope.

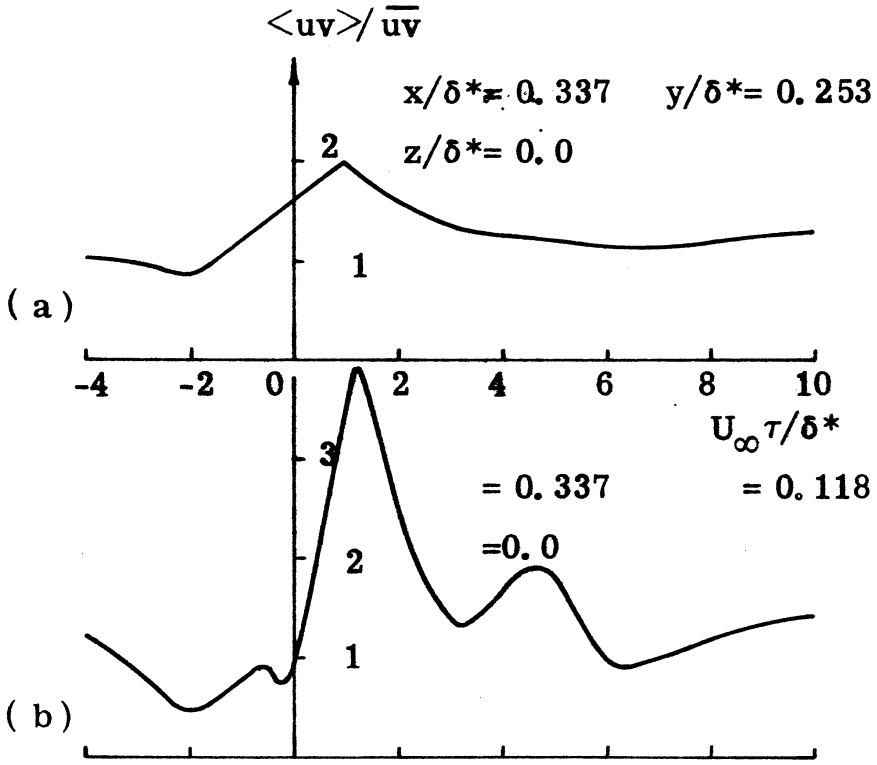

Fig. 26. Sampled Reynolds Stress.
u_w/u'_w = -1, - slope.

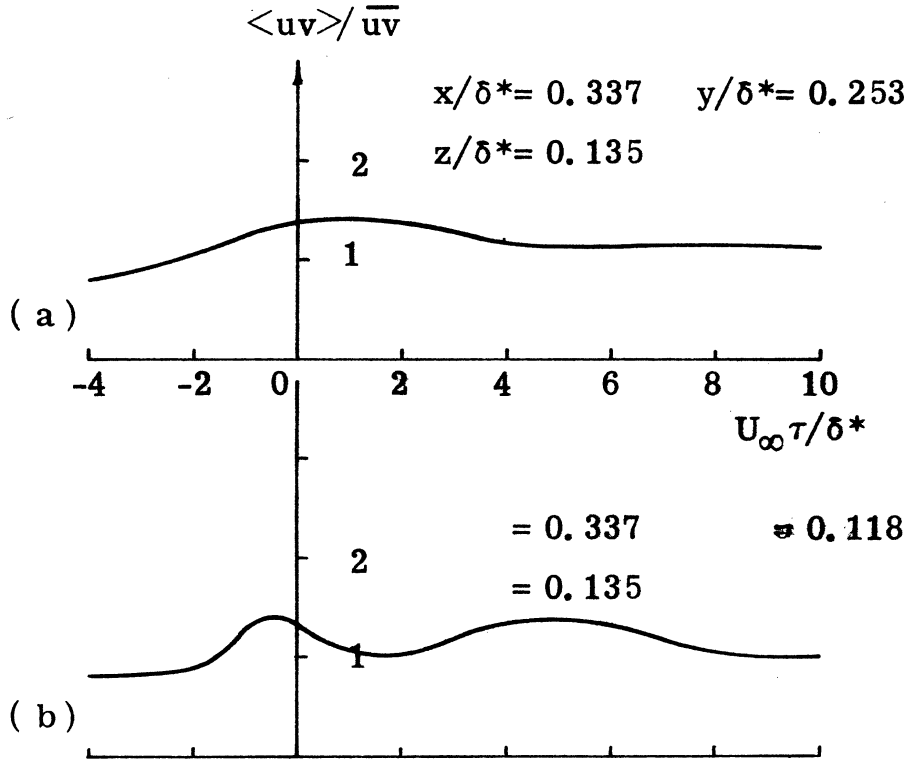

Fig. 27. Sampled Reynolds Stress.
u_w/u'_w = -1, - slope.

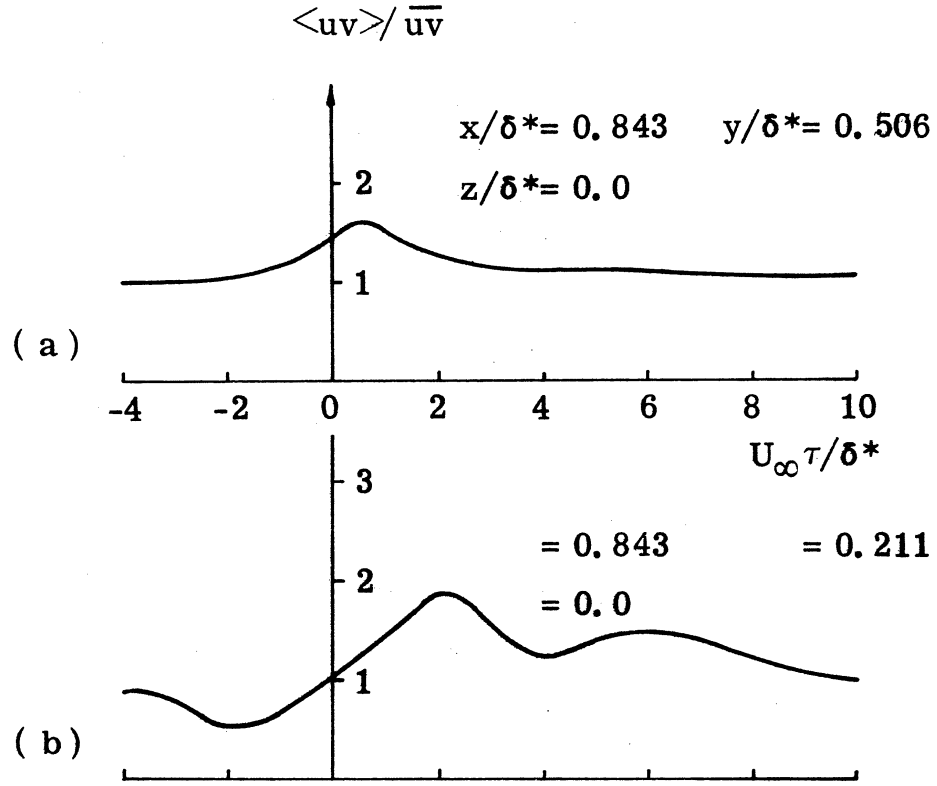

Fig. 28. Sampled Reynolds Stress.
u_w/u'_w = -1, - slope.

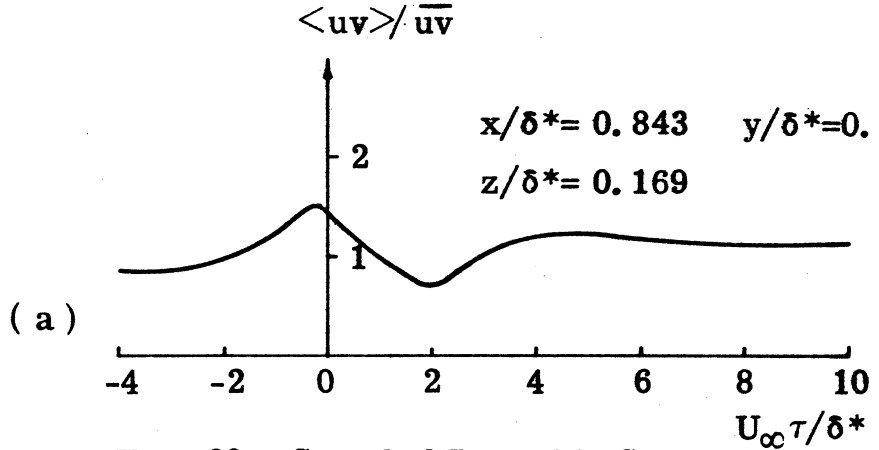

Eig. 29. Sampled Reynolds Stress.
u_w/u'_w = -1, - slope.

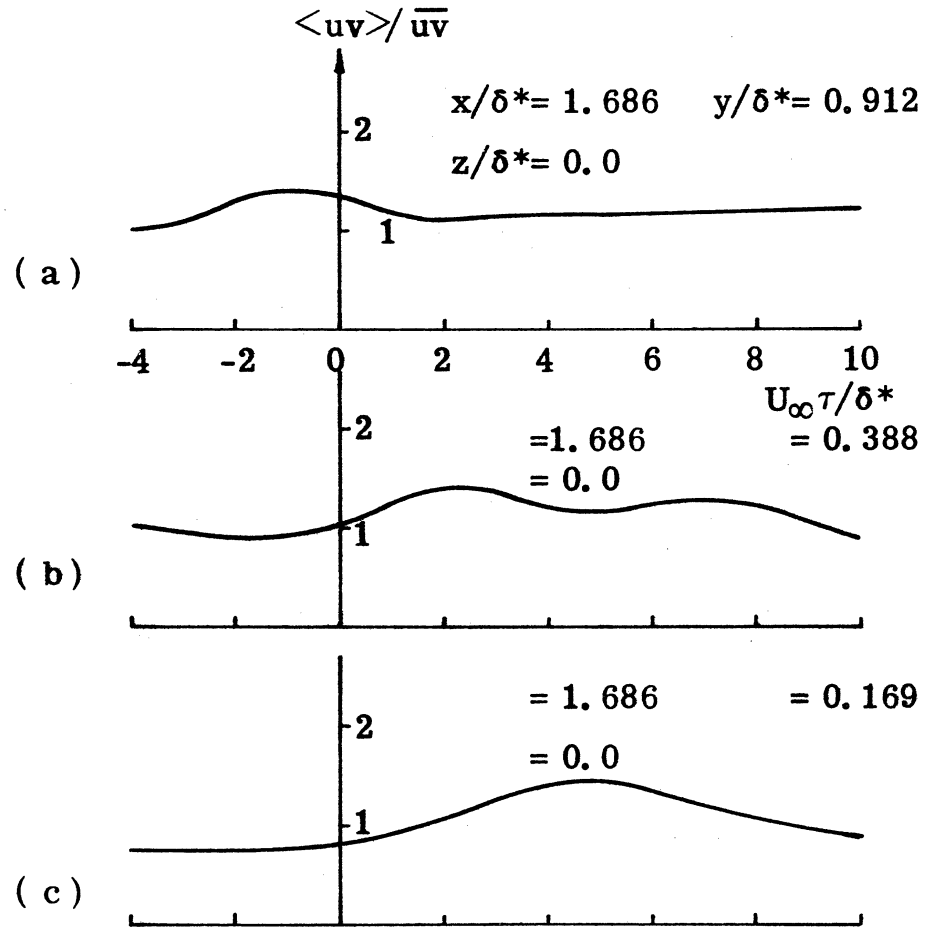

Fig. 30. Sampled Reynolds Stress.
$u_w/u'_w = -1$, - slope.

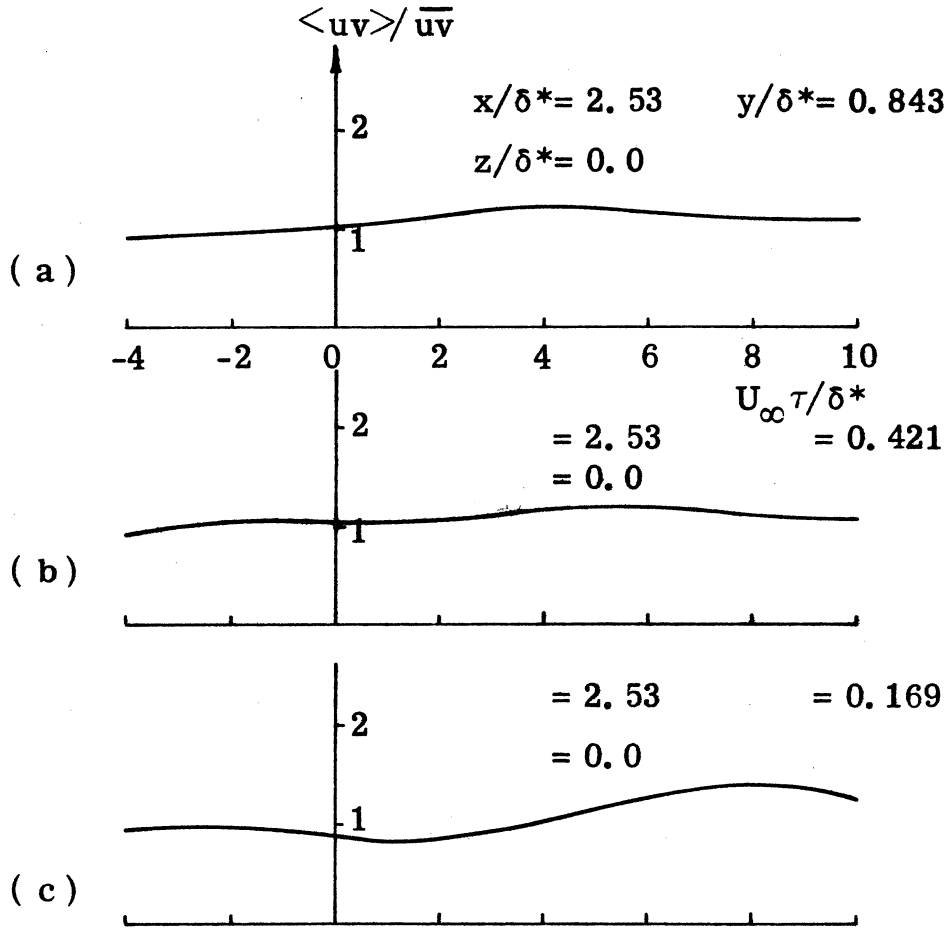

Fig. 31. Sampled Reynolds Stress.
$u_w/u'_w = -1$, - slope.

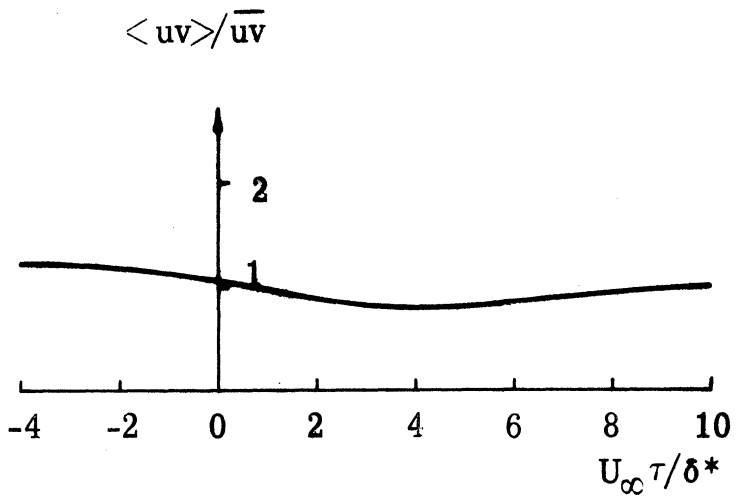

Fig. 32. Sampled Reynolds Stress Obtained using Sampling Conditions of $u_w/u'_w = +1$ and + slope of u_w at $x/\delta^* = 0.$, $y/\delta^* = 0.118$, $z/\delta^* = 0.$

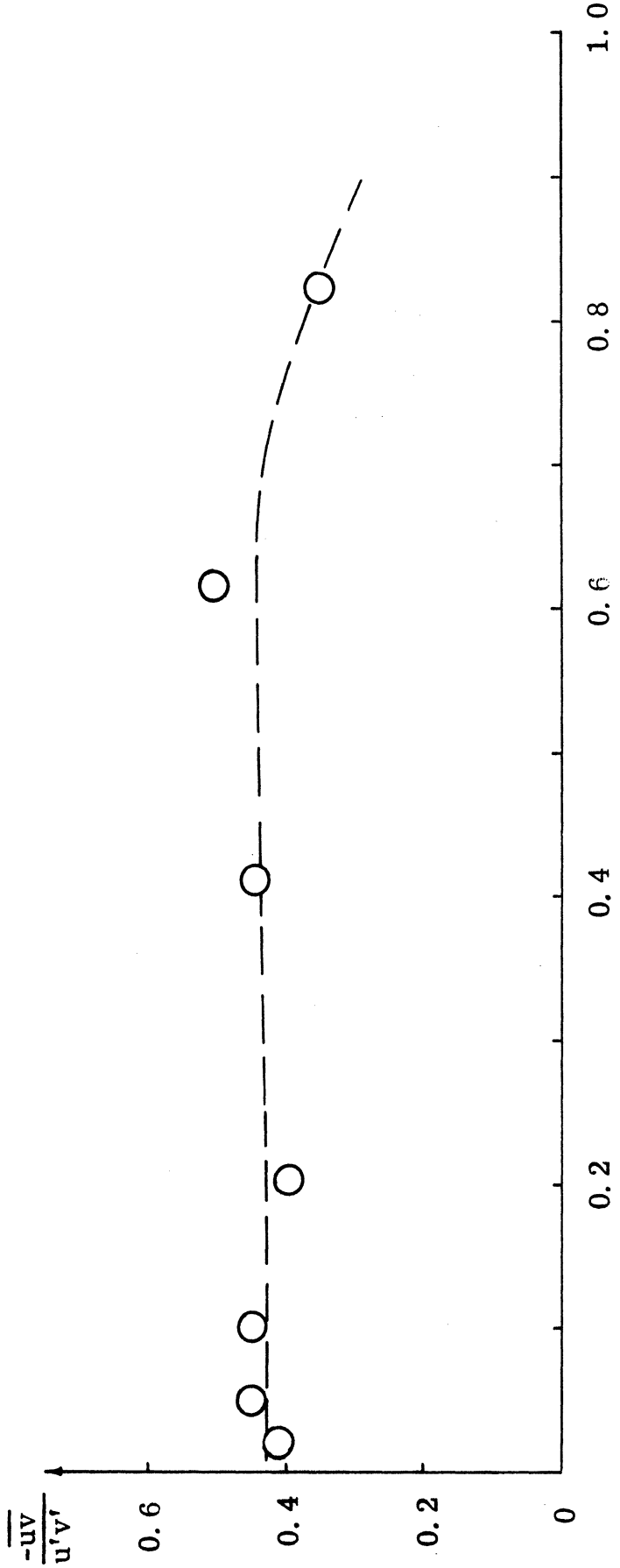

Fig. 33. Measurements of Correlation Coefficients in a Turbulent Boundary Layer with $U_\infty \approx 20$ ft/sec.

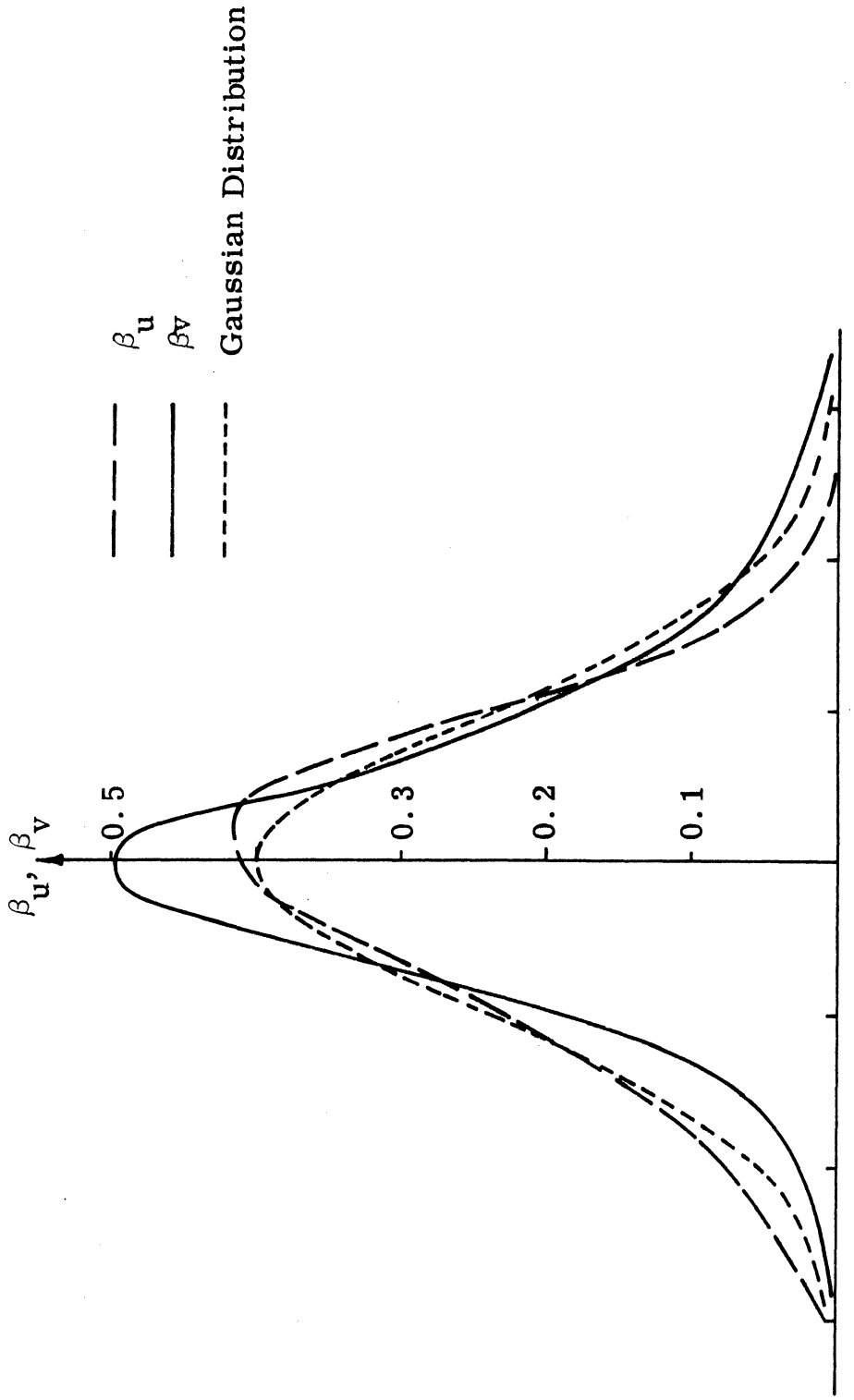

Fig. 34. Probability Density Distributions of u and v Measured at $y^+ = 30.5$ in a Turbulent Boundary Layer with $U_\infty \approx 20$ ft/sec.

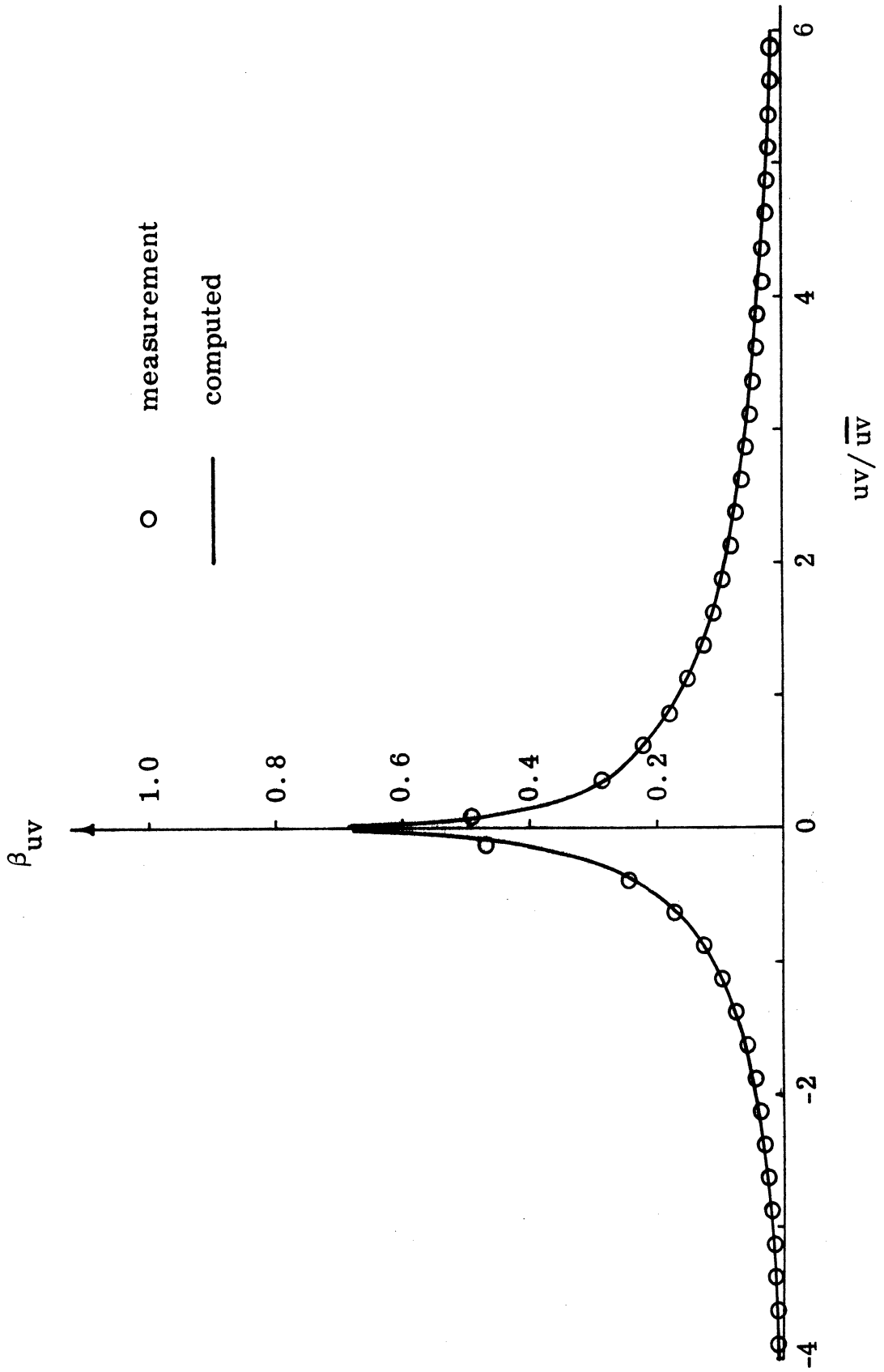

Fig. 35. Probability Density Distribution of the uv Signal Obtained from a Hot Wire Probe at a Distance of $y/\delta^* = 0.912$ from the Wall in a Turbulent Boundary Layer with $U_\infty \approx 20$ ft/sec.

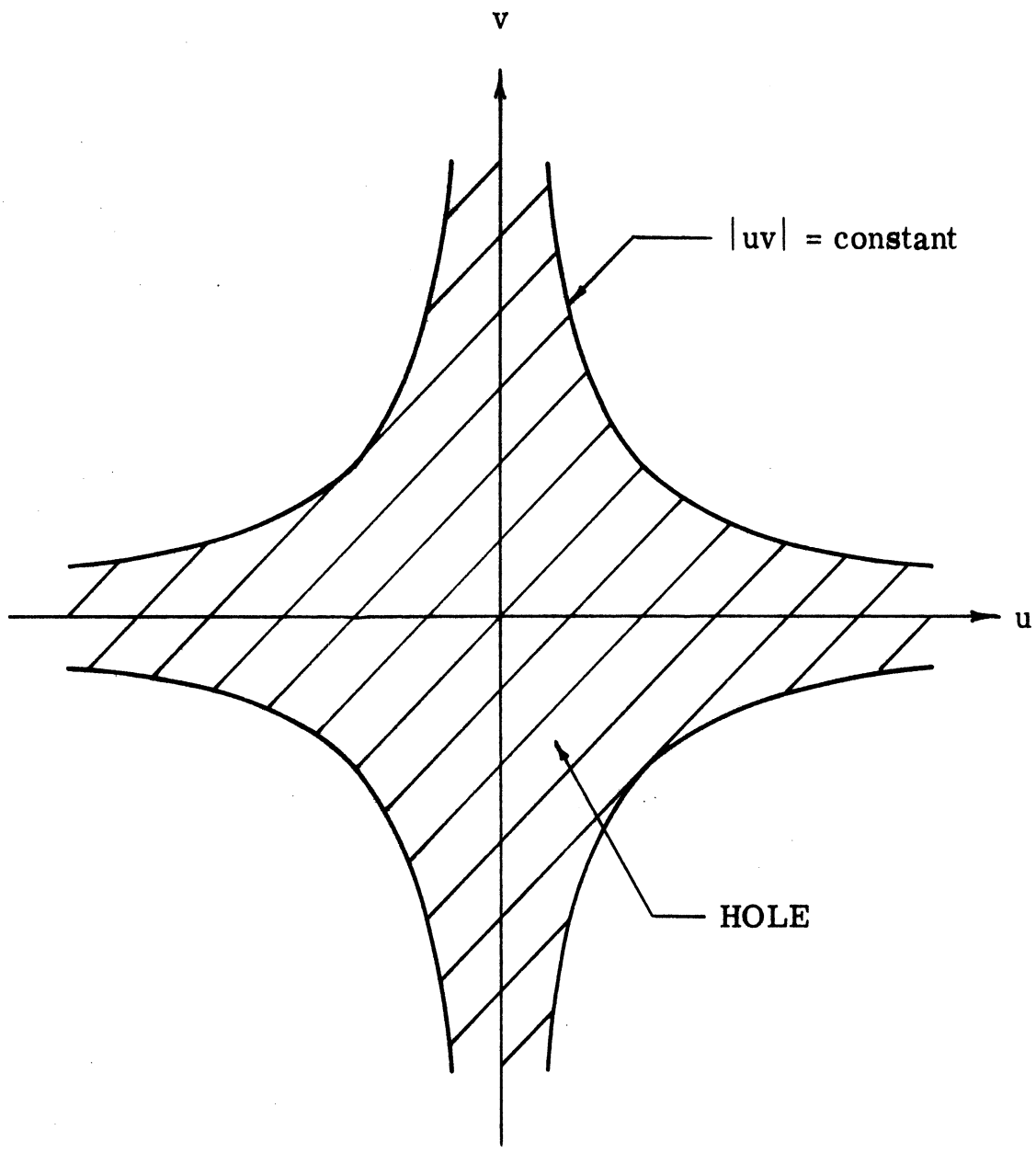

Fig. 36. Sketch of "Hole" Region in the u-v Plane.

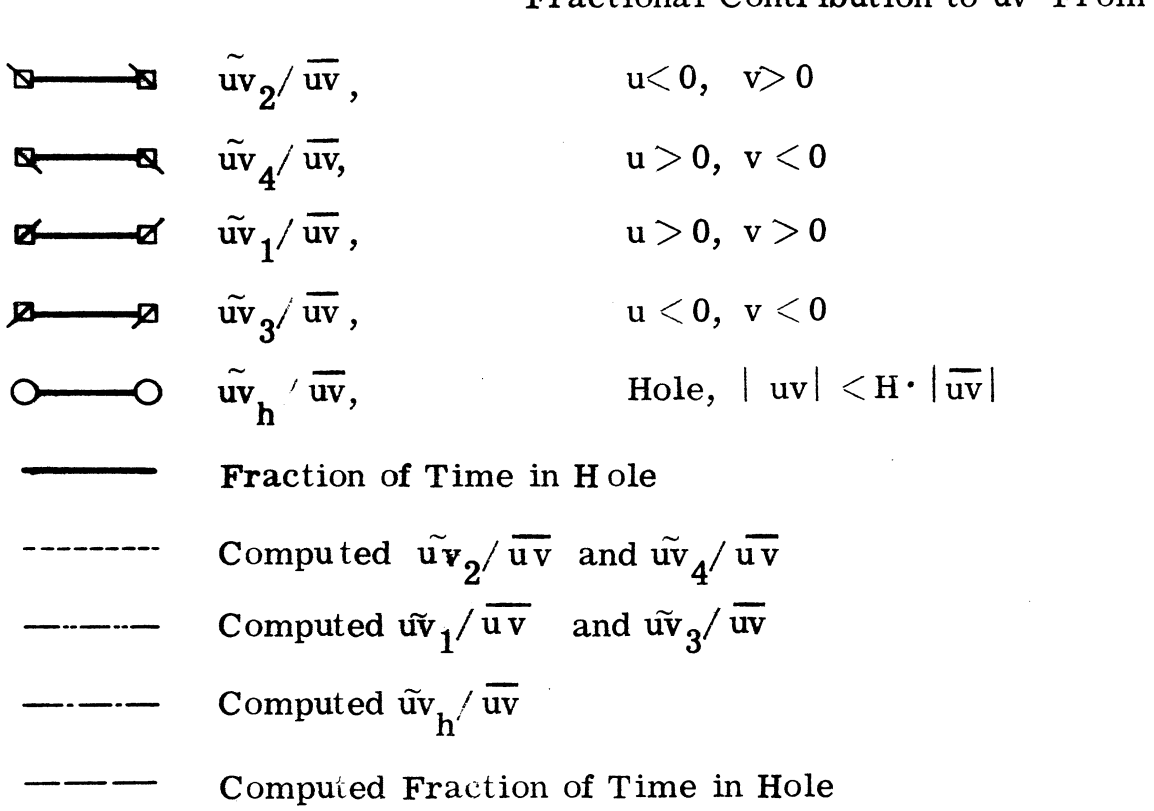

Fig. 37a. Contributions to $\overline{uv}$ from Different Events Measured at a Distance of $y/\delta = 0.021$ from the Wall in a Turbulent Boundary Layer with $U_\infty \approx 20$ ft/sec., or $Re_\theta = 4,230$.

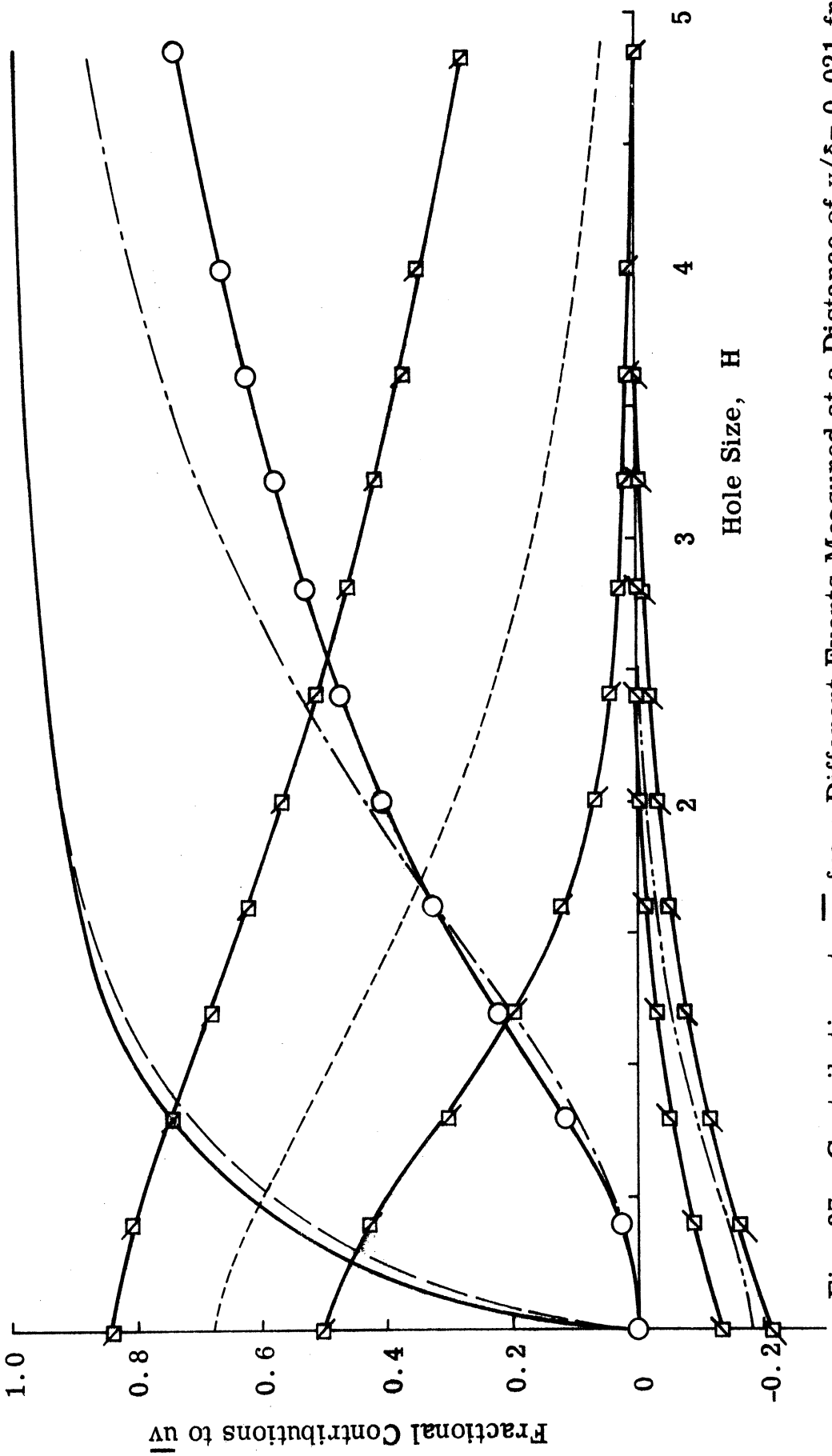

Fig. 37a. Contributions to $\overline{uv}$ from Different Events Measured at a Distance of $y/\delta = 0.021$ from the Wall in a Turbulent Boundary Layer with $U_\infty \approx 20$ ft/sec., or, $Re_\theta \approx 4,230$.

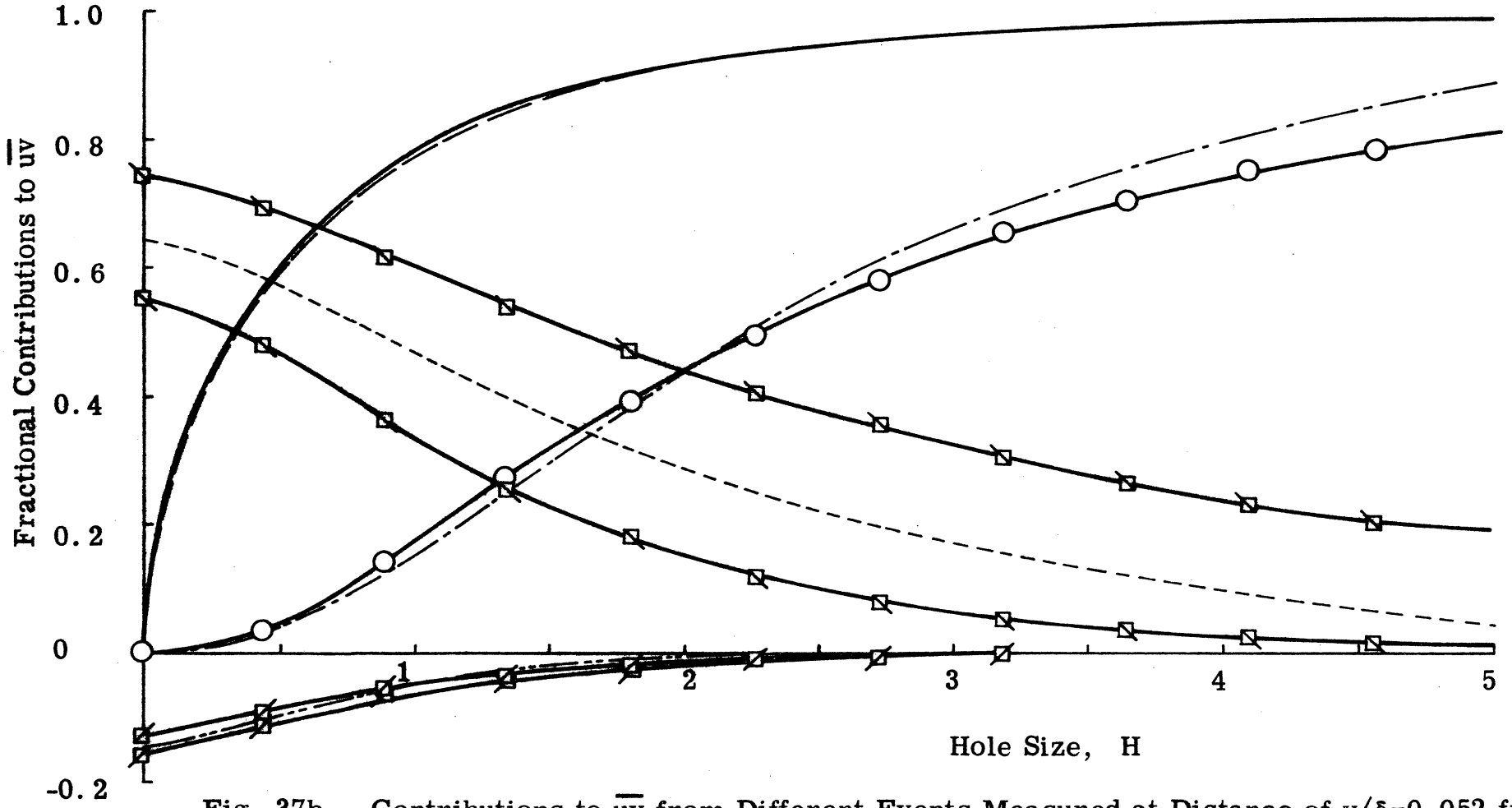

Fig. 37b. Contributions to $\overline{uv}$ from Different Events Measured at Distance of $y/\delta=0.052$ from the Wall in a Turbulent Boundary Layer with $U_\infty \approx 20$ ft/sec., or, $Re_\theta \approx 4,230$. (See Fig. 37a for Captions)

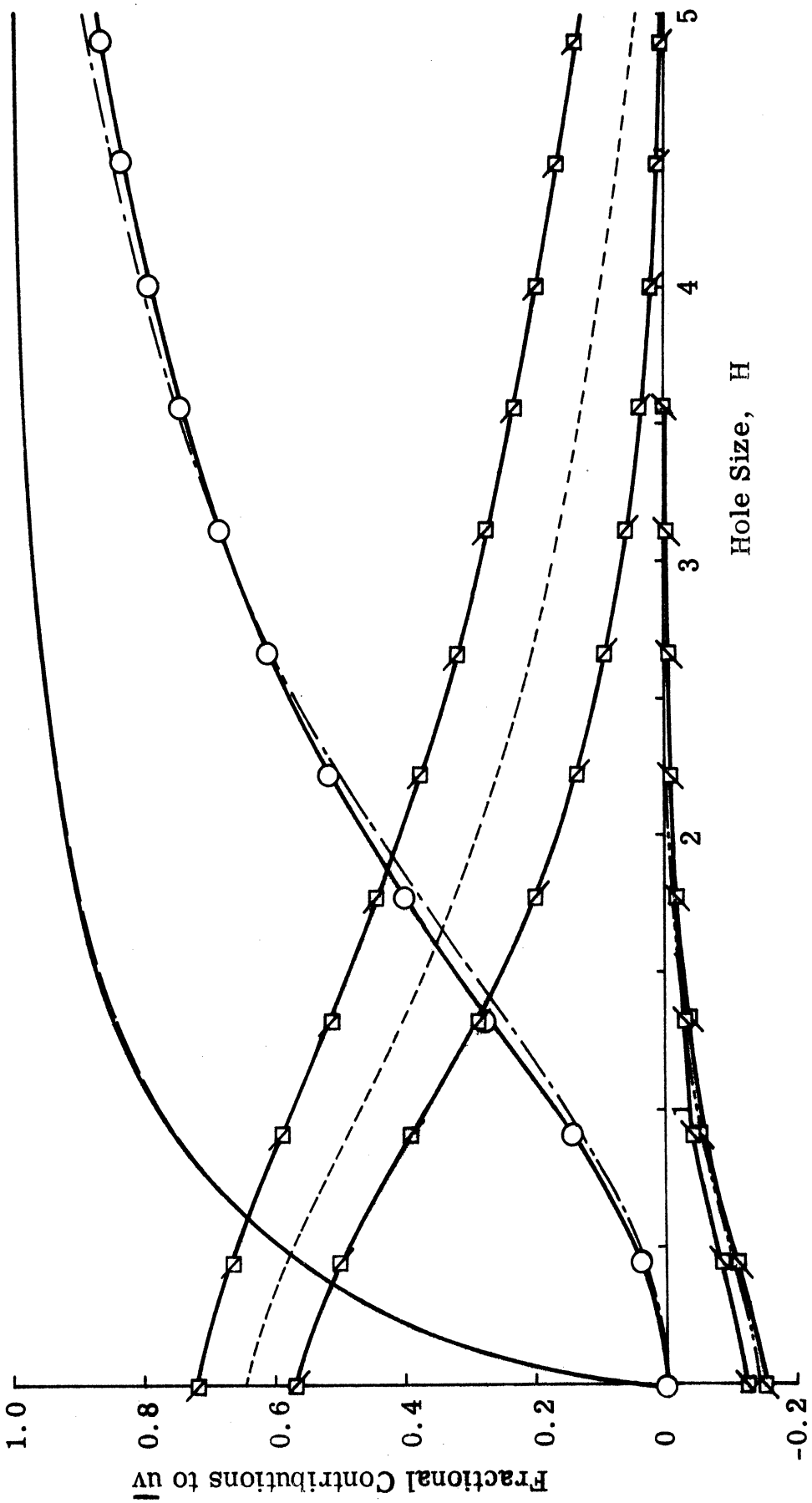

Fig. 37c. Contributions to $\overline{uv}$ from Different Events Measured at $y/\delta = 0.103$ from the Wall. $U_\infty \approx 20$ ft/sec., or, $Re_\theta \approx 4,230$. (See Fig. 37a for Captions)

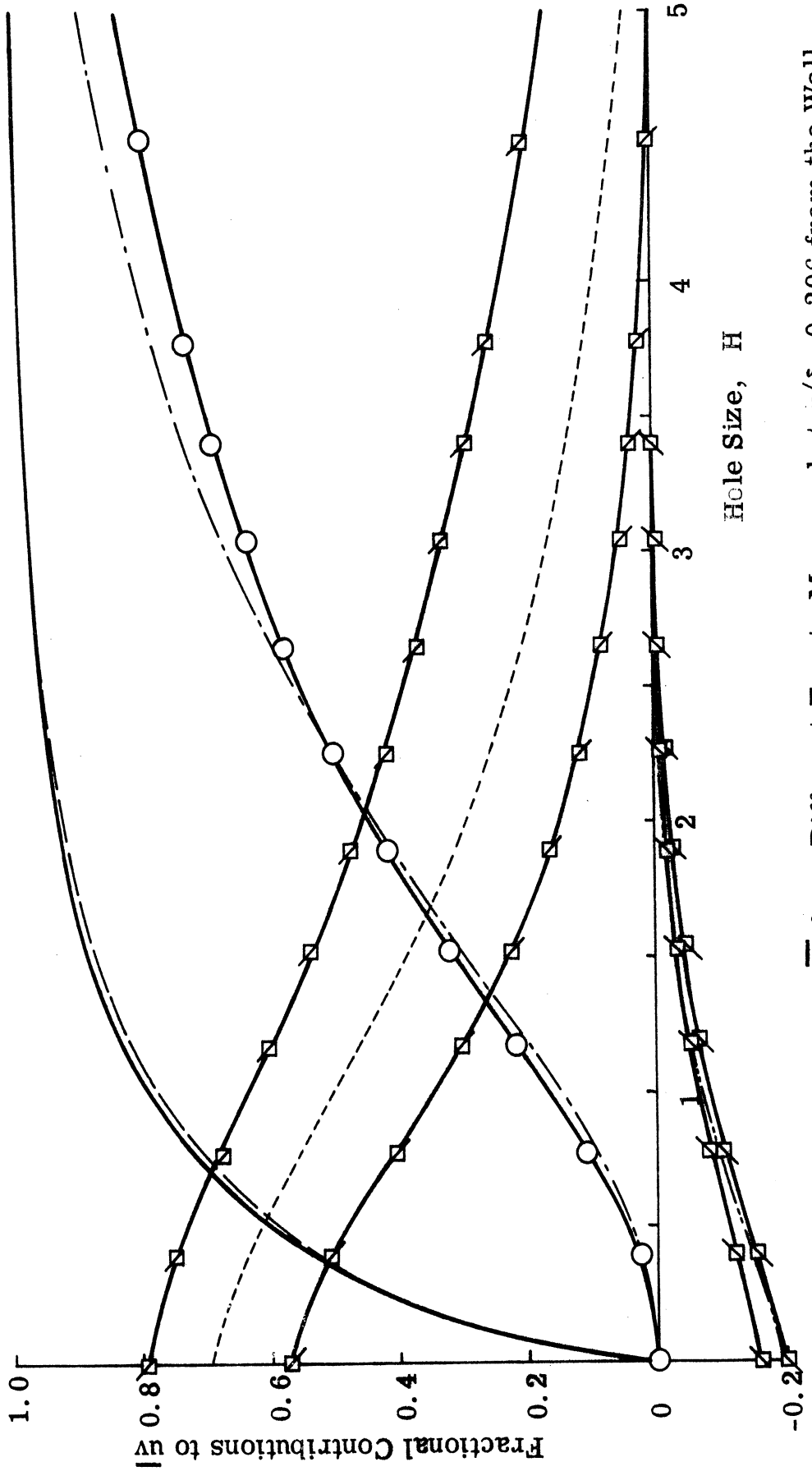

Fig. 37d. Contributions to $\overline{uv}$ from Different Events Measured at $y/\delta = 0.206$ from the Wall. $U_\infty \approx 20$ ft/sec., or, $Re_\theta \approx 4,230$. (See Fig. 37a for Captions)

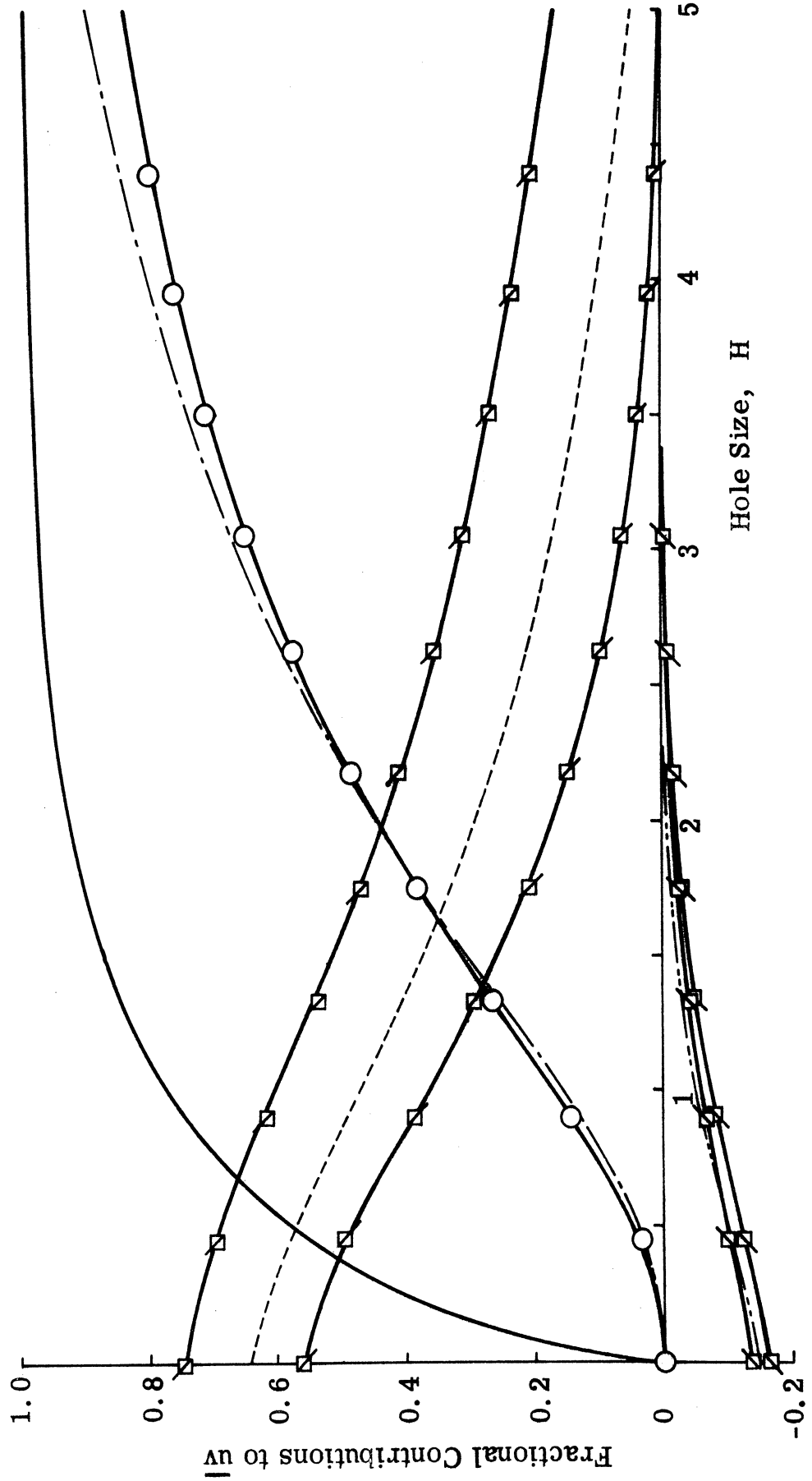

Fig. 37e. Contributions to $\overline{uv}$ from Different Events Measured at $y/\delta = 0.412$ from the Wall. $U_\infty \approx 20$ ft/sec., or, $Re_\theta \approx 4,230$. (See Fig. 37a for Captions)

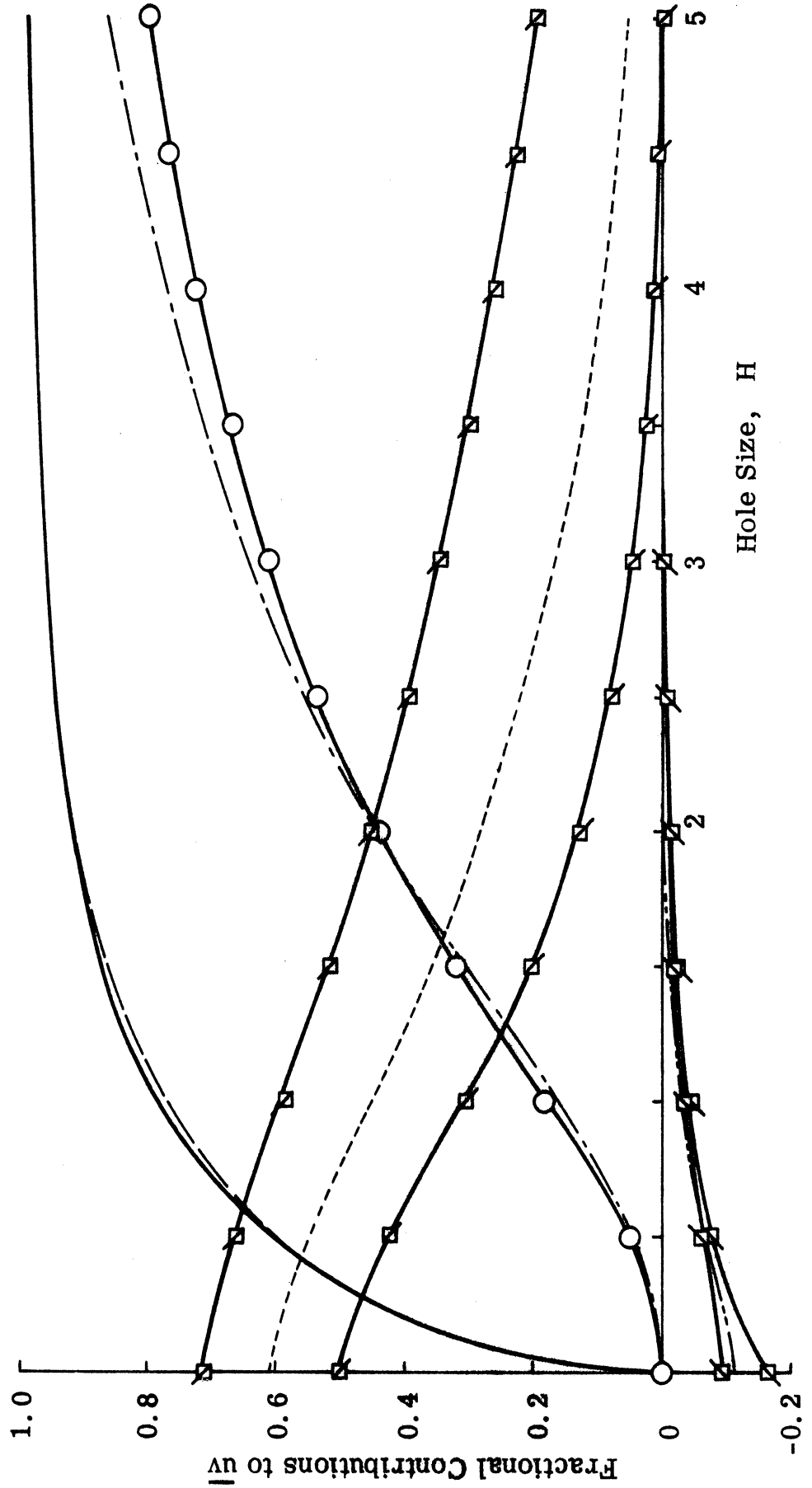

Fig. 37f. Contributions to $\overline{uv}$ from Different Events Measured at $y/\delta = 0.618$ from the Wall. $U_\infty \approx 20$ ft/sec., or, $Re_\theta \approx 4,230$. (See Fig. 37a for Captions)

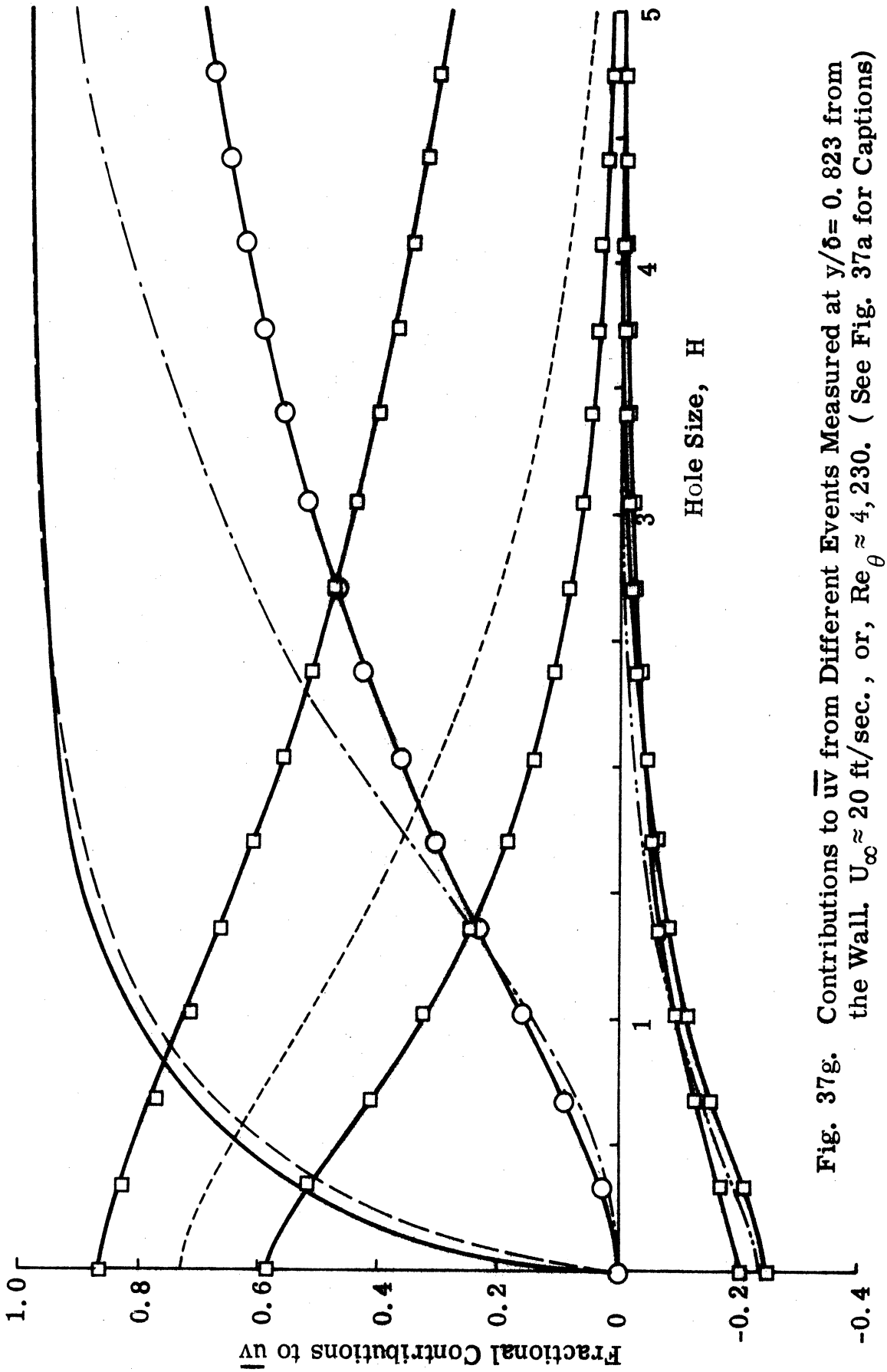

Fig. 37g. Contributions to $\overline{uv}$ from Different Events Measured at $y/\delta = 0.823$ from the Wall. $U_\infty \approx 20$ ft/sec., or, $Re_\theta \approx 4,230$. (See Fig. 37a for Captions)

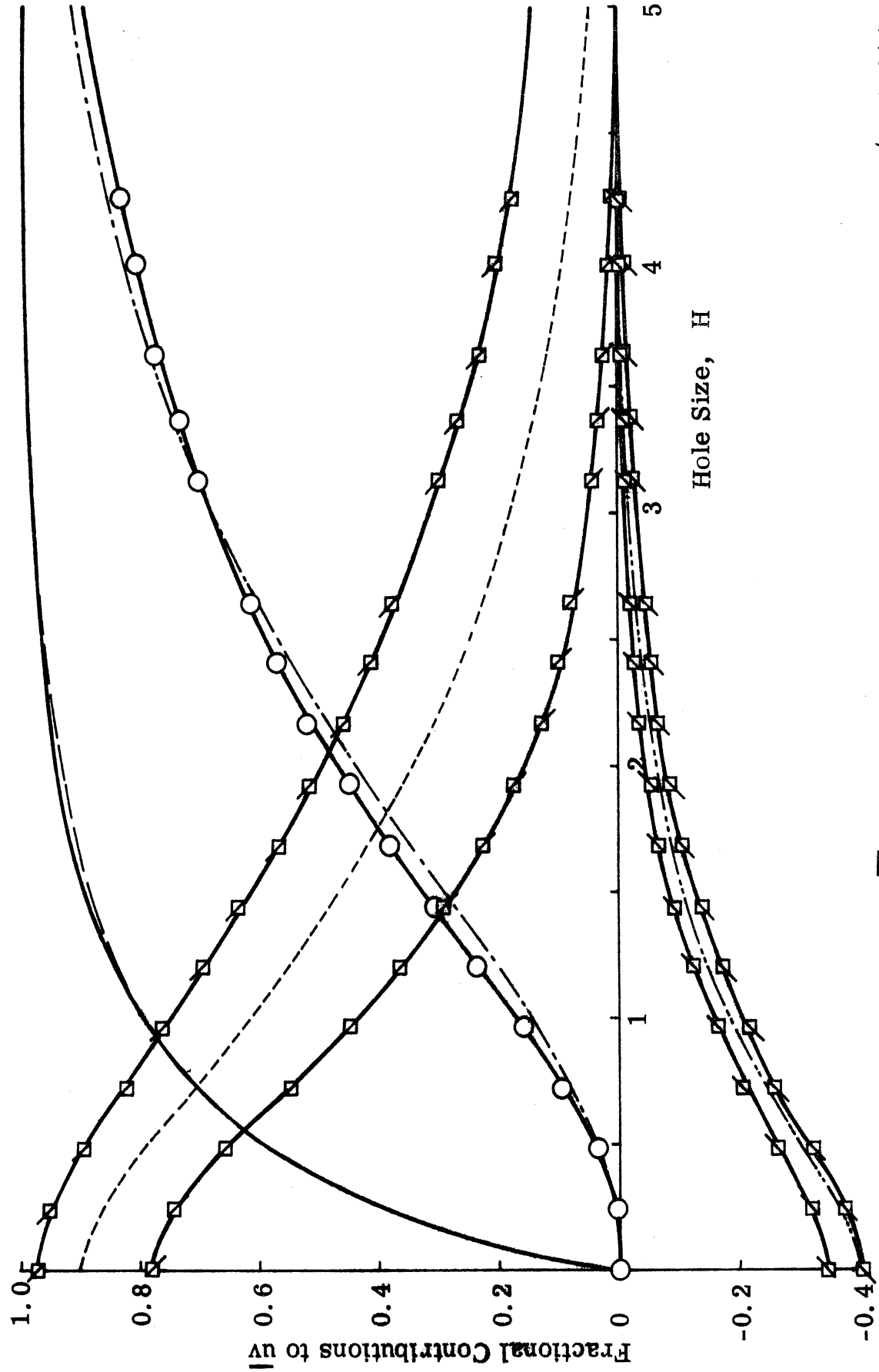

Fig. 38. Contributions to $\overline{uv}$ from Different Events Measured at a Distance of $y/\delta = 0.014$, or, $y^+ = 265$ from the Wall in a Turbulent Boundary Layer with $U_\infty \approx 200$ ft/sec., or, $Re_\theta \approx 38,000$. (See Fig. 37a for Captions)

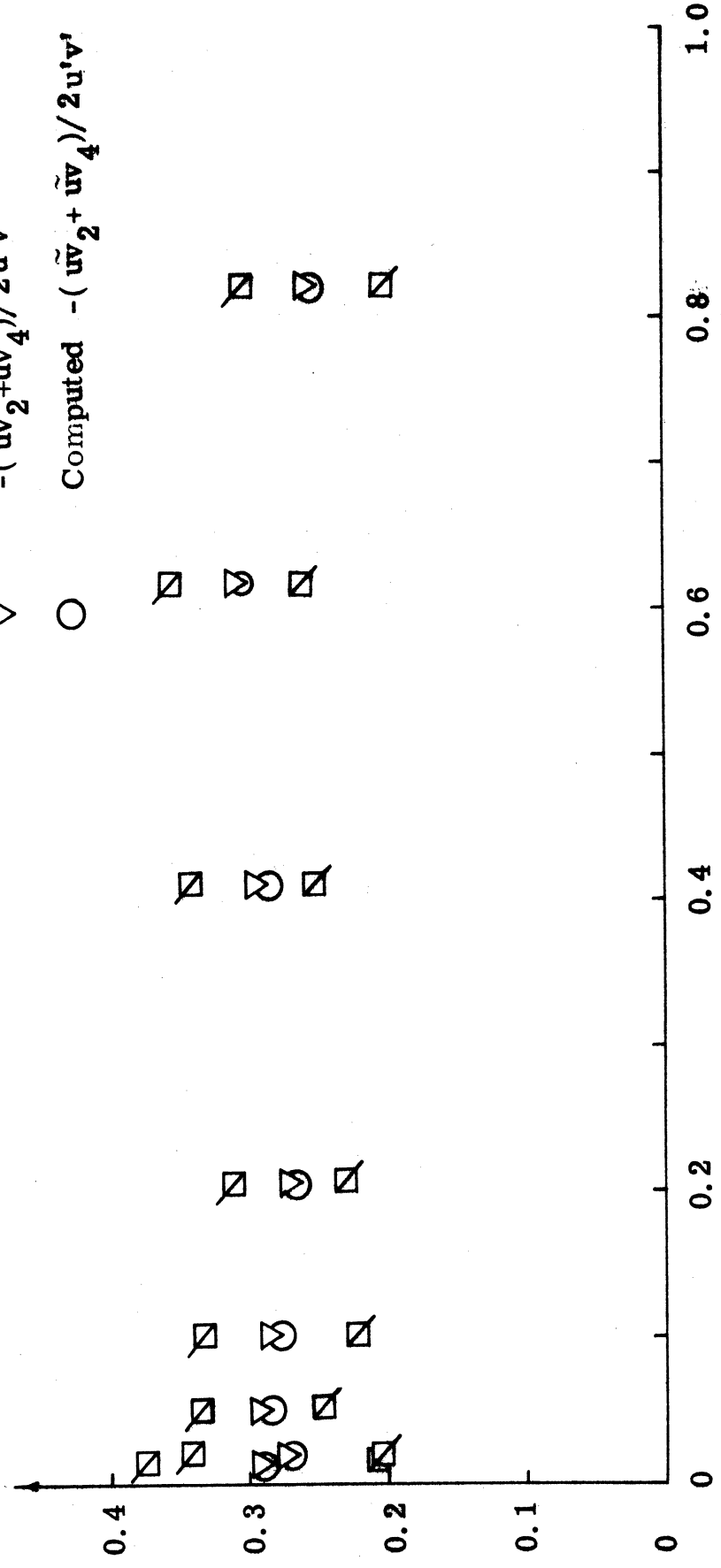

Fig. 39. Distribution of $\tilde{u}\tilde{v}_2/u'v'$ and $\tilde{u}\tilde{v}_4/u'v'$ in a Turbulent Boundary Layer. The Hole Size is Set at H = 0.

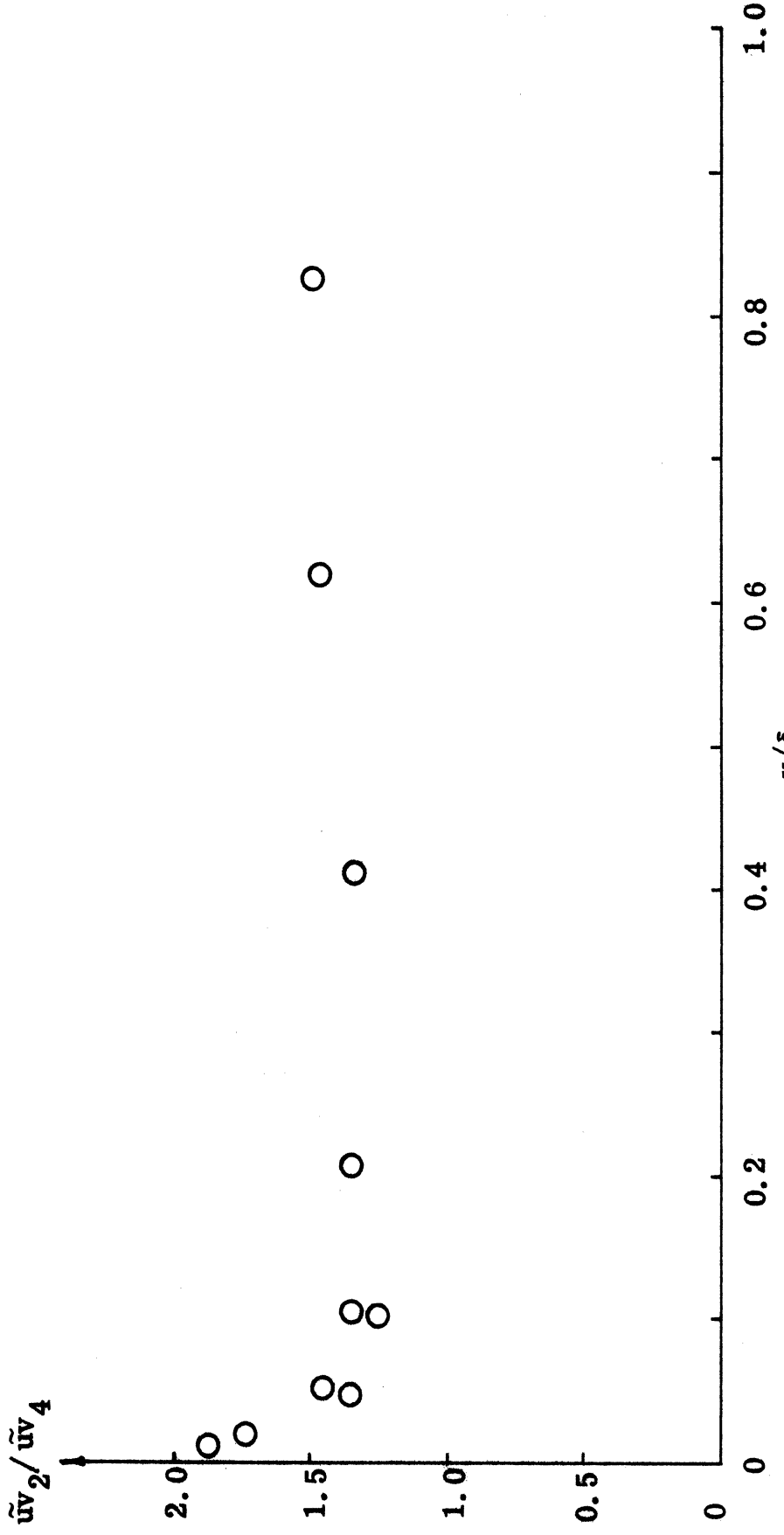

Fig. 40. Distribution of the Ratio, $\tilde{uv}_2/\tilde{uv}_4$, Set at a Hole Size of H = 0 in a Turbulent Boundary Layer with U_∞ = 20 ft/sec., δr, $Re_\theta \approx 4,230$.

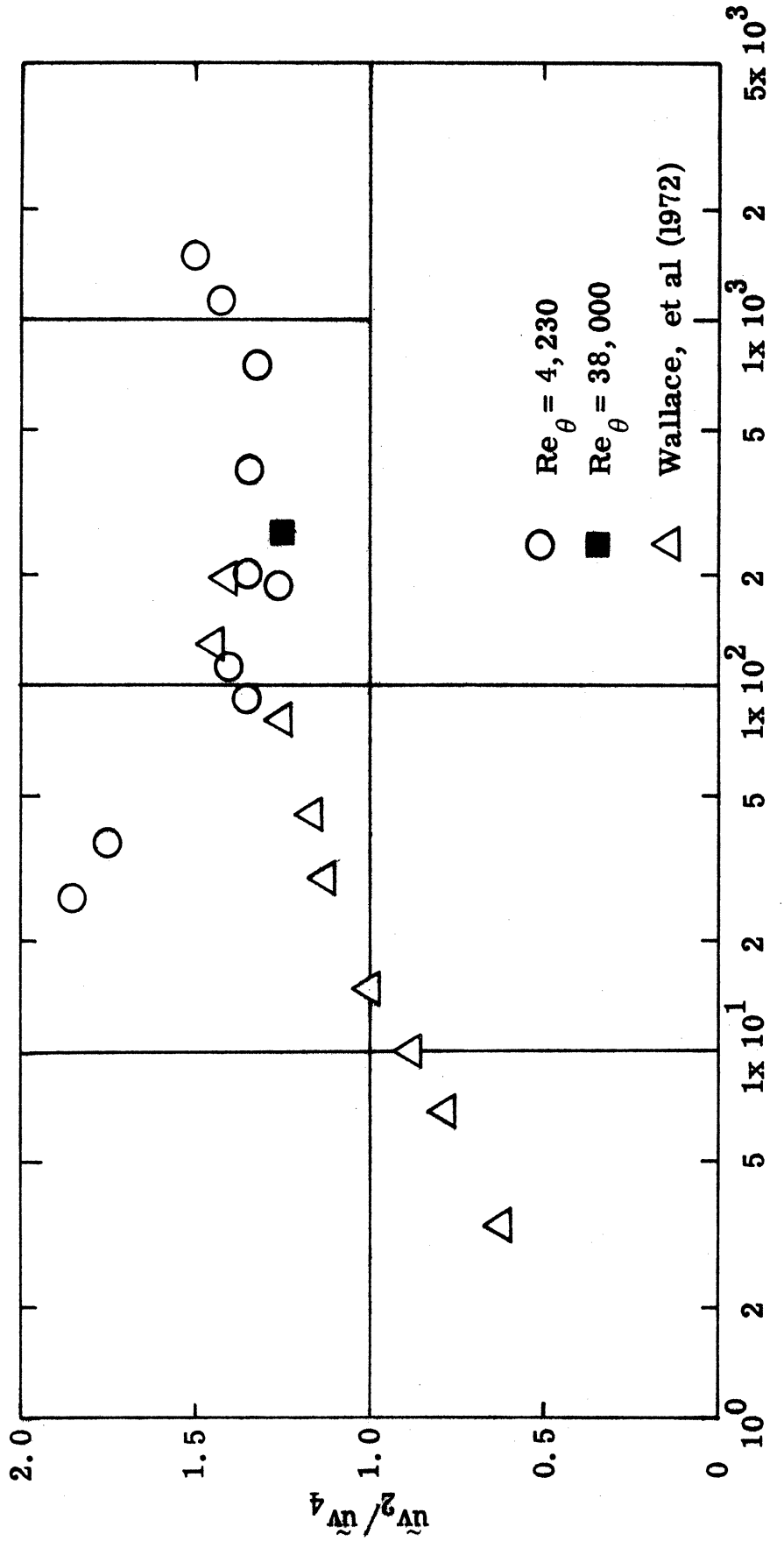

Fig. 41. The Ratio, $\tilde{uv}_2/\tilde{uv}_4$ with H=0, Scales with the Inner Flow Variables.

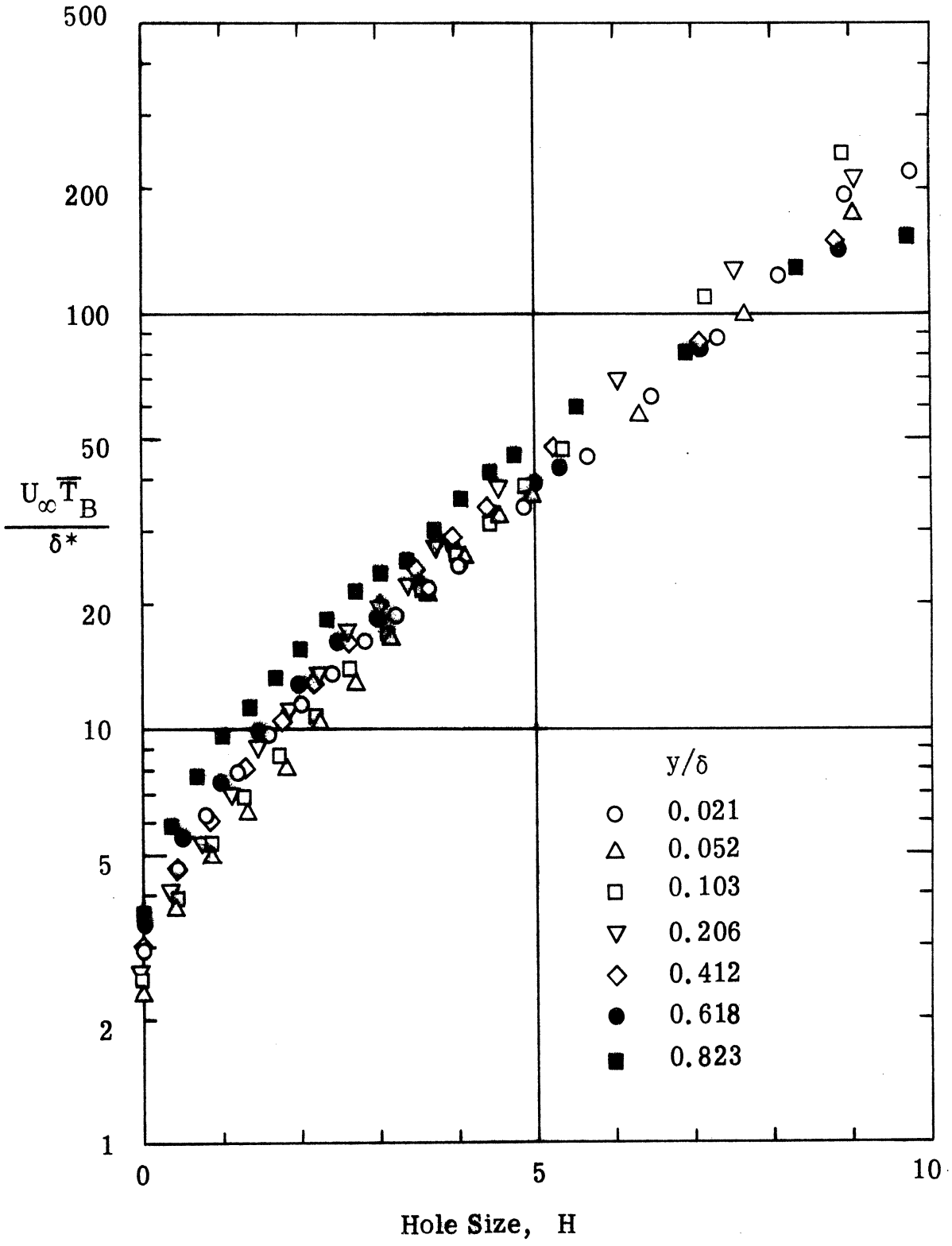

Fig. 42. Mean Time Intervals Between Bursts as a Function of Hole Size, H, Measured Across a Turbulent Boundary Layer with $U_\infty \approx 20$ ft/sec., or, $Re_\theta \approx 4,230$.

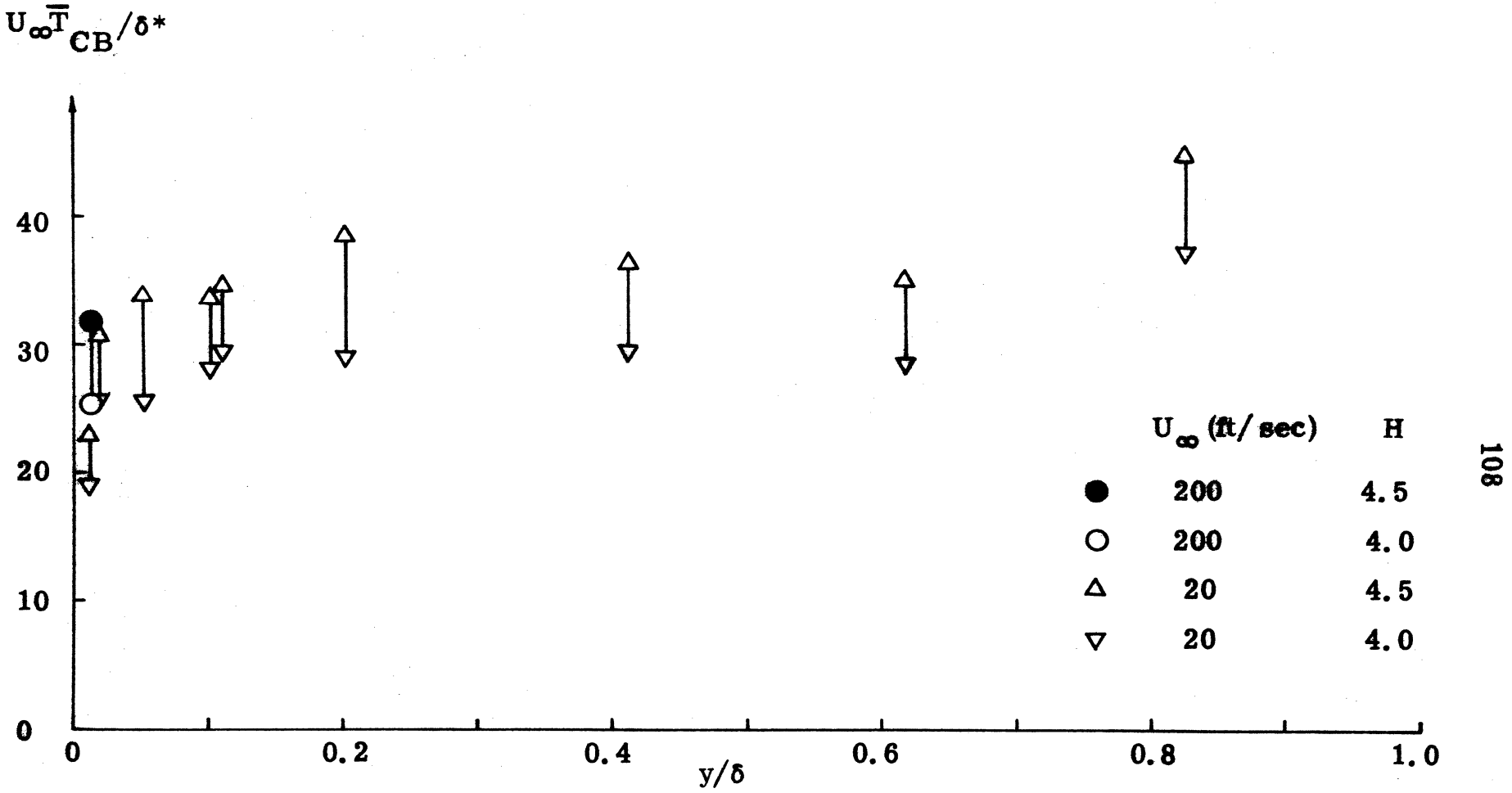

Fig. 43. Characteristic Mean Time Intervals Between Bursts Measured Across a Turbulent Boundary Layer.

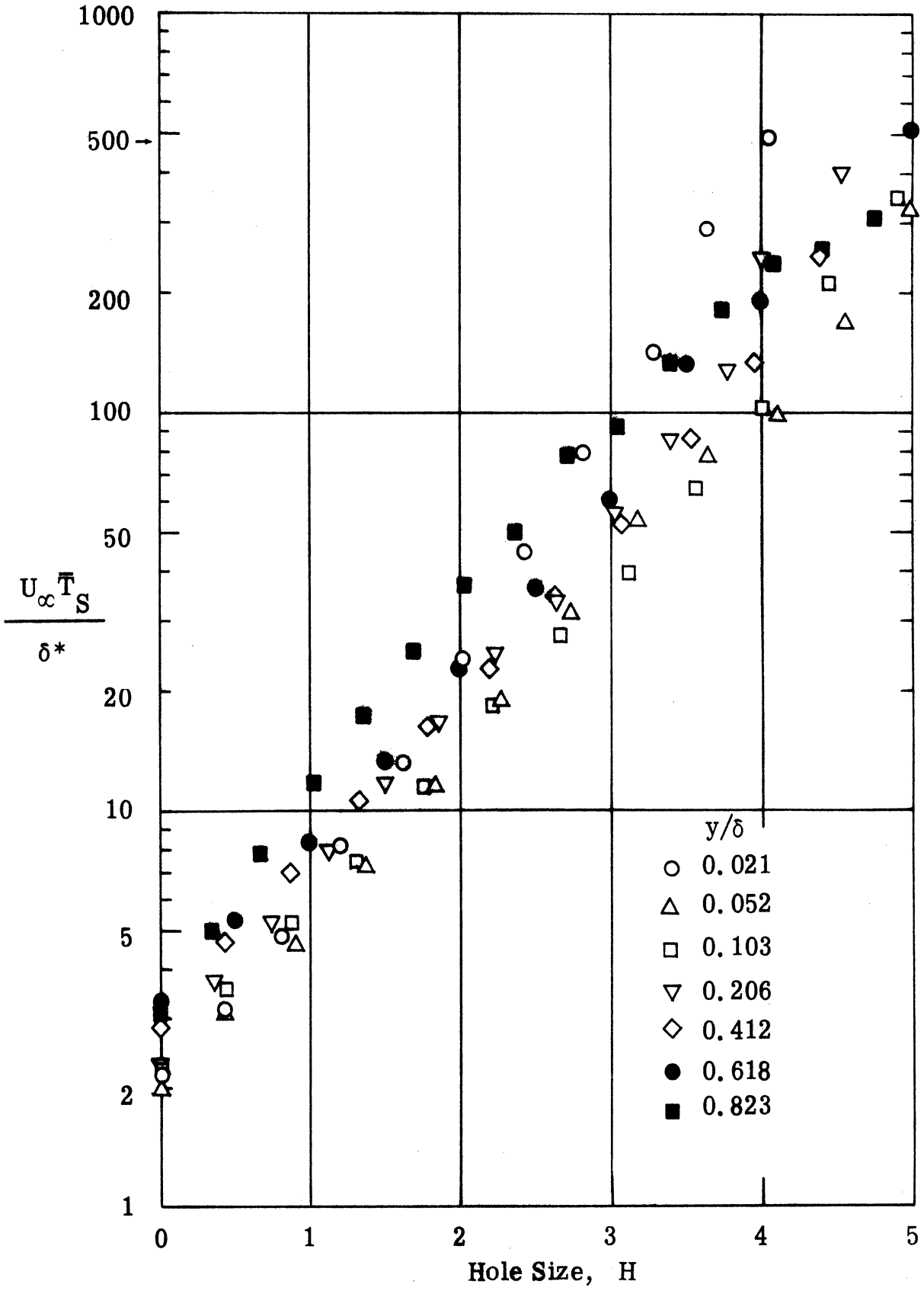

Fig. 44. Mean Time Intervals Between Sweeps as a Function of Hole Size, H, Measured Across a Turbulent Boundary Layer with $U_\infty \approx 20$ ft/sec., or, $Re_\theta \approx 4,230$.

Fig. 45. Characteristic Mean Time Interval Between Sweeps Measured Across a Turbulent Boundary Layer.

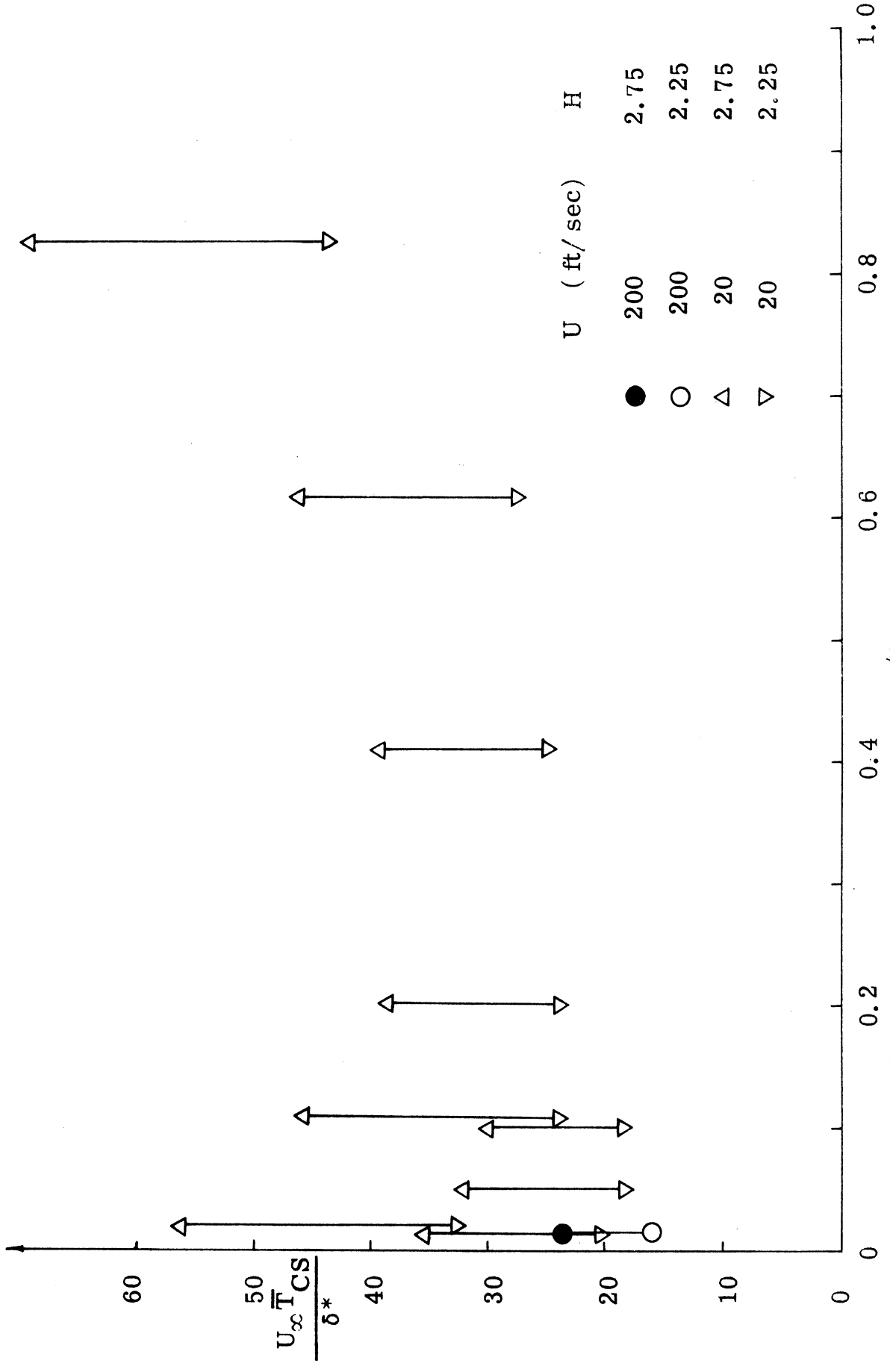
U (ft/sec) H
200 2.75
200 2.25
20 2.75
20 2.25
$\frac{U_\infty \overline{T}_{CS}}{\delta^*}$
60
50
40
30
20
10
0
0.2
0.4
0.6
0.8
1.0
y/δ

Fig. 45.

Fig. 46. Time Scales of Bursts as a Function of Hole Size, H, Measured Across a Turbulent Boundary Layer with $U_\infty \approx 20$ ft/sec., or, $Re_\theta \approx 4,230$.

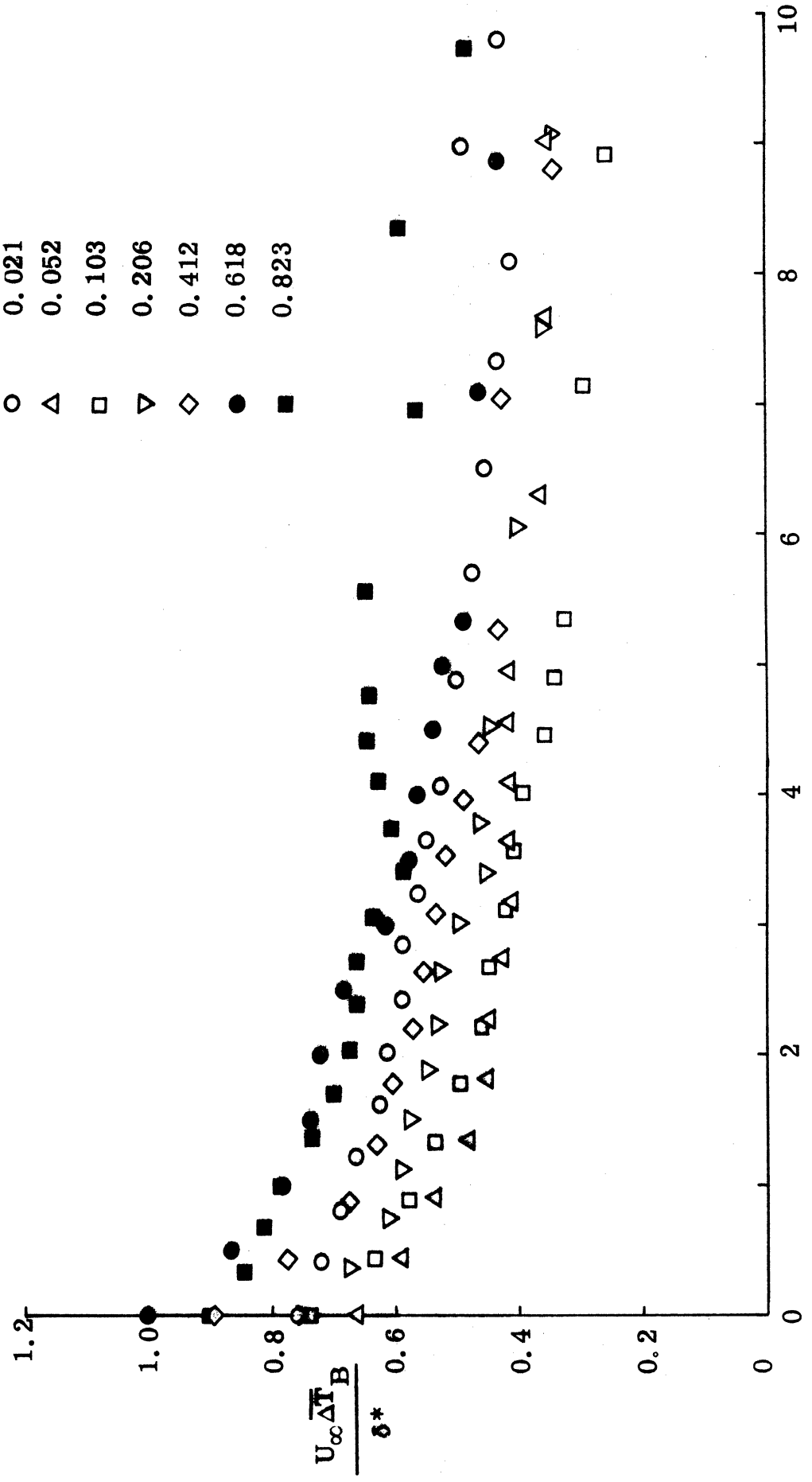
y/δ
0.021
0.052
0.103
0.206
0.412
0.618
0.823
$\frac{U_\infty \overline{\Delta T}_B}{\delta^*}$
1.2
1.0
0.8
0.6
0.4
0.2
0
0
2
4
6
8
10
Hole Size, H

Fig. 46.

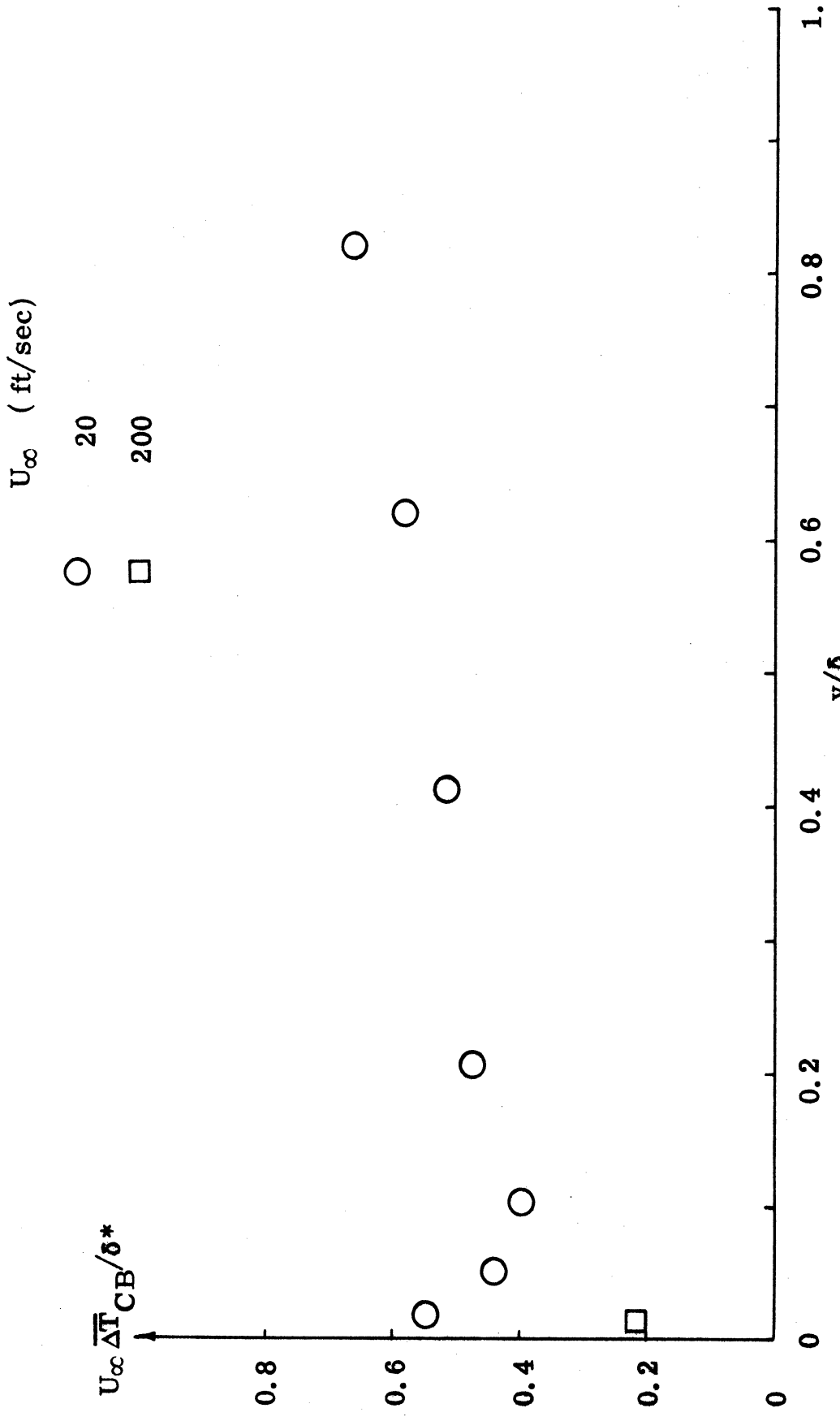

Fig. 47. Characteristic Time Scale of Bursts Measured Across a Turbulent Boundary Layer with H = 4 ~ 4.5.

Fig. 48. Time Scale of Sweeps as a Function of Hole Size, H, Measured Across a Turbulent Boundary Layer with $U_\infty \approx 20$ ft/sec., or, $Re_\theta \approx 4,230$.

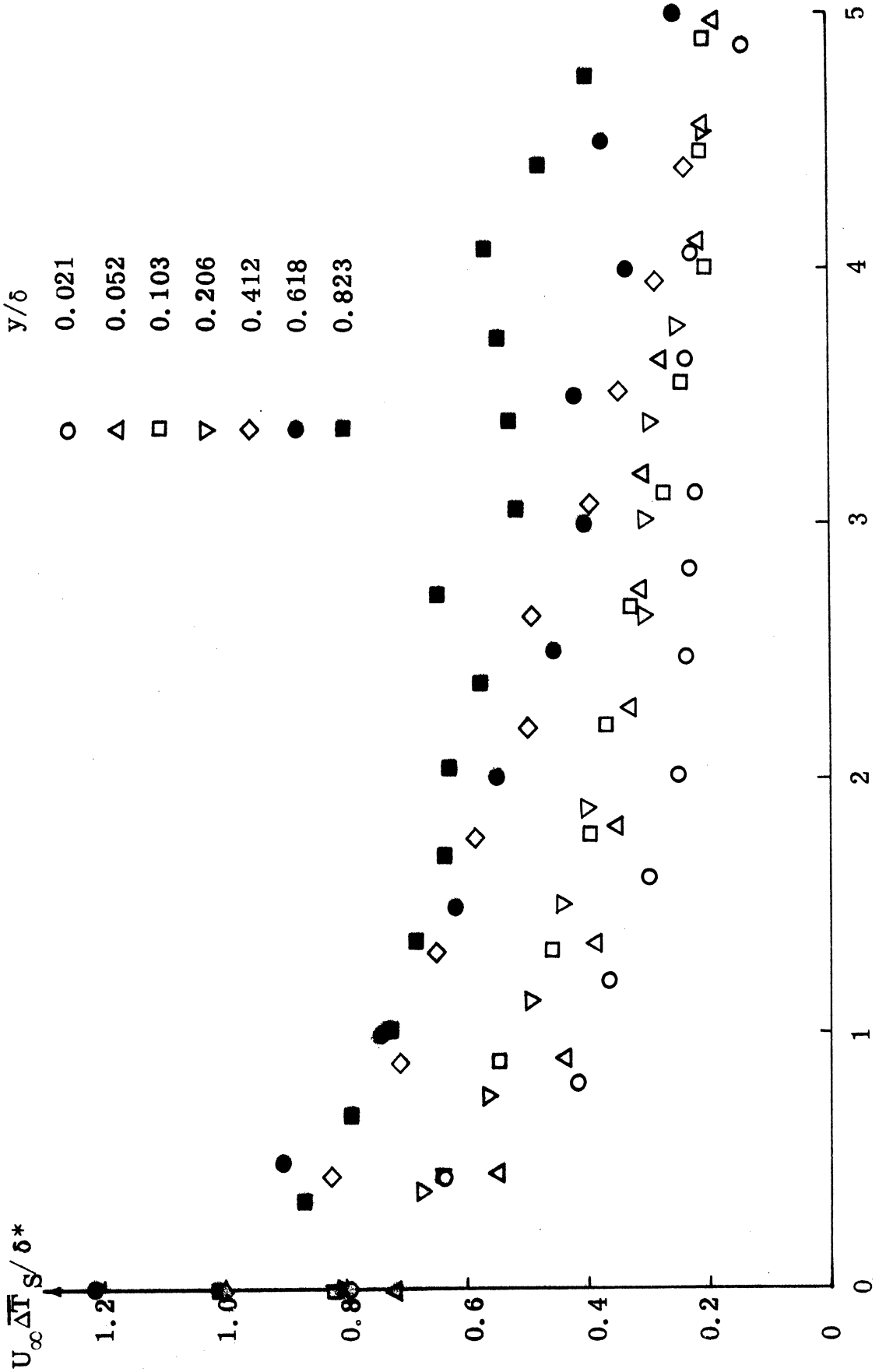
y/δ
0.021
0.052
0.103
0.206
0.412
0.618
0.823
$U_\infty \overline{\Delta T}_s / \delta^*$
1.2
1.0
0.8
0.6
0.4
0.2
0
0
1
2
3
4
5
Hole Size, H

Fig. 48.

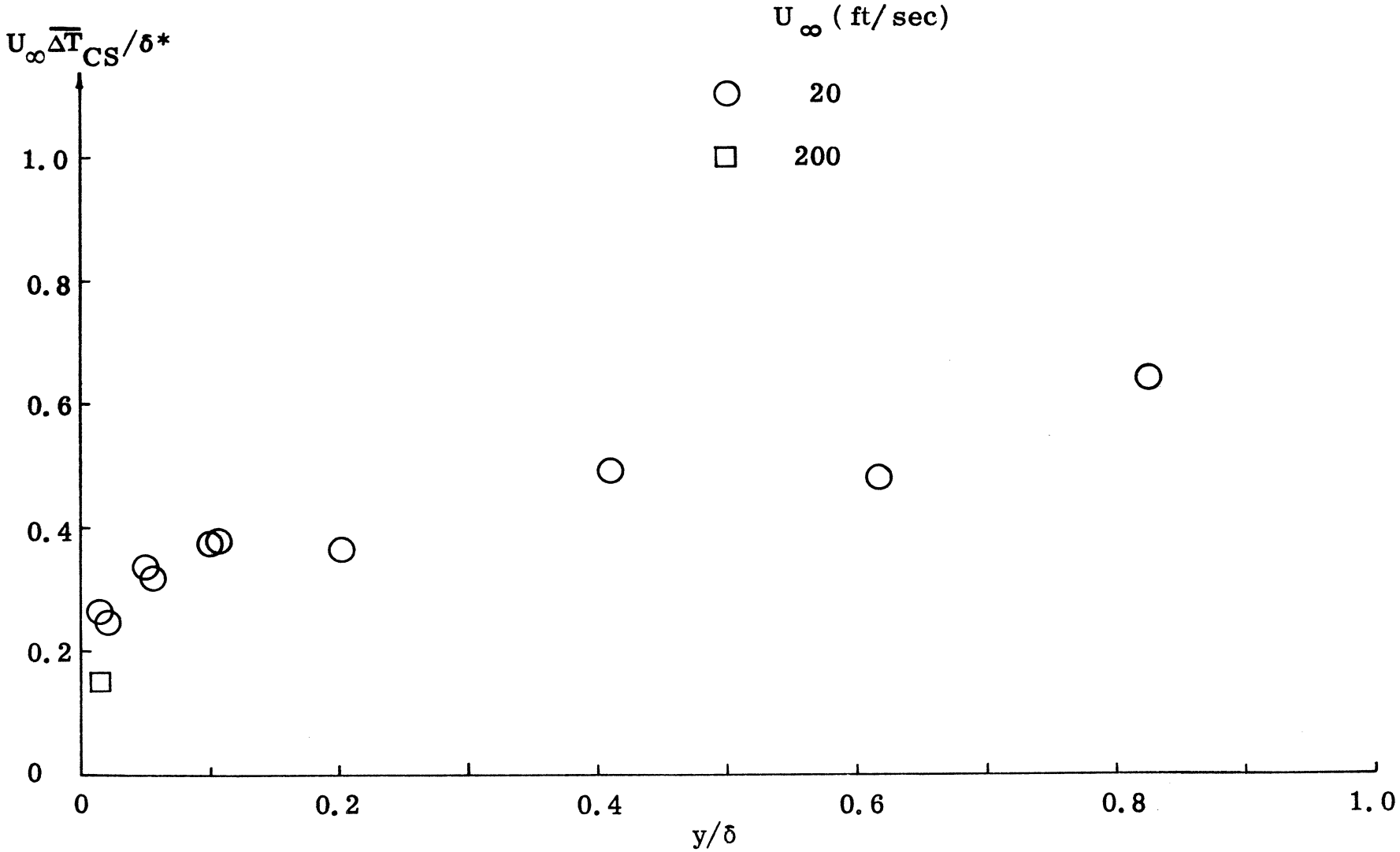

Fig. 49. Characteristic Time Scale of Sweeps Measured Across a Turbulent Boundary Layer with H ≈ 2.25 ~ 2.75.

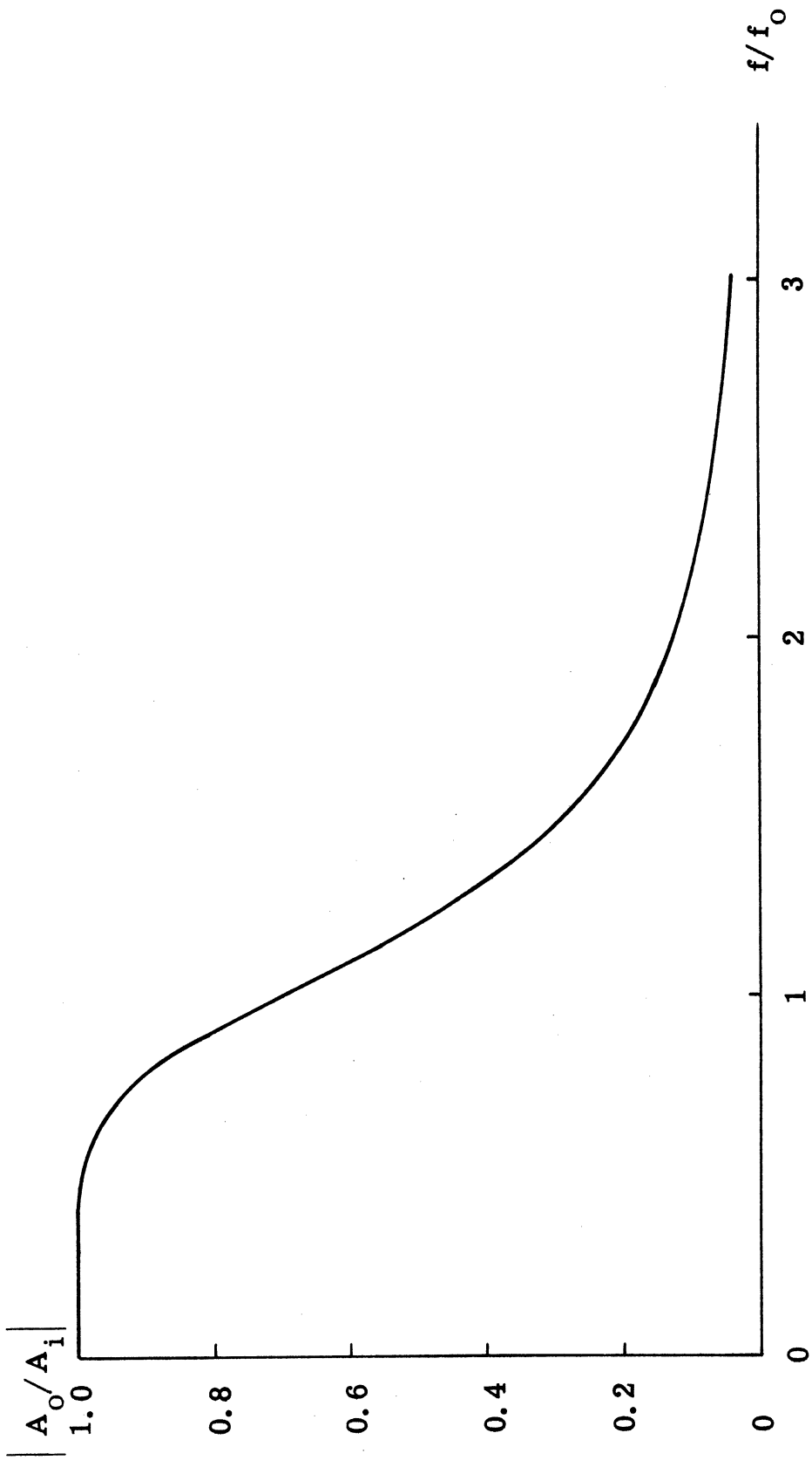

Fig. A1. Gain of the Third Order Low Pass Butterworth Filter.

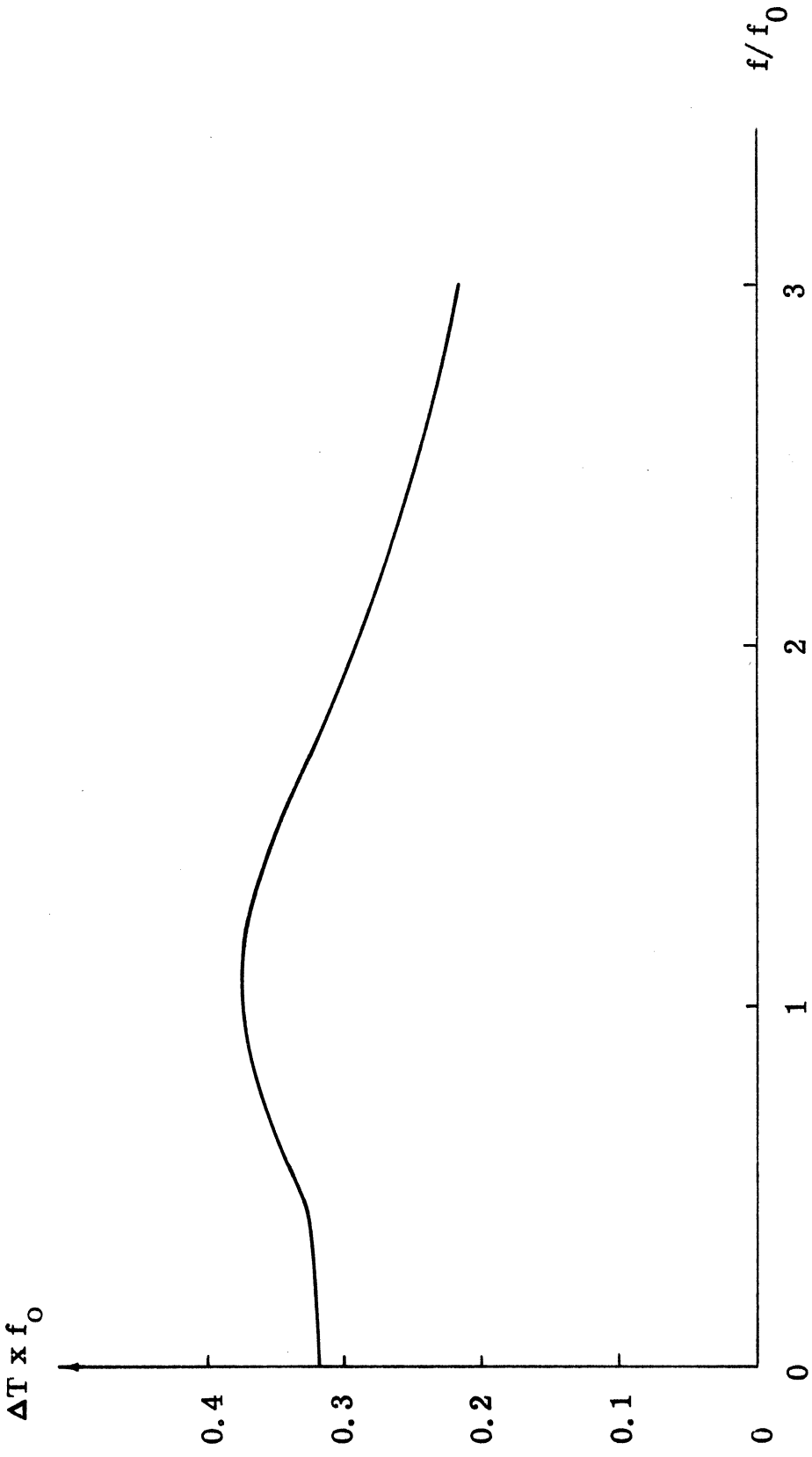

Fig. A2. Time Lag of Signal Passing Through a Third Order Low Pass Butterworth Filter.

Unclassified

Security Classification

DOCUMENT CONTROL DATA - R & D

(Security classification of title, body of abstract and indexing annotation must be entered when the overall report is classified)

1. ORIGINATING ACTIVITY (Corporate author)
The University of Michigan
Dept. of Aerospace Eng., Gas Dynamics Laboratory
Ann Arbor, Michigan 48104

2a. REPORT SECURITY CLASSIFICATION
Unclassified

2b. GROUP
Not applicable

3. REPORT TITLE

The Structure of the Reynolds Stress in a Turbulent Boundary Layer

4. DESCRIPTIVE NOTES (Type of report and inclusive dates)
Technical Report

5. AUTHOR(S) (First name, middle initial, last name)
Lu, Shui-Shong
Willmarth, William W.

6. REPORT DATE
November 1972

7a. TOTAL NO. OF PAGES
117

7b. NO. OF REFS
44

8a. CONTRACT OR GRANT NO.
N00014-67-A-0181-0015

b. PROJECT NO.

c.

d.

9a. ORIGINATOR'S REPORT NUMBER(S)
021490-2-T

9b. OTHER REPORT NO(S) (Any other numbers that may be assigned this report)

10. DISTRIBUTION STATEMENT

Approved for public release: Distribution unlimited.

11. SUPPLEMENTARY NOTES
Not applicable

12. SPONSORING MILITARY ACTIVITY
Office of Naval Research

13. ABSTRACT

Experimental studies of the structure of the Reynolds stress in a turbulent boundary layer on a smooth wall with zero pressure gradient are reported. The technique of conditional sampling is employed to study the signal, uv, obtained from hot wire probes in a x configuration. Measurements of the mean time intervals and durations of burst and sweeps are attempted. In the conditional sampling method the velocity at the edge of the viscous sublayer is used as a detector of bursts and the signal, uv, is obtained at various locations. It is found that when the velocity, u_w, at the edge of the sublayer becomes low and is decreasing, a burst occurs. The sweep event occurs when u_w becomes large and is increasing. The convection velocity of burst and sweep events are equal and are 0.8 times the local mean velocity at $y/\delta^* \sim 0.169$. Throughout the boundary layer the bursts are the largest contributors to $\overline{uv}$ and the sweeps the second largest. The mean time intervals between bursts and sweeps is roughly the same and the time intervals scale with the characteristic time of the outer flow δ/U_∞.

DD FORM 1 NOV 1473

Unclassified

Security Classification

14. KEY WORDS	LINK A		LINK B		LINK C	
	ROLE	WT	ROLE	WT	ROLE	WT
Turbulent boundary layer						
Reynolds stress						
Turbulent structure						

DISTRIBUTION LIST

Defense Documentation Center
Cameron Station
Alexandria, Virginia 22314 (12)

Technical Library
Naval Ship Research and
Development Laboratory
Annapolis, Maryland 21402

Professor Bruce Johnson
Engineering Department
Naval Academy
Annapolis, Maryland 21402

Library
Naval Academy
Annapolis, Maryland 21402

Professor W. R. Debler
Department of Engineering Mechanics
University of Michigan
Ann Arbor, Michigan 48108

Professor W. P. Graebel
Department of Engineering Mechanics
University of Michigan
College of Engineering
Ann Arbor, Michigan 48108

Professor Finn C. Michelsen
Naval Architecture and Marine
Engineering
445 West Engineering Building
University of Michigan
Ann Arbor, Michigan 48108

Dr. Francis Ogilvie
Department of Naval Architecture
and Marine Engineering
University of Michigan
Ann Arbor, Michigan 48108

Professor W. W. Willmarth
Department of Aerospace Engineering
University of Michigan
Ann Arbor, Michigan 48108

National Science Foundation
Engineering Division
1800 G. Street, NW.
Washington, D.C. 20550

Dr. S. A. Piacsek
Argonne National Laboratory
Applied Mathematics Division
9700 S. Cass Avenue
Argonne, Illinois 60439

AFOSR (REM)
1400 Wilson Boulevard
Arlington, Virginia 22204

Professor S. Corrsin
Mechanics Department
The Johns Hopkins University
Baltimore, Maryland 20910

Professor L. S. G. Kovasznay
The Johns Hopkins University
Baltimore, Maryland 20910

Professor O. M. Phillips
The Johns Hopkins University
Baltimore, Maryland 20910

Professor J. F. Kennedy, Director
Iowa Institute of Hydraulic Research
State University of Iowa
Iowa City, Iowa 52240

Librarian
Department of Naval Architecture
University of California
Berkeley, California 94720

Professor A. Thiruvengadam
Department of Mechanical Engineering
The Catholic University of America
Washington, D.C. 20017

Professor M. Holt
Division of Aeronautical Sciences
University of California
Berkeley, California 94720

Professor E. V. Laitone
Department of Mechanical Engineering
University of California
Berkeley, California 94720

Professor P. Lieber
Department of Mechanical Engineering
University of California
Institute of Engineering Research
Berkeley, California 94720

Professor J. R. Paulling
Department of Naval Architecture
University of California
Berkeley, California 94720

Professor J. V. Wehausen
Department of Naval Architecture
University of California
Berkeley, California 94720

Professor E. R. van Driest
Virginia Polytechnic Institute
and University
Department of Aerospace Engineering
Blacksburg, Virginia 24061

Commander
Boston Naval Shipyard
Boston, Massachusetts 02129

Director
Office of Naval Research
Branch Office
495 Summer Street
Boston, Massachusetts 02210

Professor M. S. Uberoi
Department of Aeronautical Engineering
University of Colorado
Boulder, Colorado 80303

Commander
Puget Sound Naval Shipyard
Bremerton, Washington 98314

Professor J. J. Foody
Chairman, Engineering Department
State University of New York
Maritime College
Bronx, New York 10465

Dr. Alfred Ritter
Assistant Head, Applied Mechanics
Department
Cornell Aeronautical Laboratory, Inc.
Buffalo, New York 14221

Dr. A.S. Iberall, President
General Technical Services, Inc.
451 Penn Street
Yeadon, Pennsylvania 19050

Professor G. H. Carrier
Department of Engineering and
Applied Physics
Harvard University
Cambridge, Massachusetts 02139

Professor G. Birkhoff
Department of Mathematics
Harvard University
Cambridge, Massachusetts 02138

Commanding Officer
NROTC Naval Administrative Unit
Massachusetts Institute of Technology
Cambridge, Massachusetts 02139

Professor M. A. Abkowitz
Department of Naval Architecture
and Marine Engineering
Massachusetts Institute of Technology
Cambridge, Massachusetts 02139

Professor A. T. Ippen
Department of Civil Engineering
Massachusetts Institute of Technology
Cambridge, Massachusetts 02139

Professor L. N. Howard
Department of Mathematics
Massachusetts Institute of Technology
Cambridge, Massachusetts 02139

Professor E. W. Merrill
Department of Mathematics
Massachusetts Institute of Technology
Cambridge, Massachusetts 02139

Professor E. Mollo-Christensen
Room 54-1722
Massachusetts Institute of Technology
Cambridge, Massachusetts 02139

Professor N. Newman
Department of Naval Architecture and
Marine Engineering
Massachusetts Institute of Technology
Cambridge, Massachusetts 02139

Professor A. H. Shapiro
Department of Mechanical Engineering
Massachusetts Institute of Technology
Cambridge, Massachusetts 02139

David M. Chase
Bolt, Beranek & Newman, Inc.
50 Moulton Street
Cambridge, Massachusetts 02138

Commander
Charleston Naval Shipyard
U. S. Naval Base
Charleston, South Carolina 29408

A. R. Kuhlthau, Director
Research Laboratories for the
Engineering Sciences
Thorton Hall, University of Virginia
Charlottesville, Virginia 22903

Director
Office of Naval Research
Branch Office
536 South Clark Street
Chicago, Illinois 60605

Library
Naval Weapons Center
China Lake, California 93555

Professor J. M. Burgers
Institute of Fluid Dynamics and
Applied Mathematics
University of Maryland
College Park, Maryland 20742

Professor Pai
Institute for Fluid Dynamics
and Applied Mathematics
University of Maryland
College Park, Maryland 20740

Acquisition Director
NASA Scientific & Technical
Information
P. O. Box 33
College Park, Maryland 20740

Professor L. Landweber
Iowa Institute of Hydraulic Research
State University of Iowa
Iowa City, Iowa 52240

Technical Library
Naval Weapons Laboratory
Dahlgren, Virginia 22448

Computation & Analyses Laboratory
Naval Weapons Laboratory
Dahlgren, Virginia 22448

Dr. C. S. Wells, Jr.
Manager - Fluid Mechanics
Advanced Technology Center, Inc.
P. O. Box 6144
Dallas, Texas 75222

Dr. R. H. Kraichnan
Dublin, New Hampshire 03444

Commanding Officer
Army Research Office
Box CM, Duke Station
Durham, North Carolina 27706

Professor A. Charnes
The Technological Institute
Northwestern University
Evanston, Illinois 60201

Dr. Martin H. Bloom
Polytechnic Institute of Brooklyn
Graduate Center, Dept. of Aerospace
Engineering and Applied Mechanics
Farmingdale, New York 11735

Technical Documents Center
Building 315
U. S. Army Mobility Equipment
Research and Development Center
Fort Belvoir, Virginia 22060

Professor J. E. Cermak
College of Engineering
Colorado State University
Ft. Collins, Colorado 80521

Technical Library
Webb Institute of Naval Architecture
Glen Cove, Long Island, New York 11542

Professor E. V. Lewis
Webb Institute of Naval Architecture
Glen Cove, Long Island, New York 11542

Professor M. Poreh
Technion-Israel Institute
of Technology
Haifa, Israel

Library MS 185
NASA, Langley Research Center
Langley Station
Hampton, Virginia 23365

Dr. B. N. Pridmore Brown
Northrop Corporation
NORAIR-Div.
Hawthorne, California 90250

Dr. J. P. Breslin
Stevens Institute of Technology
Davidson Laboratory
Hoboken, New Jersey 07030

Dr. D. Savitsky
Stevens Institute of Technology
Davidson Laboratory
Hoboken, New Jersey 07030

Mr. C. H. Henry
Stevens Institute of Technology
Davidson Laboratory
Hoboken, New Jersey 07030

Dr. J. P. Craven
University of Hawaii
1801 University Avenue
Honolulu, Hawaii 96822

Professor E. L. Resler
Graduate School of
Aeronautical Engineering
Cornell University
Ithaca, New York 14851

Professor John Miles
% I.G.P.P.
University of California, San Diego
La Jolla, California 92038

Director
Scrippe Institution of Oceanography
University of California
La Jolla, California 92037

Dr. H. Cohen
IBM Research Center
P. O. Box 218
Yorktown Heights, New York 10598

Professor A. Ellis
University of California, San Diego
Department of Aerospace & Mech. Engrg. Sci.
La Jolla, California 92037

Dr. B. Sternlicht
Mechanical Technology Incorporated
968 Albany-Shaker Road
Latham, New York 12110

Dr. Coda Pan
Mechanical Technology Incorporated
968 Albany-Shaker Road
Latham, New York 12110

Mr. P. Eisenberg, President
Hydronautics, Inc.
Pindell School Road
Howard County
Laurel, Maryland 20810

Mr. M. P. Tulin
Hydronautics, Inc.
Pindell School Road
Howard County
Laurel, Maryland 20810

Mr. Alfonso Alcedan L. Director
Laboratorio Nacional De Hydraulics
Antigui Cameno A. Ancon
Casilla Jostal 682
Lima, Peru

Commander
Long Beach Naval Shipyard
Long Beach, California 90802

Professor John Laufer
Department of Aerospace Engineering
University Park
Los Angeles, California 90007

Professor J. M. Killen
St. Anthony Falls Hydraulic Lab.
University of Minnesota
Minneapolis, Minnesota 55414

Lorenz G. Straub Library
St. Anthony Falls Hydraulic Lab.
Mississippi River at 3rd Avenue SE.
Minneapolis, Minnesota 55414

Chief of Research & Development
Office of Chief of Staff
Department of the Army
The Pentagon, Washington, D.C. 20310

Professor M. S. Plesset
Engineering Division
California Institute of Technology
Pasadena, California 91109

Professor A. Roshko
California Institute of Technology
Graduate Aeronautical Laboratories
Pasadena, California 91109

Professor T. Y. Wu
Department of Engineering
California Institute of Technology
Pasadena, California 91109

Director
Office of Naval Research
Branch Office
1030 E. Green Street
Pasadena, California 91101

Naval Ship Engineering Center
Philadelphia Division
Technical Library
Philadelphia, Pennsylvania 19112

Technical Library
Philadelphia Naval Shipyard
Philadelphia, Pennsylvania 19112

Professor R. C. Mac Camy
Department of Mathematics
Carnegie Institute of Technology
Pittsburgh, Pennsylvania 15213

Dr. Paul Kaplan
Oceanics, Inc.
Plainview, Long Island, New York 11803

Technical Library
Naval Missile Center
Point Mugu, California 93441

Technical Library
Naval Civil Engineering Laboratory
Port Hueneme, California 93041

Commander
Portsmouth Naval Shipyard
Portsmouth, New Hampshire 03801

Commander
Norfolk Naval Shipyard
Portsmouth, Virginia 23709

Professor F. E. Bisshopp
Division of Engineering
Brown University
Providence, Rhode Island 02912

Dr. L. L. Higgins
TRW Space Technology Labs, Inc.
One Space Park
Redondo Beach, California 90278

Dr. William A. Gross, Vice President
Ampex Corporation
401 Broadway
Redwood City, California 94063

Dr. H. N. Abramson
Southwest Research Institute
8500 Culebra Road
San Antonio, Texas 78228

Editor
Applied Mechanics Review
Southwest Research Institute
8500 Culebra Road
San Antonio, Texas 78206

Office of Naval Research
San Francisco Area Office
50 Fell Street
San Francisco, California 94102

Library
Pearl Harbor Naval Shipyard
Box 400
FPO San Francisco, California 96610

Technical Library
Hunters Point Naval Shipyard
San Francisco, California 94135

Librarian
Naval Ordnance Laboratory
White Oak
Silver Spring, Maryland 20910

Fenton Kennedy Document Library
The Johns Hopkins University
Applied Physics Laboratory
8621 Georgia Avenue
Silver Spring, Maryland 20910

Professor E. Y. Hsu
Department of Civil Engineering
Stanford University
Stanford, California 94305

Professor J. Ripkin
St. Anthony Falls Hydraulic Lab.
University of Minnesota
Minneapolis, Minnesota 55414

Dr. W. Silberman
St. Anthony Falls Hydraulic Lab.
University of Minnesota
Minneapolis, Minnesota 55414

Superintendent
Naval Postgraduate School
Library Code 0212
Monterey, California 93940

Professor A. B. Metzner
University of Delaware
Newark, New Jersey 19711

Technical Library
Naval Underwater Systems Center
Newport, Rhode Island 02840

Professor Dudley D. Fuller
Department of Mechanical Engineering
Columbia University
New York, New York 10027

Professor V. Castelli
Department of Mechanical Engineering
Columbia University
New York, New York 10027

Professor H. Elrod
Department of Mechanical Engineering
Columbia University
New York, New York 10027

Professor J. J. Stoker
Institute of Mathematical Sciences
New York University
251 Mercer Street
New York, New York 10003

Society of Naval Architects and
Marine Engineering
74 Trinity Place
New York, New York 10006

Engineering Societies Library
345 East 47th Street
New York, New York 10017

Office of Naval Research
New York Area Office
207 W. 24th Street
New York, New York 10011

Miss O. M. Leach, Librarian
National Research Council
Aeronautical Library
Montreal Road
Ottawa 7, Canada

Professor A. K. Ray
Department of Applied Mechanics
University of Ottawa
Faculty of Pure & Applied Science
Ottawa 2, Canada

Technical Library
Naval Ship Research and
Development Center
Panama City, Florida 32401

Technical Library
Naval Undersea R&D Center
Pasadena Laboratory
3202 E. Foothill Boulevard
Pasadena, California 91107

Dr. Andrew Fabula
Naval Undersea Research &
Development Center
Pasadena Laboratory
3202 E. Foothill Boulevard
Pasadena, California 91107

Dr. J. W. Hoyt
Naval Undersea R&D Center
Pasadena Laboratory
3202 E. Foothill Boulevard
Pasadena, California 91107

Professor A. Acosta
Department of Mechanical Engineering
California Institute of Technology
Pasadena, California 91109

Professor H. Liepmann
Department of Aeronautics
California Institute of Technology
Pasadena, California 91109

Dr. G. Kulin
National Bureau of Standards
Washington, D.C. 20234

Code 8040
Naval Research Laboratory
Washington, D.C. 20390

Code 031
Naval Ship Systems Command
Washington, D.C. 20390

Code 0341
Naval Ship Systems Command
Washington, D.C. 20390

Code 03412B (L. Benen)
Naval Ship Systems Command
Washington, D.C. 20390

Code 03412 (J. Schuler)
Naval Ship Systems Command
Washington, D.C. 20390

Code 2052
Naval Ship Systems Command
Washington, D.C. 20390

Code 6034
Naval Ship Engineering Center
Center Building
Prince George's Center
Hyattsville, Maryland 20782

Code 6101E
Naval Ship Engineering Center
Center Building
Prince George's Center
Hyattsville, Maryland 20782

Code 6110
Naval Ship Engineering Center
Center Building
Prince George's Center
Hyattsville, Maryland 20782

Code 6113
Naval Ship Engineering Center
Center Building
Prince George's Center
Hyattsville, Maryland 20782

Code 6114
Naval Ship Engineering Center
Center Building
Prince George's Center
Hyattsville, Maryland 20782

Code 6120E
Naval Ship Engineering Center
Center Building
Prince George's Center
Hyattsville, Maryland 20782

Code 6136
Naval Ship Engineering Center
Center Building
Prince George's Center
Hyattsville, Maryland 20782

Dr. A. Powell
Code 01
Naval Ship Research and
Development Center
Washington, D.C. 20034

Mr. W. M. Ellsworth
Code 0H50
Naval Ship Research and
Development Center
Washington, D.C. 20034

Central Library
Code L42
Naval Ship Research and
Development Center
Washington, D.C. 20034

Dr. W. E. Cummins
Code 500
Naval Ship Research and
Development Center
Washington, D.C. 20034

Mr. S. F. Crump
Code 513
Naval Ship Research and
Development Center
Washington, D.C. 20034

Mr. R. Wermter
Code 520
Naval Ship Research and
Development Center
Washington, D.C. 20034

Dr. P. Pien
Code 521
Naval Ship Research and
Development Center
Washington, D.C. 20034

Dr. Byrne Perry
Department of Civil Engineering
Stanford University
Stanford, California 94305

Dr. R. L. Street
Department of Civil Engineering
Stanford University
Stanford, California 94305

Professor Milton Van Dyke
Department of Aeronautical Engineering
Stanford University
Stanford, California 94305

Professor S. Eskinazi
Department of Mechanical Engineering
Syracuse University
Syracuse, New York 13210

Professor R. Pfeffer
Florida State University
Geophysical Fluid Dynamics Institute
Tallahassee, Florida 32306

Professor R. C. Di Prima
Department of Mathematics
Rensselaer Polytechnic Institute
Troy, New York 12180

Dr. Lee Segel
Department of Mathematics
Rensselaer Polytechnic Institute
Troy, New York 12180

Professor J. Lumley
Ordnance Research Laboratory
Pennsylvania State University
University Park, Pennsylvania 16801

Dr. M. Sevik
Ordnance Research Laboratory
Pennsylvania State University
University Park, Pennsylvania 16801

Dr. J. M. Robertson
Department of Theoretical and
Applied Mechanics
University of Illinois
Urbana, Illinois 61803

Technical Library
Mare Island Naval Shipyard
Vallejo, California 94592

Code 438
Office of Naval Research
Department of the Navy
Arlington, Virginia 22217 (3)

Code 461
Office of Naval Research
Department of the Navy
Arlington, Virginia 22217

Science & Technology Division
Library of Congress
Washington, D.C. 20540

Department of the Army
Coastal Engineering Research Center
5201 Little Falls Road, NW.
Washington, D.C. 20011

Code 468
Office of Naval Research
Department of the Navy
Arlington, Virginia 22217

Code 473
Office of Naval Research
Department of the Navy
Arlington, Virginia 22217

Code 481
Office of Naval Research
Department of the Navy
Arlington, Virginia 22217

Code 2627
Naval Research Laboratory
Washington, D.C. 20390 (6)

Library, Code 2620 (ONRL)
Naval Research Laboratory
Washington, D.C. 20390 (6)

Code 6170
Naval Research Laboratory
Washington, D.C. 20390

Code 4000
Director of Research
Naval Research Laboratory
Washington, D.C. 20390

Code 8030 (Maury Center)
Naval Research Laboratory
Washington, D.C. 20390

Dr. W. B. Morgan
Code 540
Naval Ship Research and
Development Center
Washington, D.C. 20034

Mr. P. Granville
Code 541
Naval Ship Research and
Development Center
Washington, D.C. 20034

Mr. J. B. Hadler
Code 560
Naval Ship Research and
Development Center
Washington, D.C. 20034

Dr. H. R. Chaplin
Code 600
Naval Ship Research and
Development Center
Washington, D.C. 20034

Mr. G. H. Gleissner
Code 800
Naval Ship Research and
Development Center
Washington, D.C. 20034

Dr. M. Strasberg
Code 901
Naval Ship Research and
Development Center
Washington, D.C. 20034

Mr. J. McCarthy
Code 552
Naval Ship Research and
Development Center
Washington, D.C. 20034

Code 03
Naval Air Systems Command
Washington, D.C. 20360

AIR 5301
Naval Air Systems Command
Department of the Navy
Washington, D.C. 20360

AIR 604
Naval Air Systems Command
Department of the Navy
Washington, D.C. 20360

Code ORD 03
Naval Ordnance Systems Command
Washington, D.C. 20360

Code ORD 035
Naval Ordnance Systems Command
Washington, D.C. 20360

Code ORD 05413
Naval Ordnance Systems Command
Washington, D.C. 20360

Code ORD 9132
Naval Ordnance Systems Command
Washington, D.C. 20360

Oceanographer of the Navy
Washington, D.C. 20390

Commander
Naval Oceanographic Office
Washington, D.C. 20390

Chief Scientist (CNM PM-1)
Strategic Systems Project Office
Department of the Navy
Washington, D.C. 20360

Technical Division (CNM PM 11-20)
Deep Submergence Systems Project Office
Department of the Navy
Washington, D.C. 20360

Dr. A. L. Slafkosky
Scientific Advisor
Commandant of the Marine Corps (Code AX)
Washington, D.C. 20380

Librarian Station 5-2
Coast Guard Headquarters
NASSIF Building
400 7th Street, S.W.
Washington, D.C. 20591

Office of Research and Development
Maritime Administration
441 G. Street, NW.
Washington, D.C. 20235

Division of Ship Design
Maritime Administration
441 G. Street, NW.
Washington, D.C. 20235